The Pennsylvania State University

The Graduate School

Department of Electrical Engineering

OPTICAL WAVE-MIXING AND PHOTOREFRACTIVITY IN LIQUID CRYSTALS

A Thesis in

Electrical Engineering

by

Jianwu Ding

Submitted in Partial Fulfillment
of the Requirements
for the Degree of

Doctor of Philosophy

May 2005

The thesis of Jianwu Ding was reviewed and approved* by the following:

Iam-Choon Khoo
Distinguished Professor of Electrical Engineering
Thesis Advisor
Chair of Committee

Kultegin Aydin
Professor of Electrical Engineering

Ruyan Guo
Professor of Electrical Engineering

Thomas Jackson
Robert E. Kirby Chair
Professor of Electrical Engineering

Mark Maroncelli
Professor of Chemistry

W. Kenneth Jenkins
Professor of Electrical Engineering
Head of the Department of Electrical Engineering

*Signatures are on file in the Graduate School

ABSTRACT

Optical wave-mixing has a lot of applications such as optical amplification, adaptive optics, hologram and optical image processing, harmonic wave generation, and multi-photon microscopy. Photorefractivity has been utilized in many important applications including high density optical data storage, image processing (correlation, pattern recognition), spatial light modulation, phase conjugation, optical limiting, simulations of neural networks and associative memories, and programmable optical interconnections. They have been investigated, theoretically and experimentally, in this thesis, in the contexts of stimulated orientational scattering and photorefractivity in liquid crystals.

Stimulated orientational scattering (SOS) is a unique optical wave-mixing phenomenon that a scattered noise beam, generated by liquid crystal director oscillation, gets amplified through its interaction with the transmitted beam and liquid crystal director reorientation grating under an intense laser illumination. In this research work, I developed the first steady-state SOS theory without the compromise of non-pump-depletion approximation and it showed good agreement with previous experimental results. Based on the prediction of the developed theory, I successfully implemented polarization conversion in the infrared wavelength regime (1.55 μm) and the experimental observations agree well with the numerical simulation. The control of external low frequency AC electric field to the stimulated orientational scattering was experimentally investigated as well.

Furthermore, I investigated the dynamics of this liquid crystal director reorientational process by analyzing the Fourier spectrum of the stimulated signal under various input laser intensity. The influence of the modulating AC field to the stimulated signal was also studied. The oscillating frequency of the liquid crystal director grating agreed with theoretically calculated characteristic frequency when the input laser intensity exceeds the threshold value.

In addition, I have theoretically and experimentally studied the photorefractivity in nematic liquid crystals. Based on the transport band model, the generated space charge field was developed and showed the similar spatial distribution as the illuminating optical field. With the help of an externally applied DC field, the space charge field is able to induce liquid crystal director reorientation and analytical solutions have been derived for both the director reorientational angle and the resulting refractive index grating. The relationship between the first order diffraction efficiency and various material parameters has been discussed in details and shown to be in good agreement with experimental observations. Single-wall carbon nanotube doped nematic liquid crystal films showed a big increase in the effective optical nonlinearity compared with previous reported result in C60 doped photorefractive liquid crystals. The generation of the diffractive grating in the pure and Methyl-red doped liquid crystal has also been theoretically studied and the absence of the two-beam amplification has been explained as well.

In the last, this investigation in the optical wave-mixing and photorefractivity in liquid crystal is concluded and the future works are proposed.

TABLE OF CONTENTS

LIST OF FIGURES

LIST OF TABLES

ACKNOWLEDGEMENTS

I wish to express my gratitude to my thesis advisor, Professor Iam-Choon Khoo, for his patient guidance and encouragement through the course of this work. I would also like to thank my thesis committee members for their advice and suggestions. I am deeply indebted to my previous and present labmates, Michael Wood, Min-Yi Shih, Andres Diaz, Yana Williams, Kan Chen and Jae-Hong Park for their technical assistance and friendship.

I would also like to express my appreciation to my wife for her endless support and patience. My deepest appreciation goes out to my family. I will be forever indebted to my parents for the moral support they provided throughout my entire college career.

Chapter 1

Introduction

Liquid crystal is an intermediate state between liquid and solid. On one hand, it can flow like liquid. On the other hand, there is some order in the arrangement of the liquid crystal molecules and these molecules can form certain crystalline structure. Most liquid crystal molecules are large and anisotropic. As a result, there is anisotropy in their mechanical, electrical, magnetic, and optical properties. Due to the rather weak inter-molecular force, the liquid crystal director (the axis of preferred orientation of liquid crystal molecules) will reorient under the influence of an externally applied field (optical, electric or magnetic), or the applied anchoring surfactant. Liquid crystal's large anisotropy and ability to reorient its director underline almost all the known orientational effects of liquid crystalline materials.

In addition to their duality of liquid and crystal phases, liquid crystals [Khoo 1994b] possess some unique properties which make them very good materials for a wide range of applications:

- A large optical birefringence (0.15~0.2).
- Good transparency over a wide wavelength regime ranging from 0.4 μm to 20 μm.
- Adaptability. Their physical properties can be changed by adding or altering the concentration of various types of dopants.

- Flexibility. As liquids, liquid crystals can be configured in a multitude of different geometries to suit various applications.

All these unique properties of liquid crystals make them essential components in a wide variety of applications such as flat panel displays, light valves, spatial light modulators, storage devices, optical image processing devices and much more. Liquid crystals will continuously find roles in scientific research and industrial development.

1.1 General Background of Wave-Mixing in Nematic Liquid Crystals

Liquid crystals are optically anisotropic materials, and their local optical properties depend on the direction of the optical axis, which is determined by the average orientation of the liquid crystal molecules, also known as liquid crystal director. The director can be influenced by the electric field of an incoming light wave. Thus, an intense laser can disturb the liquid crystal director and thereby alter the optical properties of liquid crystal media which it propagates through. Typically, a nematic liquid crystal will have a third-order nonlinear optical susceptibility $\chi^{(3)}$ on the order of ~ 10^{-22} to 10^{-23} Cm/V^3 [Khoo 1994b], which is about eight orders of magnitude larger than that of CS_2, a well-known nonlinear crystal. This large nonlinear optical susceptibility makes liquid crystals excellent media for various optical wave-mixing phenomena and allows the observations of nonlinear optical effects at relatively much lower laser power.

Orientational nonlinearity and wave-mixing phenomena in liquid crystals have received a great deal of attention over the past several decades. Among those phenomena,

the stimulated orientational scattering [Tabiryan 2001] and photorefractive effect [Khoo 1995] in nematic liquid crystals are of the primary research objects in this thesis report because they provide direct revelation of the intensive interaction between optical field(s) and the liquid crystal director, and have many potential applications.

Stimulated orientational scattering in liquid crystals describes such a two-wave-mixing phenomenon that a weak scattered noise light, generated by a disturbance in the liquid crystal director orientation due to the impinging intensive optical wave, gets amplified through its interaction with the nematic liquid crystals (NLC) and the pump laser. A diagram illustrating this phenomenon is shown in Figure 1.1. A pump laser is focused onto a NLC film and disturbs the alignment of nearby liquid crystal molecules. This disturbance causes fluctuation of refractive index distribution in the NLC film and scatters a small portion of the input laser. The scattered noise beam in turn interacts with the transmitting laser beam and nearby NLC molecules and causes the rearrangement of the NLC molecules when it satisfies the “phase-matching” condition. When the input laser power is low, the power of the scattering noise beam is linearly proportional to the input laser power. When the pump laser is strong enough, it will strongly interact with the generated noise signal and the reoriented liquid crystal director. Through this intense interaction the scattered noise at the orthogonal polarization (relative to the input laser) will get amplified when it satisfies the phase-matching condition.

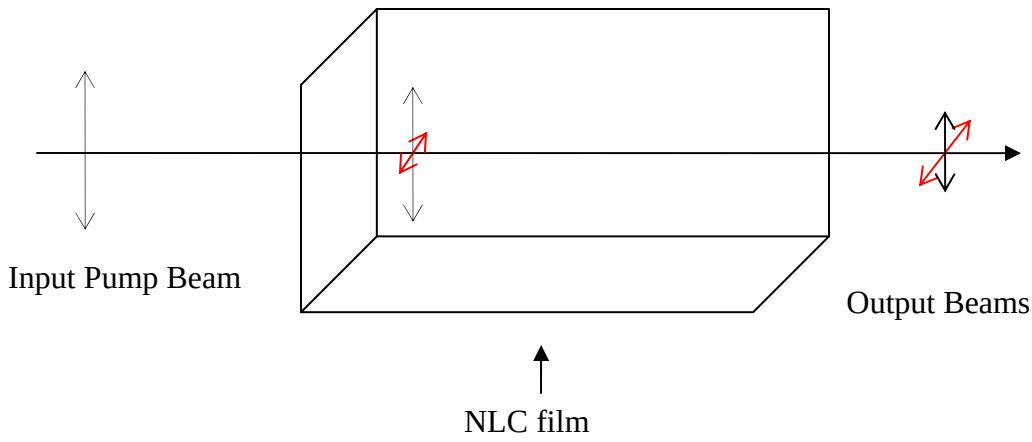

Figure 1.1: Illustration of stimulated orientational scattering.

Generally speaking, photorefractivity stands for the light induced refractive index change in a medium. In liquid crystalline materials, photorefractive (PR) effect refers to the spatial modulation of the refractive index, which is induced by the light-generated space charge field when the medium is illuminated by an inhomogeneous optical field. Most of the previous works in liquid crystal photorefractivity have been focused on the four-wave-mixing interaction and the reorientation of the liquid crystal director due to the light-induced space charge field in a photo-sensitive dye-doped liquid crystal [Gunter 1989]. Recent discoveries of photo-induced diffractive grating in Methyl-red doped nematic liquid crystals and pure nematic liquid crystals have triggered a lot of interest in the so-called surface photorefractive effect. Diffractive gratings formed in this surface photorefractive liquid crystals do not show any sign of two-beam amplification and suggest that there is no phase shift between the input optical field and the induced

refractive index grating. On the contrary, there is a $\pi/2$ phase shift and two-beam amplification in the photorefractive materials involving photon-induced space charge field. In this thesis report, the generation of periodic director reorientation gratings and the resulting refractive index gratings due to both bulk- and surface- activated photorefractive effects in liquid crystalline materials under the illumination of periodic optical field will be presented.

1.2 Significance of Stimulated Scattering

As one of the most fundamental optical phenomena, scattering is attributed to the fluctuation or non-uniform distribution of refractive index in a medium. It has been studied since as early as the beginning of the modern optics when Lord Rayleigh explained why the sky is blue. The process of light scattering can be divided into linear and nonlinear regimes. In linear scattering, the properties of a medium are not affected by the incident light. The scattered or transmitted light bears the information of the physical properties of the material. Nonlinear optical scattering occurs when an incident light interacts intensively with a medium and modifies its optical/physical properties. The scattered or transmitted light will have the information of this strong interaction between the light and the material.

Scattering of light in liquid crystals originates from the non-uniform distribution of the optical dielectric constant $\varepsilon(\vec{r})$. Due to the dielectric anisotropy, director axis fluctuation will induce disturbances in the refractive index distribution in nematic liquid crystals. Because of the relatively weak inter-molecular force in liquid crystals, a laser

beam will be able to cause director fluctuation in a liquid crystal film, especially in a thick film, and then generate scattered noise light. By studying the scattered light, one can extract the information of the liquid crystal director reorientation processes. Stimulated orientational scattering serves as one of the most direct and simple techniques to study the orientational optical nonlinearity of liquid crystals and the interaction between liquid crystals and optical field(s). Furthermore, the knowledge of how the scattered noise grows into a coherent laser is also applicable for other coherent optical wave-mixing processes.

From the fact that the amplified noise beam in the stimulated orientational scattering possesses polarization orthogonal to the original linearly-polarized input laser, stimulated orientational scattering effect has a great potential to act as an all-optical polarization switcher. Since liquid crystals have a good transparency over a wide range of wavelength regime, this non-resonant all-optical liquid crystal polarization switcher would find its usage in a wide spectrum of applications from the visible to the infrared regimes.

1.3 Significance of Photorefractive Study

Proposed applications of the photorefractive effect (PRE) include optical image processing, high density optical data storage, optical computing, communications, image processing, neutral networks, associative memories, phase conjugation, laser resonators, and many others [Yeh 1993, Sturman 1992, Heanue 1994, Pepper 1990, Solymar 1996]. Image processing applications include image correlation, image amplification, and

dynamic novelty filtering. Data can be stored in photorefractive data cubes in the form of three-dimensional phase holograms which have very high density and fast parallel optical access. The PRE has been used to correct image distortions suffered by optical beams in inhomogeneous or turbulent media. Photorefractive crystals such as $LiNbO_3$ have been used to demonstrate many of the proposed applications and to study the physics of the photorefractive effect. In the pursuit of more efficient photorefractive material, liquid crystals were found to be a very good candidate because they provide much larger nonlinearity (implying larger diffraction efficiency, thus stronger photorefractive effect) than traditional inorganic photorefractive crystals due to their large optical anisotropy and director reorientation capability.

Understanding of photorefractive effect in liquid crystals requires the knowledge of space charge field generation (in bulk-activated photorefractive liquid crystals) and surface torques (in surface-activated photorefractive liquid crystals) and the resulting liquid crystal director reorientation. To date, there is no complete theoretical analysis for both bulk- and surface- activated photorefractivity in liquid crystalline materials. The detailed knowledge of the generation of the liquid crystal director orientational grating can provide direction in optimizing experimental parameters and in developing more photo-sensitive dopants to satisfy specific applications' need and to improve diffraction efficiency. Recently invented single-wall and multi-wall carbon nanotubes have shown to enhance optical nonlinearity and improve the diffractive efficiency of the photorefractive liquid crystals when used as photo-sensitive dopants.

1.4 Statement of Objectives and Organization of Materials

The purpose of this research work is to investigate the wave-mixing and photorefractivity of nematic liquid crystals in the context of stimulated orientational scattering and photorefractivity in nematic liquid crystal films, both theoretically and experimentally.

The supra wave-mixing and photorefractive effects are directly related to the unique optical/mechanical properties and orientational nonlinearity of the liquid crystals. Chapter 2 gives detailed background knowledge of nematic liquid crystals and their orientational nonlinearity. In chapter 3, steady-state stimulated orientational scattering in liquid crystal films and waveguides is discussed in details, including theoretical modeling and experimental observations in both visible and infrared wavelength regimes. The dynamic study and Fourier spectrum analysis of stimulated scattering in liquid crystals are presented in chapter 4. Chapter 5 is dedicated to photorefractive effect of nematic liquid crystals, including detailed theoretical analysis and comprehensive experimental observations. Final conclusions and suggestions for future work are summarized in chapter 6.

Chapter 2

Orientational Nonlinearity of Nematic Liquid Crystals

Liquid crystal is a unique type of material possessing one or more intermediate states between normally encountered solid and liquid phases. It exhibits many crystalline properties of solids, such as birefringence, anisotropies, and crystal-like x-ray diffraction patterns, yet capable of flowing like a liquid. As a result, numerous applications of liquid crystals have been found in the areas of flat-panel displays, image processing, optical storage, sensor protection and tunable-bandgap photonic structures [see, for example, Khoo 1994a].

The basis of the majority of liquid crystal electro-optical effects is found in the reorientation of its director (axis of the preferred orientation of liquid crystal molecules) under the influence of an externally applied field (optical, electric or magnetic). Anisotropy in the dielectric properties of liquid crystals is the origin for the director reorientation, whereas the dynamics of this reorientation process depends on the initial director orientation and liquid crystal viscosity. Optical properties of a liquid crystal material are changed as a result of this director (optical axis) reorientation. Thereby the understanding of nonlinear orientational effects in liquid crystals relies on the knowledge of both the physical and the optical properties of nematic liquid crystals. In this chapter, a general review of nematic liquid crystals and their orientational optical nonlinearity is presented.

2.1 Basics of Liquid Crystals

Liquid crystals are well-known for their applications in flat-panel display technology. However, recent studies [see, for example, Gunter 1989] showed that they also are highly nonlinear optical materials. Typically, a nematic liquid crystal (NLC) has an optical nonlinearity 10^8 times larger than that of CS_2, a standard Kerr medium. Therefore, many nonlinear optical phenomena, which usually happen only with high power lasers, can be observed in a NLC medium with low-power lasers [Khoo 1994a]. Table 2.1 shows the comparison of effective nonlinear index coefficients among different optical materials.

Table 2.1: Refractive Index Coefficients of Nonlinear Optical Materials

Materials	Order of Magnitude of n_2 (cm^2/W)
Nematic Liquid Crystal	
Purely optically induced or thermal effect	10^{-4}
Excited dopant assisted	10^{-3}
Photorefractive -C60 doped	10^{-3}
Photorefractive -methyl-red doped	**10**
BMAB doped NLC	**>2**
Cis-trans isomer	10^{-3}
GaAs bulk	10^{-5}
GaAs MQW	10^{-3}
Photorefractive crystals and polymers	10^{-4}
Bacteriorhodopsin	10^{-3}
Organic Polymers	10^{-13}

Liquid crystals are composed of fairly large rod-like organic molecules which tend to align along a common direction parallel to their long axis. Figure 2.1 shows the basic molecular structures of the most common liquid crystal mixture E7. In general, liquid crystal molecules, as shown in Figure 2.2**,** comprise a side chain R, two or more aromatic rings A and A', connected by linkage group X, and at the other end connected by a terminal group R' [Khoo 1994a]. Most of liquid crystals are benzene derivatives containing aromatic rings. Typically, liquid crystals are named after their linkage groups.

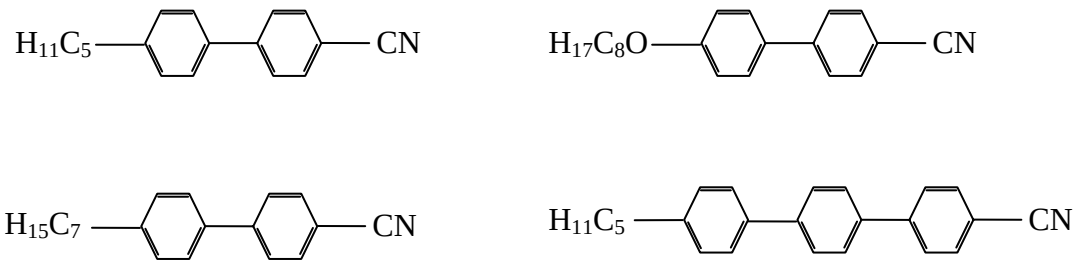

Figure 2.1: Chemical structure of E7

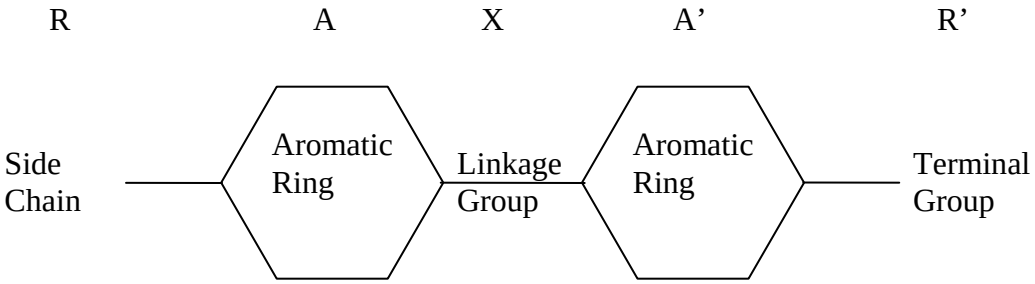

Figure 2.2: Molecular structure of a typical liquid crystal

In general, liquid crystals may be classified by their physical parameters associated with liquid crystalline phases: Lyotropic, polymeric and thermotropic. Lyotropic liquid crystals are mainly used in biological studies. Polymeric liquid crystals are basically the polymer version of monomers, and are characterized by much higher

viscosity than monomers. Typically polymeric liquid crystals are used for optical storage. Figure 2.3 shows the structures of typical polymeric liquid crystals. Thermotropic liquid crystals are the most widely used and extensively studied liquid crystalline materials because of their impressive nonlinear optical properties. There are three main types of thermotropic liquid crystals, i.e., nematic, cholesteric and smectic, classified by their orientational and positional orders respectively.

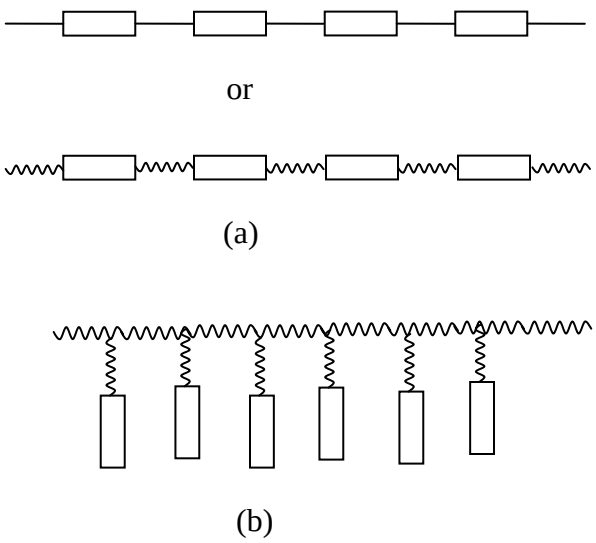

Figure 2.3: Polymeric liquid crystals: (a) main chain; (b) side chain

In the nematic phase of liquid crystals (NLC), there is a long-range order of molecular orientation, while positions of molecules are totally disordered as shown in Figure 2.4. The direction of the preferred molecules orientation (imposed by the boundary plates) is denoted by the director $\vec{n}$, which is a unit vector to denote an average

direction that a domain of liquid crystal molecules aligns to. At a given temperature, the direction of individual liquid crystal molecular fluctuates around the NLC director. A physical parameter S is used to measure how well the liquid crystal molecules align along the director. $S = 1$ means all the molecules are in line with the NLC director while $S = 0$ represents the totally disordered state (no preferred orientation at all). Generally, nematic liquid crystal molecules are centro-symmetric.

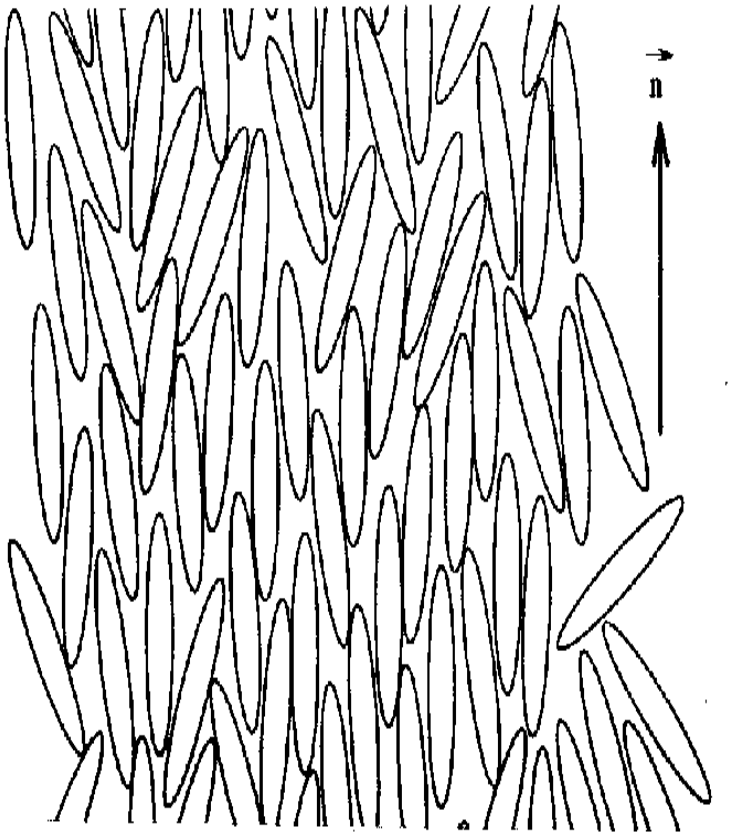

Figure 2.4: Molecular alignment of nematic liquid crystal

Cholesteric liquid crystals are fabricated by adding chiral molecules into nematic liquid crystals to form a chiral structure. Hence, they are also known as chiral nematic liquid crystals, and resemble nematic liquid crystals in all physical properties except the

molecules tend to align in a helical manner as shown in Figure 2.5. This added feature provides faster switching performance and makes cholesteric liquid crystals useful in applications such as flat-panel display and smart-pixel technology [Johnson 1993].

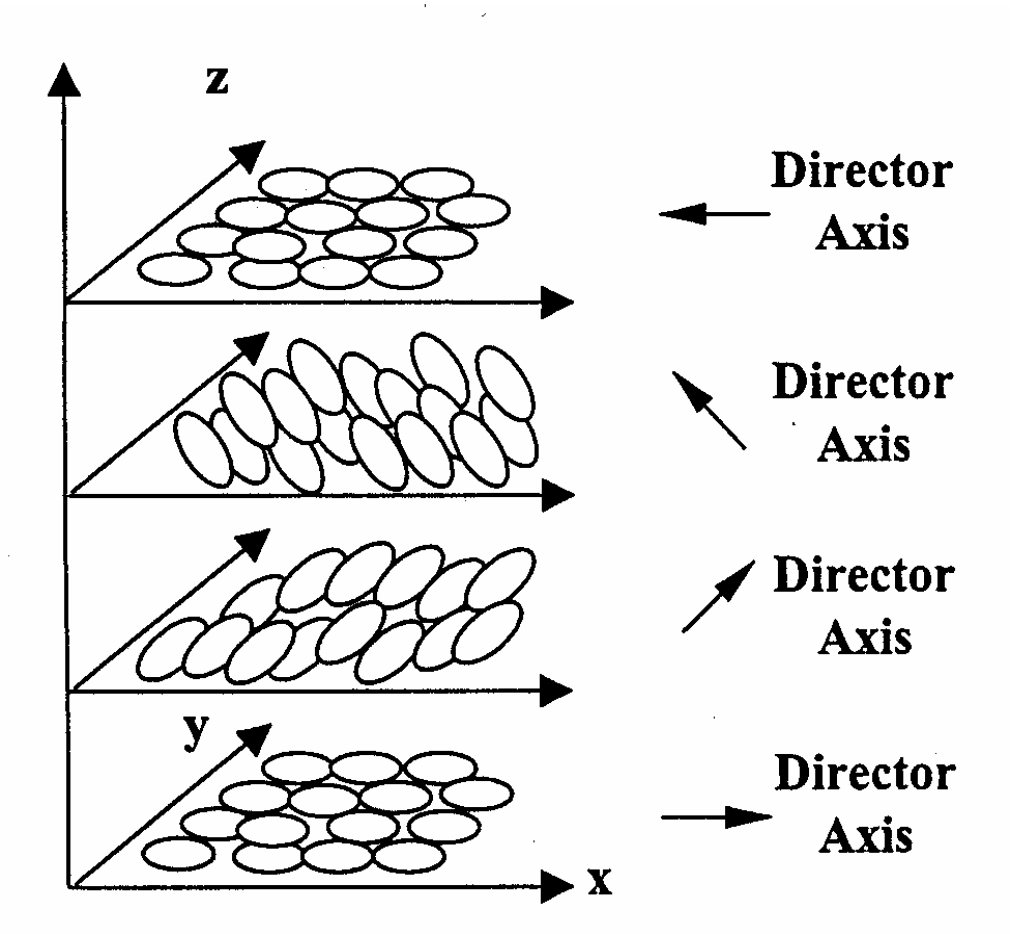

Figure 2.5: Molecular alignment of chiral nematic liquid crystal

Smectic liquid crystals are the closest to solid in structure and have both orientational and positional order in molecular arrangement. Different from the nematic phase, the position of molecules in smectic liquid crystals is correlated in some ordered pattern. There are several sub-phases of smectics according to the arrangement or the ordering of molecules and their structural symmetry properties. They are generally used

in practical electro- and opto-optical modulation devices. This report will focus on the most widely studied liquid crystals in nonlinear optics - nematic liquid crystals.

2.2 Nematic Liquid Crystals

Nematic liquid crystals are the most extensively studied liquid crystals and they are the best examples of the dual nature of liquid crystals: fluidity and crystalline structure. Without any external alignment, there are multiple domains in nematic liquid crystal bulk. The whole sample appears milky while each domain has its own preferred director and cause refractive index disparity throughout the bulk. The crystalline properties become apparent when molecules in such milky liquid are well organized using appropriate aligning surfactants or electric, magnetic fields.

In laboratories, there are two commonly used alignments: homogeneous (or planar) and homeotropic as shown in Figure 2.6 (a) and (b), respectively. A liquid crystal film consisting of a liquid crystal layer of desired thickness is sandwiched between two surface-treated glass slides. To create homeotropic alignment, the cell walls are coated with a polar surfactant such as HTAB (hexadecyl-trimethyl-ammonium-bromide) whose molecules tend to align perpendicular to the walls and thus impart a homeotropic alignment of liquid crystals [Khoo 1994b].

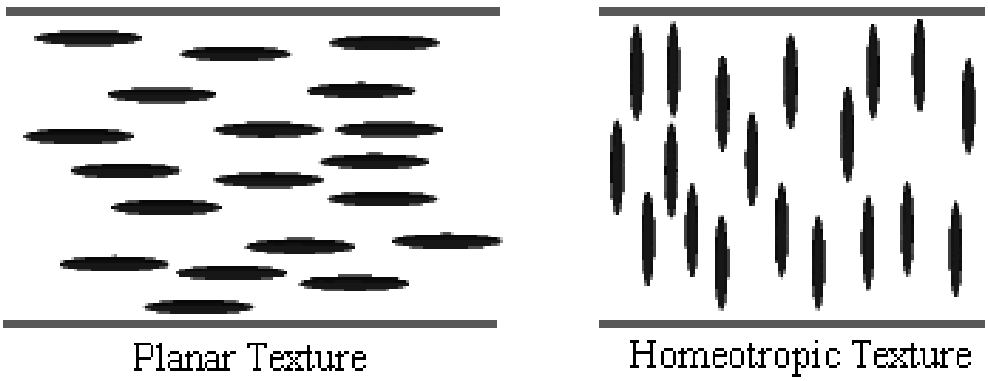

Figure 2.6: Nematic liquid crystal alignment: (a) planar; (b) homeotropic

Planar alignment can be achieved in many ways. A simple yet effective method is to first coat the cell walls with some polymer such as PVA (polyvinyl alcohol), and then rub it uni-directionally with a lens tissue. This process creates micro-grooves on the polymer coating and facilitates the alignment of the long axis of liquid crystal molecules along the rubbed direction (i.e., on the plane of the cell wall). An alternative method is to deposit silicon oxide obliquely onto the cell wall. Besides these two standard cell alignments, there are many other variations such as hybrid, twisted, super-twisted and fingerprint tailored alignments for specific applications.

At a given temperature, the direction of each liquid crystal molecule fluctuates around the director. These orientational fluctuations and the correlation of liquid crystal molecules are described by an order parameter:

$$S = \frac{1}{2}\left\langle 3\cos^2\theta - 1 \right\rangle \qquad \text{Equation 2.1}$$

where θ is the angle between the long axis of individual liquid crystal molecule and the liquid crystal director. $S = 1$ denotes the perfect alignment state while $S = 0$ means that

liquid crystal molecules are totally disordered (no preferred direction). In the nematic phase, S is a function of the temperature as:

$$S = (1 - \frac{T}{T_c})^{\beta} \qquad \text{Equation 2.2}$$

where Tc is the critical temperature above which liquid crystals change into isotropic phase from the nematic phase.

Any external field which changes the state of $\vec{n}$ or S will change the optical refractive index, and further, change the state (phase and/or amplitude) of light passing through the liquid crystal sample. If the change in the refractive index results from light-induced nonlinear reorientation of the liquid crystal director or causes nonlinear modification in phase or magnitude of the transmitted light, the phenomena is called orientational nonlinear optical effect.

2.3 Orientational Nonlinearity of Nematic Liquid Crystals

When a NLC is in its single crystal state, it acts just like a uni-axial crystal. However, due to the extremely large anisotropy and the rather weak inter-molecular force in liquid crystals, even a very small external perturbation (caused by electrical field, optical field, pressure, or temperature) can easily induce a reorientation of the NLC director. Because of the large birefringence of NLCs, any small director reorientation means an enormous change in the refractive index of the medium.

In a lab reference system defined by Cartesian coordinates, the tensor of the optical dielectric permittivity of nematic liquid crystal is described as: [Tabiryan 1986]

$$\varepsilon_{ij} = \varepsilon_{\perp}\delta_{ij} + \varepsilon_a n_i n_j \qquad \text{Equation 2.3}$$

where $\varepsilon_a = \varepsilon_{\parallel} - \varepsilon_{\perp}$ is the dielectric anisotropy of nematic liquid crystals, and the subscripts *i, j=x, y, z* denote the projection components on the axis of different Cartesian coordinates.

If a director reorientation occurs, the liquid crystal director will change as:

$$n_i = n_i^{\,0} - \delta n_i \qquad \text{Equation 2.4}$$

where $n_i^{\,0}$ denotes the initial director orientation. The dielectric permittivity changes into:

$$\begin{aligned} \varepsilon_{ij} &= \varepsilon_{\perp}\delta_{ij} + \varepsilon_a (n_i^{\,0} + \delta n_i)(n_j^{\,0} + \delta n_j) \\ &\approx \varepsilon_{\perp}\delta_{ij} + \varepsilon_a n_i^{\,0} n_j^{\,0} + \varepsilon_a (n_i^{\,0}\delta n_j + n_j^{\,0}\delta n_i) \\ &= \varepsilon_{ij}^{\,0} + \delta\varepsilon_{ij} \end{aligned} \qquad \text{Equation 2.5}$$

where $\varepsilon_{ij}^{\,0}$ represents the unperturbed dielectric permittivity tensor and $\delta\varepsilon_{ij}$ is the induced change of the dielectric tensor caused by an external perturbation. The resulting change of the refractive index is:

$$\begin{aligned} \delta n &= n - n^0 \\ &= \sqrt{\varepsilon} - \sqrt{\varepsilon^0} \\ &= \sqrt{\varepsilon^0 + \delta\varepsilon} - \sqrt{\varepsilon^0} \\ &\approx \sqrt{\varepsilon^0}\left(1 + \frac{\delta\varepsilon}{2\varepsilon^0}\right) - \sqrt{\varepsilon^0} \\ &= \frac{\delta\varepsilon}{2n^0} \end{aligned} \qquad \text{Equation 2.6}$$

It is apparent that the change of the refractive index is proportional to the change of the dielectric tensor. Due to the extremely large birefringence ($\varepsilon_a \approx 0.65$) and the rather weak inter-molecular bonding, even a small disturbing optical field can cause the

reorientation of the liquid crystal director and induce significant change in the refractive index distribution which in turn changes the system response to the incoming optical field(s).

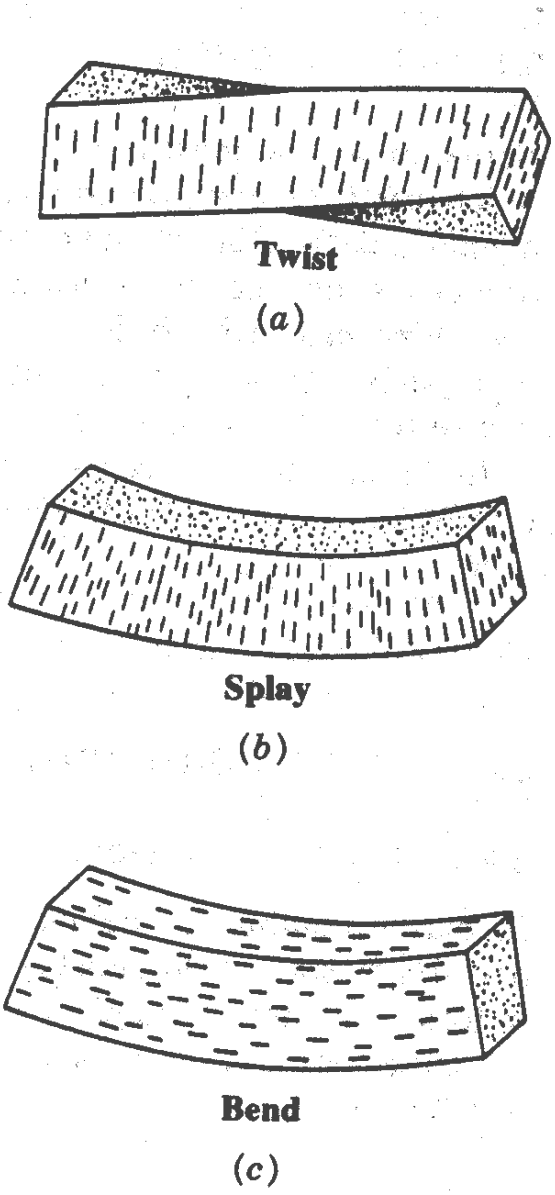

Figure 2.7: (a) twist deformation in a nematic liquid crystal; (b) splay deformation; (c) bend deformation.

Upon application of an external field, NLCs will undergo deformations just as any solid. Three principal distinct director axis deformations are twist, splay, and bend as shown in Figure 2.7. The free energy density associated with these deformations is given by:

$$\begin{aligned} \text{splay: } f_1 &= \frac{1}{2} K_1 \left(\nabla \cdot \hat{n}\right)^2, \\ \text{twist: } f_2 &= \frac{1}{2} K_2 \left(\hat{n} \cdot \nabla \times \hat{n}\right)^2, \\ \text{bend: } f_3 &= \frac{1}{2} K_3 \left(\hat{n} \times \nabla \times \hat{n}\right)^2, \end{aligned} \qquad \text{Equation 2.7}$$

where K_1, K_2, and K_3 are the respective Frank elastic constants. Establishment of the equilibrium state in a director reorientation process at a constant temperature is described by the so-called Euler-Lagrange-Rayleigh equation as: [Tabiryan 1986]

$$\frac{\partial}{\partial x_j} \frac{\delta f}{(\partial U_m / \partial x_j)} - \frac{\delta f}{\delta U_m} - \frac{\delta R}{\delta \dot{U}_m} = 0 \qquad \text{Equation 2.8}$$

where U_m's are the independent variables of the system. f is the total free energy and R is the dissipative function density of the system. The dissipative function density R is defined as:

$$R = \frac{1}{2} \eta \dot{\hat{n}}^2 \qquad \text{Equation 2.9}$$

where η is the viscosity constant of the NLC medium.

When there are other forces such as surface alignment forces, external electric or magnetic field(s), or applied optical field(s), the total free energy has to be expanded to include the free energy due to these external forces as:

$$f = f_{elastic} + f_{surface} + f_{applied} \qquad \text{Equation 2.10}$$

where $f_{elastic} = f_1 + f_2 + f_3$ is the sum of free energy arising from elastic deformations of a NLC medium.The reorientation process of the NLC director resulting from these external forces will be discussed in the following section.

2.4 Reorientation of Nematic Liquid Crystal Molecules

Due to the rather weak inter-molecular force, the local arrangement of liquid crystal molecules can be influenced by external forces even in a well-aligned liquid crystal film [Khoo 1994b]. This post-sample-preparation reorientation capability of liquid crystal enables one to change the liquid crystal director orientation, and in turn changes the optical properties of liquid crystal samples. In this section, some popular reorientation techniques of nematic liquid crystals are introduced.

2.4.1 Alignment by Electric and/or Magnetic Field

When an electric or magnetic field is applied to a NLC cell, it places a torque on the rod-like NLC molecules. For an applied electric field $\vec{E}$, the induced displacement $\vec{D}$ has the form:

$$\vec{D} = \varepsilon_{\perp}\vec{E} + (\varepsilon_{\parallel} - \varepsilon_{\perp})(\hat{n}\cdot\vec{E})\hat{n} \qquad \text{Equation 2.11}$$

The molecular torque associated with the electric field is given by:

$$\begin{aligned}\Gamma_E &= \vec{D}\times\vec{E} \\ &= (\varepsilon_{\parallel} - \varepsilon_{\perp})(\hat{n}\cdot\vec{E})(\hat{n}\times\vec{E}) \\ &= \varepsilon_a(\hat{n}\cdot\vec{E})(\hat{n}\times\vec{E})\end{aligned} \qquad \text{Equation 2.12}$$

Similarly, the magnetic torque density is expressed as:

$$\Gamma_E = \chi_a{}^m (\hat{n} \cdot \vec{H})(\hat{n} \times \vec{H}) \qquad \text{Equation 2.13}$$

where $\hat{n}$ is the NLC director, ε_a and $\chi_a{}^m$ are the corresponding anisotropy of the dielectric permittivity and the magnetic susceptibility. For positive anisotropic liquid crystal ($\varepsilon_a > 0$), the induced torque tends to align NLC molecules to the direction of the applied field in order to minimized the free energy. Because of the strong anchoring forces at the NLC cell boundaries, the applied field has to exceed a certain threshold value called "Freedericksz Transition Threshold" to induce observable reorientation in the NLC medium. When passing the Freedericksz threshold, the reorientation angle of the liquid crystal director increases with the increase of the applied field. However, the reorientation of the NLC molecules is not uniform across the cell. There is hardly any reorientation in the region close to the cell boundaries because of the surfactant anchoring force, while the applied field plays a dominant role in the bulk.

In CGS units, the Freedericksz threshold in a NLC cell when an electric field is applied perpendicular to the NLC director's initial alignment is give as: [Khoo 1994b]

$$E_f = \frac{\pi}{d}\sqrt{\frac{4\pi K_{ii}}{\varepsilon_a}} \qquad \text{Equation 2.14}$$

where the subscript $i = x, y, z$ denotes the projection component on the axis of different Cartesian coordinates, K_{ii} is the splay coefficient, d is the thickness of the NLC cell and ε_a is the dielectric anisotropy. The larger the splay coefficient, the more electric torque is needed to surpass the inter-molecular interaction and reorient the NLC director. For a thinner NLC cell, the surfactant has a larger influence and a stronger external field is

needed to reorient the NLC director to the same extent when other parameters remain the same. This inverse relationship between the film thickness and the magnitude of the aligning field implies that a NLC film can not be too thin in order to maintain the capability of reorienting its director under external field(s). If the sample is too thick, the NLC molecules in the bulk may not be able to align well due to their weak inter-molecular force.

2.4.2 Alignment by an Optical Field

When a plane wave optical field impinges on the NLC medium, the free energy of the system due to the optical dipolar interaction is given by:

$$f_{light} = -\frac{1}{2}\varepsilon_{ij}E_iE_j \qquad \text{Equation 2.15}$$

Where the subscripts $i\ j$ =*x*, *y*, *z* denotes the projection components on the axis of different Cartesian coordinates, ε_{ij} is the NLC dielectric tensor, E_i is the electric field component along the respective Cartesian axis. Minimizing this free energy gives the torque due to the optical field which is the same as the one due to an electric field:

$$\Gamma_{light} = \varepsilon_a(\hat{n}\cdot\vec{E})(\hat{n}\times\vec{E}) \qquad \text{Equation 2.16}$$

The reorientation process of the NLC director will be discussed in a greatly simplified example as shown in Figure 2.8. In this example, a linearly polarized laser is incident on a homeotropically aligned NLC cell at an angle β. This optical field will induce a reorientation angle θ of the director in a NLC cell with thickness *d*. The torque equation in this medium is:

$$K_1 \frac{d^2\theta}{dz^2} + \frac{\varepsilon_a \left|\vec{E}\right|^2}{16\pi} \sin 2(\beta + \theta) = 0 \qquad \text{Equation 2.17}$$

When the reorientation angle θ is small, under the so-called hard-boundary condition (the director axis will be fixed at the boundary due to the strong anchoring force of the aligning surfactant), the director reorientation angle has an analytical solution as [Khoo 1994b]:

$$\theta(z) = \frac{\varepsilon_a \left|\vec{E}\right|^2}{32\pi K_1} \sin 2\beta [d \cdot z - z^2] \qquad \text{Equation 2.18}$$

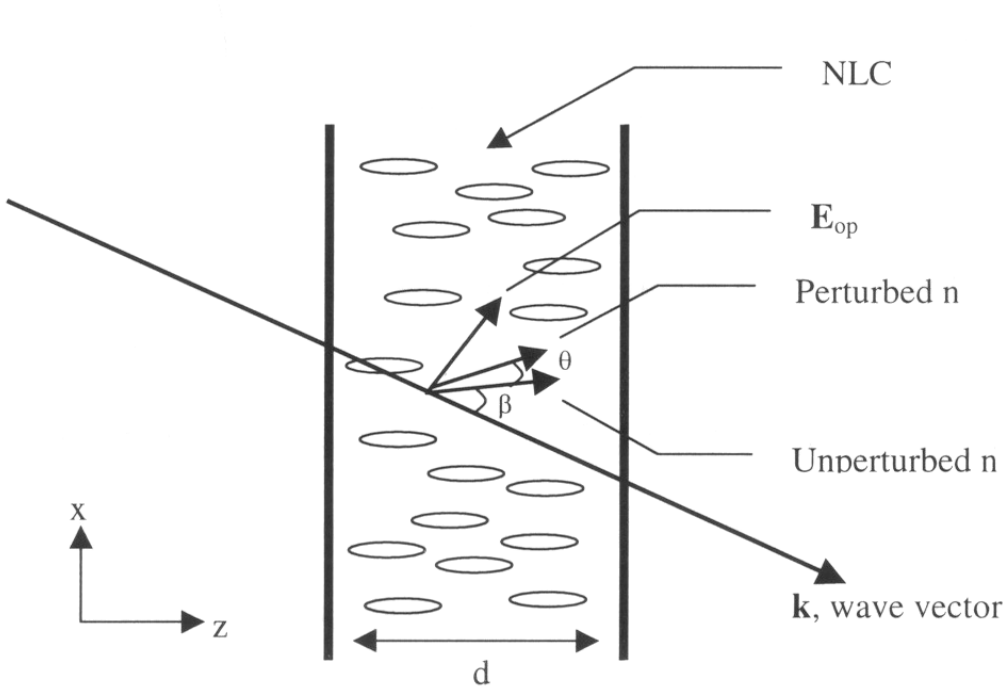

Figure 2.8: Interaction of a linearly polarized laser and a homeotropically aligned NLC film.

From Equation 2.18, the reorientational angle is quadratically dependent on the magnitude of the applied optical field or linearly proportional to the irradiative light

intensity, and it is inversely proportional to the splay elastic constant of the NLC medium. A smaller elastic constant means weaker inter-molecular forces and gives a larger reorientation angle under the same experimental conditions. As discussed before, in a thicker sample the influence of the boundary anchoring force is much weaker in the bulk and yields larger director reorientation movement under the same disturbing force. The director reorientational angle is linearly proportional to the sample thickness as shown in Equation 2.18 that the increase in the sample thickness generally allows larger reorientational angle when other parameters remain the same.

2.4.3 Laser Induced Dye-Assisted NLC Molecular Reorientation

Recently, a great deal of interest has arisen in dye-doped liquid crystals in the pursuit of supra-nonlinear, functionalized active photonic materials and devices [Barbero 2002, Kaczmark 2002]. It has been shown that some absorbing dye molecules, once photo-excited, are able to exert an intermolecular torque large enough to influence the orientation of NLC molecules. In particular, Janossy et al [Janossy 1992] have observed that some classes of anthraquinone dyes, under a linearly polarized laser illumination, will align themselves in the direction of the input laser polarization and help the NLC director reorient toward the laser polarization direction. On the other hand, some other dye-doped liquid crystals will align themselves in the direction orthogonal to the laser polarization and the wave vector as reported by Gibbons et al [Gibbons 1991]. This response will in fact deteriorate the reorientation effort initiated by the input optical field.

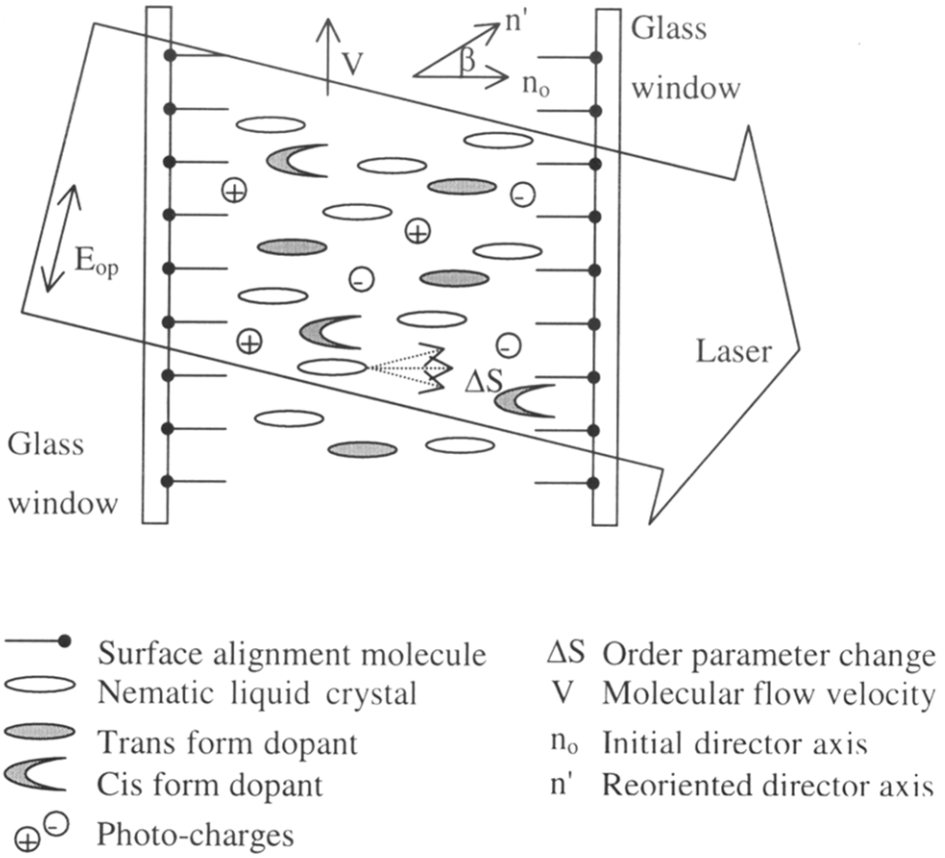

Figure 2.9: Schematic diagram of the propagation of an optical field in dye-doped NLC film

Figure 2.9 illustrates a schematic diagram of the propagation of an optical field in a photo-sensitive dye doped NLC film. By means of being photo-ionized to generate photo-charges and form space charge field, or being photo-isomerized, these photo-active dyes are able to influence the local NLC molecules' alignment and reorient the NLC director. Combing with its large optical anisotropy, this unique reorientation property makes liquid crystal a highly nonlinear optical material for a wide range of applications.

Chapter 3

Stimulated Orientational Scattering of Nematic Liquid Crystals

Nematic liquid crystals (NLC) are optically anisotropic materials, and their local optical properties are determined by the orientation of the optical axis, the NLC director. The director orientation, on the other hand, can be influenced by an external field such as a polarized light. Thus an intense laser can alter the optical properties of a liquid crystal medium as it propagates, through it and influence the light transmission subsequently. Stimulated orientational scattering (SOS) in a nematic liquid crystal (NLC) film, in which a weak scattered noise grows into a strong signal via the optical wave mixing effect, was first predicted and observed more than a decade ago by Tabiryan [Tabiryan 1986]. This orientational dynamics has since been utilized in various applications such as chaotic study in liquid crystals [Cipparrone 1993]. Tabiryan's analysis was successful in explaining the exponential growth of the stimulated signal when it is small and negligible compared to the input pump beam. But this theory is limited by the non-pump-depletion assumption, which becomes inappropriate when the generated signal becomes comparable or even exceeds the transmitted wave as reported in Khoo's experimental observation in 1995 [Khoo 1995]. Further study is needed in order to have a better understanding of the NLC director's reorientation dynamics and the interaction between a NLC system and optical field(s).

3.1 General Principles

Because of the rather weak intermolecular forces in NLC, even a very small external perturbation can easily induce a reorientation of the NLC director. This reorientation (even small reorientation) will cause a significant change in the refractive index of a NLC medium thanks to NLCs' large birefringence. In general, a small perturbation in NLC molecular alignment, such as a heat-induced local density fluctuation, can produce a disparity in the optical dielectric constant $\varepsilon(\vec{r})$ of a NLC medium. This perturbation in optical dielectric constant causes scattering loss for the light propagating through it [Hayer 1978]. The resulting scattered or transmitted light, in terms of spatial or temporal frequency or intensity, can reflect the physical properties of a nematic liquid crystal medium or reveal the interaction mechanism between optical field(s) and material, especially under intense laser illumination.

As a result of fluctuations of the optical dielectric constant, an incident light beam will be scattered. The direction, polarization, and spectrum of the scattered light depend on the optical-geometrical configuration. In the case of nematic liquid crystals, the differential scattering cross section from a linearly polarized light beam is expressed as [Khoo 1994b]:

$$\frac{d\sigma}{d\Omega} = \frac{\varepsilon_a{}^2 \omega^4}{c^4} V k_B T \left[\frac{\cos^2(\theta/2)}{K_1 q^2} + \frac{\sin^2(\theta/2)}{K_2 q^2}\right] \qquad \text{Equation 3.1}$$

where $\theta \in (0, 90^o)$ is the angle between incident beam and the scattered beam, K_1 K_2 are the splay and twist Frank elastic constants of liquid crystal respectively, V is the volume of the medium, $\vec{q}$ and ω are the wave vector and frequency difference between the input

and the scattered beam, k_B is Boltzmann's constant, T is the medium temperature, and ε_a is the dielectric anisotropy. Equation 3.1 has two important inferences:

- The scattering inside a well-aligned NLC media is intense at the cross-polarization direction where $\theta = 90^o$ (i.e. when the scattered light is orthogonally polarized to the incident optical field).
- The scattering is particularly strong at small angles $\theta \approx 0$.

The scattered noise at the cross-polarization, $\theta = 90^o$, is of great importance because it has the potential to get amplified and even start lasing when its wave vector and frequency satisfy the phase-matching condition.

3.2 Current Status

A typical stimulated orientational scattering configuration is shown in Figure 3.1. A linearly polarized light beam enters a homogeneously aligned liquid crystal film with the director parallel to the input laser's polarization. The scattered noise beam interacts with the input laser through the grating they formed in the NLC film and grows into an observable signal due to the energy transfer from the input pump beam. The first theoretical work on this effect was done by N. V. Tabiryan in 1986 [Tabiryan 1986]. Starting from the Euler-Lagrange-Rayleigh equation which describes the establishment of the equilibrium state in this NLC director reorientation process, he derived the director reorientation induced by the input linearly polarized laser and the scattered cross-polarized noise beam as:

$$\theta_0(z,t) = \frac{\varepsilon_0 \varepsilon_a}{2K_2 q^2} \frac{E_x E_y^*}{1 - i\Omega\eta / K_2 q^2} \qquad \text{Equation 3.2}$$

where E_x and E_y are the electric fields of the input and scattered beam respectively, q and Ω are the wave vector and frequency of the NLC director's orientational grating, η is the viscosity of the NLC film and K_2 is the bending elastic constant of the NLC medium.

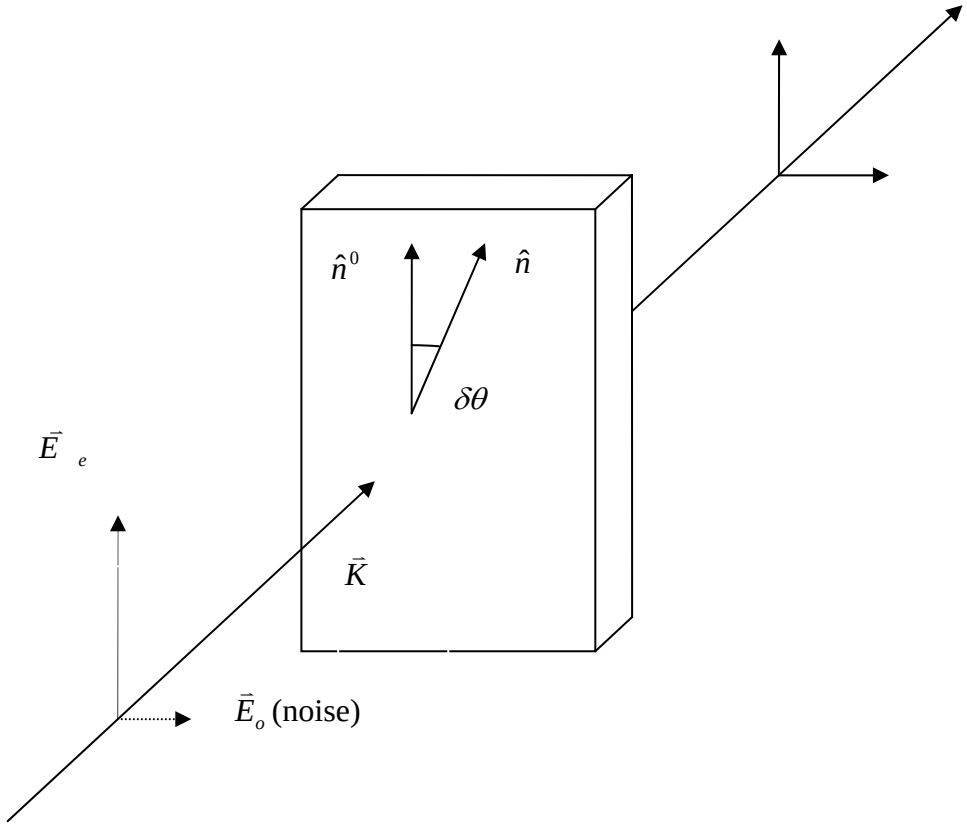

Figure 3.1: Schematic configuration of stimulated orientational scattering in a nematic liquid crystal film.

Using the coupled wave equations under the so-called non-pump-depletion approximation, Tabiryan predicted that the amplification coefficient of the noise signal has the exponential form

$$I_{noise} = I_0 e^{gd} \qquad \text{Equation 3.3}$$

The gain factor g has the following expression:

$$g = \frac{\Omega\eta / K_2 q^2}{1+(\Omega\eta / K_2 q^2)^2} \frac{k_y \varepsilon_0 \varepsilon_a{}^2 |E_x|^2}{2K_2 q^2} \qquad \text{Equation 3.4}$$

The exponential gain of the signal wave E_y is the result of energy transferring from the pumping wave E_x. The amplification to the noise signal only appears at $\Omega > 0$ due to the grating phase relaxational shift. The gain coefficient g is proportional to the pump intensity $I_x = |E_x(z)|^2$ and reaches the maximum at

$$\Omega = K_2 q^2 / \eta \qquad \text{Equation 3.5}$$

The amplification coefficient is quadratically proportional to the dielectric anisotropy of the NLC medium. The larger the anisotropy, the stronger the reorientational nonlinearity and the more energy transfer to the stimulated noise beam.

The first observation of the stationary SOS effect in a NLC film was made in 1987 [Khoo 1987]. An o-type wave was incident on a homogeneous liquid crystal (5CB) film of 110 μm thick. An Argon laser was used (λ = 0.48 μm). The stimulated signal showed exponential gain with respect to the input beam intensity as predicted in Tabiryan's theoretical work [Tabiryan 1986]. Later in 1990 [Sukhov 1990], Sukhov reported the forward SOS for the normal incidence of an e-wave onto a planar liquid

crystal 5CB film. The pump radiation was generated by a pulse Ruby laser. The transient SOS theory was used for the comparison and the experimental results were in a good agreement with Tabiryan's theory with respect to both the exponential growth of the stimulated noise beam and the value of the gain coefficient.

Tabiryan's theory works well in explaining the SOS effect when the stimulated output is negligibly small compared to the transmitted pump wave. But the non-pump depletion approximation becomes invalid when the stimulated signal becomes comparable to the transmitted pump beam or even stronger than the transmitted pump beam as in the experimental observation by Khoo [Khoo 1995]. SOS effect is an all-optical non-resonant effect and has many potential applications such as polarization conversion, optical phase conjugation, and all-optical beam amplifications. A complete SOS theory without the non-pump-depletion approximation is important to explain the intensive interaction between optical fields and anisotropic liquid crystals and to provide directions for further scientific research and device development. The need for a complete SOS analysis sets the starting point for the work reported here.

It has been noticed that in Tabiryan's SOS analysis the gain coefficient of the stimulated noise is independent on the irradiative laser wavelength. This means that this effect is a non-resonant nonlinear phenomenon suitable for a wide wavelength regime. Accordingly, the SOS effect in the infrared or other wavelength region could be employed. The most important of all, the potential usage of this polarization effect in fiber communications (1.55 μm) makes the SOS research in the near infrared wavelength very attractive. Since a NLC film can be made as thin as 100 ~ 200 μm, it is capable of

acting as an integrated photonic component for polarization conversion or other functions.

3.3 Theoretical Analysis

Stimulated orientational scattering stems from the intensive interaction among the NLC director, the input pump laser and the scattered light beam. The complete understanding of this wave-mixing process requires the knowledge of both the coupled-wave equations and the NLC director reorientation dynamics. The coupled wave equations describe the energy transfer between the transmitted and the generated beams through a NLC medium, whereas the direction and magnitude of the energy transfer depend on the reorientation of the NLC director. The analysis of the reorientation process of the NLC director explains how the NLC director reorients under the influence of the transmitted and generated beams. The reoriented NLC director forms a moving grating which works as a bridge to transfer energy between the two beams and changes the intensities of both the transmitted and generated beams. The change in optical intensities then brings an impact in the reorientation process of the NLC director and modifies the director reorientation angle. In the following sections, both processes will be analyzed and the steady-state SOS effect will be numerically simulated.

3.3.1 Coupled Wave Equations in a Nonlinear Medium

When a number of plane-wave optical fields are normally incident on a medium, the total field has the form:

$$\vec{E}(z,t) = \sum_{\alpha} \frac{1}{2} \vec{A}^{\alpha}(z,t) e^{i(\omega^{\alpha} t - \vec{k}^{\alpha} \cdot \vec{r})} + c.c. \qquad \text{Equation 3.6}$$

where α =1,2,…, *M*, and *M* is the number of incident light waves. The *z* direction is defined as the direction normal to the material's surface. $A^{\alpha}(z,t)$ denotes the amplitude of the α^{th} wave which is slowly varying compared to the rapidly-changing phase term. *c.c.* stands for the complex conjugate terms. $\vec{k}^{\alpha}$ is the wave vector of the α^{th} wave.

The system response to the input optical field is expressed as:

$$\vec{D} = \varepsilon_0 \vec{E} + \vec{P} \qquad \text{Equation 3.7}$$

where $\vec{D}$, $\vec{E}$ and $\vec{P}$ are the electric displacement, electric field and electric-dipole polarization respectively, ε_0 is the dielectric constant. In nonlinear optics, the polarization $\vec{P}$ is usually expanded into the following form:

$$\begin{aligned} \vec{P} &= \vec{P}_L + \vec{P}_{NL} \\ &= \chi^{(1)}\vec{E} + \chi^{(2)} \cdot \vec{E}\vec{E} + \chi^{(3)} \cdot \vec{E}\vec{E}\vec{E} + \ldots \end{aligned} \qquad \text{Equation 3.8}$$

where $\chi^{(1)}$, $\chi^{(2)}$, $\chi^{(3)}$, .., are known as the linear, second, third, and higher order optical susceptibility tensors. All materials possess odd-order susceptibilities, but only those materials without inversion symmetry have the even order susceptibilities [Shen 1984]. Different optical phenomena are associated with different optical susceptibility(s) of the material(s).

The analysis of the coupled wave equations starts from the Maxwell's equations:

$$\nabla \cdot \vec{D} = \rho \qquad \text{Equation 3.9}$$

$$\nabla \cdot \vec{B} = 0 \qquad \text{Equation 3.10}$$

$$\nabla \times \vec{E} = -\frac{\partial \vec{B}}{\partial t} \qquad \text{Equation 3.11}$$

$$\nabla \times \vec{H} = \frac{\partial \vec{D}}{\partial t} + \vec{J} \qquad \text{Equation 3.12}$$

In this research work, I am primarily interested in the solution of these equations with no free charges and no free currents because there is no free charge distribution or external applied current in a NLC film in the SOS effect. We also assume that the material is nonmagnetic which is true for nematic liquid crystal films. So that,

$$\rho = 0 \qquad \text{Equation 3.13}$$

$$\vec{J} = 0 \qquad \text{Equation 3.14}$$

$$\vec{B} = \vec{H} \qquad \text{Equation 3.15}$$

Plugging the above condition Equation 3.13-15**,** into the Maxwell's Equation 3.9-12, one gets:

$$\nabla \times \nabla \times \varepsilon_0 \vec{E} + \frac{1}{c^2}\frac{\partial^2 \vec{D}}{\partial t^2} = 0 \qquad \text{Equation 3.16}$$

Or :

$$\nabla \times \nabla \times \vec{E} + \frac{1}{c^2}\frac{\partial^2 \vec{E}}{\partial t^2} = -\mu \frac{\partial^2 \vec{P}}{\partial t^2} \qquad \text{Equation 3.17}$$

Using vector analysis, the first term in the right hand side can be simplified as:

$$\nabla \times \nabla \times \vec{E} = \nabla(\nabla \cdot \vec{E}) - \nabla^2 \vec{E} \qquad \text{Equation 3.18}$$

In an isotropic media with no free charge,

$$\nabla \cdot \vec{D} = \varepsilon_0 \nabla \cdot \vec{E} = 0 \qquad \text{Equation 3.19}$$

This equation implies that the first term in the right hand-side of Equation 3.18 vanishes in an isotropic source-free medium. However in most nonlinear optical materials which are not isotropic, this term is generally non-vanishing due to the more general relationship between $\vec{D}$ and $\vec{E}$. Fortunately, this term can often be shown to be negligibly small in liquid crystals [Khoo 1994a] and can be omitted using the so-call slowly-varying-envelope-approximation (SVEA).

Combing Equations 3.17 and 3.18, the wave equation can be expressed as:

$$\nabla^2 \vec{E} - \frac{1}{c^2}\frac{\partial^2 \vec{E}}{\partial t^2} = \mu \frac{\partial^2 \vec{P}}{\partial t^2} \qquad \text{Equation 3.20}$$

If the input light consists of a number of monochromatic plane waves as in Equation 3.6, by assuming the dielectric tensor does not change with time, the wave equation in steady–state can be further simplified as:

$$\nabla^2 E_i(z,t) + \frac{\omega_i^{\,2}}{c^2}\varepsilon_0 \varepsilon_{ik}^0 E_k(z,t) = -\frac{\omega_i^{\,2}}{c^2}\varepsilon_0 \delta\varepsilon_{ik} E_k(z,t) \qquad \text{Equation 3.21}$$

where the subscript $i\ j = x, y, z$ denotes the projection component on the axis of different Cartesian coordinates, In the above wave equation, the polarization expansion has only been kept to the second order. Higher order optical susceptibility components are generally much smaller in liquid crystals and are neglected in the remaining analysis. The above equation is suitable even at the transient case as long as the time that light propagates through the material (~L/c < 10^{-11} s) is much shorter than the response time of the nonlinear process in the material. This condition is almost always satisfied for nematic liquid crystal films whose response time is in the range of μs ~ ms and typical thickness of 20 ~ 200 μm.

Equation 3.21 serves as the basic field equations to describe how optical fields are modulated and interact with the induced dielectric tensor disturbance which has the form:

$$\delta\varepsilon = \delta\varepsilon(z,t)e^{i(\Omega t - \vec{q}\cdot\vec{r})} \qquad \text{Equation 3.22}$$

On the other hand, the modification to the material's optical properties is determined by the reaction of the medium to the light field(s). In the case of liquid crystal, this change in optical properties is directly related to the NLC director and described by the director reorientation equation, which will be elaborately explained in the subsequent section.

Equation 3.21 describes a situation in which the wave E_i is coupled with the wave E_k through the dielectric tensor grating component $\delta\varepsilon_{ik}$. However, the combination of the coupling is not arbitrary. It is governed by the so-called phase-matching condition:

$$\vec{k}^{\,i} = \vec{q} + \vec{k}^{\,k} \qquad \text{Equation 3.23}$$

which is also known as Bragg's condition in crystal optics. The growth of the wave E_i requires that the oscillations of the source E_k and the wave E_i are in phase throughout the medium, or phase-matched, both temporally and spatially. The spatial phase matching is imposed by the wave-vector Equation 3.24 and the temporal phase matching condition is described by

$$\omega^i = \Omega + \omega^k \qquad \text{Equation 3.24}$$

In the case of the SOS effect, the change in the dielectric tensor comes from the reorientation of the NLC director (optical axis) since the dielectric tensor is dependent on the NLC director's orientation angle. The director reorientation process is discussed in the following section.

3.3.2 NLC Director Dynamics

As mentioned before, the SOS theory was first theoretically analyzed in [Tabiryan 1986]. The establishment of the equilibrium state of liquid crystal medium is governed by the principle that the total free energy $F = \int f d^3\vec{r}$ in a system at a constant temperature must have the minimum value when the system reaches the equilibrium state. The equation describing the establishment of the equilibrium state is the so-called Euler-Lagrange-Rayleigh (ELR) equation:

$$\frac{\partial}{\partial x_j}\frac{\delta f}{\delta(\partial U_m/\partial x_j)} - \frac{\delta f}{\delta U_m} - \frac{\delta R}{\delta \dot{U}_m} = 0 \qquad \text{Equation 3.25}$$

where U_m's are the independent variables of the system, *f* is the total free energy density and *R* is the dissipative function density of the system, x_j represents the Cartesian coordinates *x, y* and *z*.

For a NLC cell with a director vector $\vec{n}$ and a dielectric tensor ε_{ij} irradiated by a laser with electric field $\vec{E}$, the free energy density *f* is the sum of the elastic energy density f_{elastic} for director's orientation induced deformations:

$$f_{elastic} = \frac{1}{2}K_1(\nabla \bullet \vec{n})^2 + \frac{1}{2}K_2(\vec{n} \bullet (\nabla \times \vec{n}))^2 + \frac{1}{2}K_3(\vec{n} \times (\nabla \times \vec{n}))^2 \qquad \text{Equation 3.26}$$

and the electromagnetic free energy density f_{light}:

$$f_{light} = -\frac{1}{2}\varepsilon_{ij}E_iE_j \qquad \text{Equation 3.27}$$

The dissipative function density R is:

$$R = \frac{1}{2}\eta\dot{\vec{n}}^2 \qquad \text{Equation 3.28}$$

where η is the viscosity coefficient of the NLC medium.

The schematic diagram of the SOS effect is depicted in Figure 3.1. The input light is linearly polarized in the *x*-direction as the electric field $\vec{E}_i = \{E_x, 0, 0\}$ and the stimulated scattering noise is polarized in the y-direction as $\vec{E}_s = \{0, E_y, 0\}$. Thus, the total electric field inside the NLC sample is expressed as $\vec{E} = \{E_x, E_y, 0\}$. Since the electric fields are only in *x-y* plane and change along the *z*-direction, it will induce director reorientation in the *x-y* plane and the magnitude of the reorientation angle will vary along

the *z*-axis. The director of the nematic liquid crystal under this electric field and optical-geometry configuration is expressed as:

$$\vec{n} = \{\cos\theta(z,t), \sin\theta(z,t), 0\} \qquad \text{Equation 3.29}$$

The corresponding dielectric tensor is expressed as:

$$\varepsilon = \begin{pmatrix} \varepsilon_\perp + \varepsilon_a \cos^2\theta(z,t) & \varepsilon_a \cos\theta(z,t)\sin\theta(z,t) & 0 \\ \varepsilon_a \cos\theta(z,t)\sin\theta(z,t) & \varepsilon_\perp + \varepsilon_a \sin^2\theta(z,t) & 0 \\ 0 & 0 & \varepsilon_\perp \end{pmatrix} \qquad \text{Equation 3.30}$$

By some straight-forward analytical manipulations the free energy due to the optical fields has the form:

$$f_{light} = -\frac{1}{2}\varepsilon_0[(\varepsilon_\perp + \varepsilon_a \cos^2\theta(z,t))|Ex|^2 + \varepsilon_a \cos\theta(z,t)\sin\theta(z,t) (ExEy^* + Ex^*Ey) + (\varepsilon_\perp + \varepsilon_a \sin^2\theta(z,t))|Ey|^2] \qquad \text{Equation 3.31}$$

Under the general conditions of the SOS effect, the reorientation angle of the NLC director is very small. Then the director vector can be simplified as:

$$\vec{n} = \{1, \theta(z,t), 0\} \qquad \text{Equation 3.32}$$

Similarly, the free energy due to the optical fields can be simplified as:

$$f_{light} = -\frac{1}{2}\varepsilon_0[(\varepsilon_{\|} - \varepsilon_a\theta^2(z,t))|Ex|^2 + \varepsilon_a\theta(z,t)(ExEy^* + Ex^*Ey) + (\varepsilon_\perp + \varepsilon_a\theta^2(z,t))|Ey|^2] \qquad \text{Equation 3.33}$$

Thus the gradient and curl of the NLC director can be solved as:

$$\nabla \cdot \vec{n} = 0$$
$$\nabla \times \vec{n} = \{\frac{d\theta(z,t)}{dz}, 0, 0\}$$
$$\dot{\vec{n}} = \{0, \frac{d\theta(z,t)}{dt}, 0\}$$
$$\dot{\vec{n}}^2 = \dot{\vec{n}} \cdot \dot{\vec{n}} = \{0, [\frac{d\theta(z,t)}{dt}]^2, 0\}$$

Equation 3.34

Plugging the above inferences back into the elastic free energy Equation 3.26, one arrives at:

$$\begin{aligned} f_{elastic} &= \frac{1}{2} K_1 (\nabla \bullet \vec{n})^2 + \frac{1}{2} K_2 (\vec{n} \bullet (\nabla \times \vec{n}))^2 + \frac{1}{2} K_3 (\vec{n} \times (\nabla \times \vec{n}))^2 \\ &= \frac{1}{2} K_2 (\{1, \theta(z,t), 0\} \bullet \{\frac{d\theta(z,t)}{dz}, 0, 0\})^2 \\ &\quad + \frac{1}{2} K_3 (\{1, \theta(z,t), 0\} \times \{\frac{d\theta(z,t)}{dz}, 0, 0\})^2 \\ &= \frac{1}{2} [K_2 + K_3 \theta^2(z,t)] \left(\frac{d\theta(z,t)}{dz} \right)^2 \end{aligned}$$

Equation 3.35

As mentioned before, the reorientation angle is small. For this reason, the second term in the free elastic energy containing the square of $\theta(z,t)$ is negligible compared to the first term. Then the free elastic energy can be simplified as:

$$f_{elastic} = \frac{1}{2} K_2 \left(\frac{\partial \theta(z,t)}{\partial z} \right)^2$$

Equation 3.36

After treating $\theta(z,t)$ as the independent variable, the first term in the ELR equation can be expressed as:

$$\frac{\partial}{\partial x_j} \frac{\delta f}{\delta(\partial U_m / \partial x_j)} = \frac{\partial}{\partial x} \frac{\delta f}{\delta(\partial \theta / \partial x)} + \frac{\partial}{\partial y} \frac{\delta f}{\delta(\partial \theta / \partial y)} + \frac{\partial}{\partial z} \frac{\delta f}{\delta(\partial \theta / \partial z)}$$

Equation 3.37

Since $\theta(z,t)$ is independent of x and y, the first two terms in the right hand side then equal to 0. Careful derivation yields a rather simple expression for the first term in the ELR equation:

$$\begin{aligned}
\frac{\partial}{\partial x_j}\frac{\delta f}{\delta(\partial U_m/\partial x_j)} &= \frac{\partial}{\partial z}\frac{\delta f}{\delta(\partial\theta/\partial z)} \\
&= \frac{\partial}{\partial z}[\frac{\delta(f_{light}+f_{elastic})}{\delta(\partial\theta/\partial z)}] \\
&= -\frac{1}{2}\frac{\partial}{\partial z}[\frac{\delta(\varepsilon_0(\varepsilon_{\parallel}-\varepsilon_a\theta^2)|Ex|^2)}{\delta(\partial\theta/\partial z)}+\frac{\delta(\varepsilon_0\varepsilon_a\theta(ExEy^*+Ex^*Ey))}{\delta(\partial\theta/\partial z)} \\
&\quad +\frac{\delta(\varepsilon_0(\varepsilon_{\perp}+\varepsilon_a\theta^2)|Ey|^2)}{\delta(\partial\theta/\partial z)}-\frac{\delta(K_2\left(\frac{\partial\theta}{\partial z}\right)^2)}{\delta(\partial\theta/\partial z)}] \\
&= \frac{\partial}{\partial z}[K_2\frac{\partial\theta(z,t)}{\partial z}] \\
&= K_2\frac{\partial^2\theta(z,t)}{\partial z^2}
\end{aligned}$$

Equation 3.38

Following a similar procedure, the second term in the ELR equation can also be analytically solved:

$$\begin{aligned}
-\frac{\delta f}{\delta U_m} &= -\frac{\delta f}{\delta\theta} \\
&= -\frac{\delta(f_{light}+f_{elastic})}{\delta\theta} \\
&= \frac{1}{2}[\frac{\delta(\varepsilon_0(\varepsilon_{\parallel}-\varepsilon_a\theta^2)|Ex|^2)}{\delta\theta}+\frac{\delta(\varepsilon_0\varepsilon_a\theta(ExEy^*+Ex^*Ey))}{\delta\theta} \\
&\quad +\frac{\delta(\varepsilon_0(\varepsilon_{\perp}+\varepsilon_a\theta^2)|Ey|^2)}{\delta\theta}-\frac{\delta(K_2\left(\frac{\partial\theta}{\partial z}\right)^2)}{\delta\theta}] \\
&= \frac{1}{2}\varepsilon_0\varepsilon_a(ExEy^*+Ex^*Ey)+\varepsilon_0\varepsilon_a\theta(|Ey|^2-|Ex|^2)
\end{aligned}$$

Equation 3.39

The third term of the ELR equation can be expressed as:

$$
\begin{aligned}
-\frac{\delta R}{\delta \dot{U}_m} &= -\frac{\delta R}{\delta(d\theta/dt)} \\
&= -\frac{1}{2}\eta \frac{\delta \dot{n}^2}{\delta(d\theta/dt)} \\
&= -\frac{1}{2}\eta \frac{\delta[\frac{d\theta(z,t)}{dt}]^2}{\delta(d\theta/dt)} \\
&= -\eta \frac{d\theta(z,t)}{dt}
\end{aligned}
\qquad \text{Equation 3.40}
$$

Thus, the equation governing the director behavior of nematic liquid crystals is simply expressed as:

$$\eta \frac{\partial \theta(z,t)}{\partial t} - K_2 \frac{\partial^2 \theta(z,t)}{\partial z^2} = \frac{1}{2}\varepsilon_0 \varepsilon_a [(ExEy^* + Ex^* Ey) + 2\theta(z,t)(|Ey|^2 - |Ex|^2)] \qquad \text{Equation 3.41}$$

From the above equation, it is natural to express the director reorientation angle as:

$$\theta(z,t) = \theta_0(z,t) e^{i(\vec{q}\cdot\vec{r} - \Omega t)} + c.c \qquad \text{Equation 3.42}$$

and $\vec{q} = \vec{k}_x - \vec{k}_y$, $\Omega = \omega_x - \omega_y$, $\theta_0(z,t)$ is the amplitude of the director orientation.

The dielectric tensor in an anisotropic liquid crystal with the director oriented at the angle $\theta_0(z,t)$ has the form of:

$$\delta\varepsilon = \begin{pmatrix} \varepsilon_\perp + \varepsilon_a \cos^2\theta(z,t) & \varepsilon_a \cos\theta(z,t)\sin\theta(z,t) & 0 \\ \varepsilon_a \cos\theta(z,t)\sin\theta(z,t) & \varepsilon_\perp + \varepsilon_a \sin^2\theta(z,t) & 0 \\ 0 & 0 & \varepsilon_\perp \end{pmatrix} \qquad \text{Equation 3.43}$$

The change in the dielectric tensor due to the reorientation of the director can be expressed as:

$$\delta\varepsilon = \begin{pmatrix} \varepsilon_\perp + \varepsilon_a \cos^2\theta(z,t) & \varepsilon_a \cos\theta(z,t)\sin\theta(z,t) & 0 \\ \varepsilon_a \cos\theta(z,t)\sin\theta(z,t) & \varepsilon_\perp + \varepsilon_a \sin^2\theta(z,t) & 0 \\ 0 & 0 & \varepsilon_\perp \end{pmatrix} - \begin{pmatrix} \varepsilon_\perp + \varepsilon_a & 0 & 0 \\ 0 & \varepsilon_\perp & 0 \\ 0 & 0 & \varepsilon_\perp \end{pmatrix}$$

$$= \varepsilon_a \begin{pmatrix} -\sin^2\theta(z,t) & \frac{1}{2}\sin 2\theta(z,t) & 0 \\ \frac{1}{2}\sin 2\theta(z,t) & \sin^2\theta(z,t) & 0 \\ 0 & 0 & 0 \end{pmatrix} \qquad \text{Equation 3.44}$$

In the SOS effect, the input plane wave is propagating along the z direction with wave vector $\vec{k}_x$ and frequency ω_x,

$$\begin{aligned} \vec{E}_x &= \hat{e}_x E_x e^{i(\vec{k}_x \cdot \vec{r} - \omega_x t)} + c.c. \\ &= \hat{e}_x E_x e^{i(k_x z - \omega_x t)} + c.c. \end{aligned} \qquad \text{Equation 3.45}$$

As mentioned before these input waves will generate scattering light beams in various directions and frequencies because of the induced director fluctuation, the induced density fluctuation, and thermal effects. Among all these noise fields only those satisfying the phase-matching conditions (as denoted in Equation 3.23 and Equation 3.24**)** will coherently interact with the input wave throughout the whole sample. The phase-matched noise field with wave vector $\vec{k}_y$ and frequency ω_y is expressed as:

$$\begin{aligned} \vec{E}_y &= \hat{e}_y E_y e^{i(\vec{k}_y \cdot \vec{r} - \omega_y t)} + c.c. \\ &= \hat{e}_y E_y e^{i(k_y z - \omega_y t)} + c.c. \end{aligned} \qquad \text{Equation 3.46}$$

After plugging $\delta\varepsilon$ into the coupled-wave Equation 3.21 and neglecting those terms that do not satisfy the phase-matching conditions, the coupled equations between the input pump beam and the stimulated signal can be expressed as:

$$\frac{d^2E_x(z)}{dz^2}+k_x^2E_x(z)=E_x(z)\varepsilon_x\frac{\omega_x^{\,2}}{c^2}\sin^2\theta$$
$$-\frac{1}{2}\varepsilon_aE_y(z)\frac{\omega_x^{\,2}}{c^2}\sin 2\theta\exp(-iqz+i\Omega t) \qquad \text{Equation 3.47}$$

$$\frac{d^2E_y(z)}{dz^2}+k_y^2E_y(z)=-E_y(z)\varepsilon_y\frac{\omega_y^{\,2}}{c^2}\sin^2\theta$$
$$-\frac{1}{2}\varepsilon_aE_x(z)\frac{\omega_y^{\,2}}{c^2}\sin 2\theta\exp(iqz-i\Omega t) \qquad \text{Equation 3.48}$$

Under the small angle approximation, the above two equation can be further simplified as:

$$\frac{d^2E_x(z)}{dz^2}+k_x^2E_x(z)=E_x(z)\varepsilon_x\frac{\omega_x^{\,2}}{c^2}\theta^2(z,t)$$
$$-\varepsilon_aE_y(z)\frac{\omega_x^{\,2}}{c^2}\theta(z,t)\exp(-iqz+i\Omega t) \qquad \text{Equation 3.49}$$

$$\frac{d^2E_y(z)}{dz^2}+k_y^2E_y(z)=-E_y(z)\varepsilon_y\frac{\omega_y^{\,2}}{c^2}\theta^2(z,t)$$
$$-\varepsilon_aE_x(z)\frac{\omega_y^{\,2}}{c^2}\theta(z,t)\exp(iqz-i\Omega t) \qquad \text{Equation 3.50}$$

The above two equations plus the director orientation Equation 3.41 will govern the interaction between nematic liquid crystals and optical waves.

3.3.3 Steady State Stimulated Orientational Scattering

The geometry under consideration is depicted in Figure 3.1. The input pump beam lies in the *x*-direction and propagates along the *z*-direction while the phase-matching

noise field lies in the *y*-direction and propagates along the *z*-axis. The induced liquid crystal director reorientation is in the *x*-*y* plane and the magnitude of this orientation varies along the *z*-axis. Due to the strong anchoring of the surfactant on the cell walls, the variation of the liquid crystal director is still relatively small even at the occurrence of a strong SOS effect. As it will be shown later, the reorientation angle indeed is within several degrees and can be treated as a small variable under the first-order approximation.

Since the SOS effect investigated here is under the continuous-wave illumination, all the equations will be simplified to steady-state status.

The liquid crystal used in the SOS study is E7 (EM Chemicals). By rubbing the PVA coating on the substrates, the NLC film is originally aligned homogeneously. The sample is positioned such that the polarization of the input pump beam is parallel to the NLC director, which means the input beam is an e-wave.

Based on the above experimental configuration, the variance of relative dielectric constant of the NLC film can be expressed as:

$$\begin{aligned}\delta\varepsilon &= \begin{pmatrix} \varepsilon_\perp + \varepsilon_a \cos^2\theta(z,t) & \varepsilon_a \cos\theta(z,t)\sin\theta(z,t) & 0 \\ \varepsilon_a \cos\theta(z,t)\sin\theta(z,t) & \varepsilon_\perp + \varepsilon_a \sin^2\theta(z,t) & 0 \\ 0 & 0 & \varepsilon_\perp \end{pmatrix} - \begin{pmatrix} \varepsilon_\perp + \varepsilon_a & 0 & 0 \\ 0 & \varepsilon_\perp & 0 \\ 0 & 0 & \varepsilon_\perp \end{pmatrix} \\ &= \varepsilon_a \begin{pmatrix} -\sin^2\theta(z,t) & \frac{1}{2}\sin 2\theta(z,t) & 0 \\ \frac{1}{2}\sin 2\theta(z,t) & \sin^2\theta(z,t) & 0 \\ 0 & 0 & 0 \end{pmatrix} \\ &= \varepsilon_a \begin{pmatrix} -\theta^2(z,t) & \theta(z,t) & 0 \\ \theta(z,t) & \theta^2(z,t) & 0 \\ 0 & 0 & 0 \end{pmatrix}\end{aligned} \qquad \text{Equation 3.51}$$

By treating the director reorientational angle θ as a small variable, the coupled-wave equations and the director equation are:

$$\frac{d^2E_x(z)}{dz^2} + k_x^2 E_x(z) = E_x(z)\varepsilon_x \frac{\omega_x^{\ 2}}{c^2}|\theta|^2 - \varepsilon_a E_y(z)\frac{\omega_x^{\ 2}}{c^2}\theta\exp(-iqz + i\Omega t) \qquad \text{Equation 3.52}$$

$$\frac{d^2E_y(z)}{dz^2} + k_y^2 E_y(z) = -E_y(z)\varepsilon_y \frac{\omega_y^{\ 2}}{c^2}|\theta|^2 - \varepsilon_a E_x(z)\frac{\omega_y^{\ 2}}{c^2}\theta\exp(iqz - i\Omega t) \qquad \text{Equation 3.53}$$

$$\eta\frac{\partial\theta(z,t)}{\partial t} - K_2\frac{\partial^2\theta(z,t)}{\partial z^2} = \frac{1}{2}\varepsilon_0\varepsilon_a[(ExEy^* + Ex^*Ey) + 2\theta(z,t)(|Ey|^2 - |Ex|^2)] \qquad \text{Equation 3.54}$$

Under the slowly-varying-envelope-approximation (SVEA):

$$\left|k^{\alpha 2}A_j^\alpha\right| >> \left|k^\alpha\frac{\partial A_j^\alpha}{\partial z}\right| >> \left|\frac{\partial^2 A_j^\alpha}{\partial z^2}\right| \qquad \text{Equation 3.55}$$

Equations 3.52 - 54 can be simplified as:

$$\frac{dE_x(z)}{dz} = \frac{i\varepsilon_a k_x}{2}[-2E_x(z)|\theta(z,t)|^2 + E_y(z)\theta(z,t)] \qquad \text{Equation 3.56}$$

$$\frac{dE_y(z)}{dz} = \frac{i\varepsilon_a k_y}{2}[2E_y(z)|\theta(z,t)|^2 + E_x(z)\theta^*(z,t)] \qquad \text{Equation 3.57}$$

$$[K_2q^2 - i\eta\Omega + \varepsilon_0\varepsilon_a(|Ey|^2 - |Ex|^2)]\theta(z,t) = \frac{1}{2}\varepsilon_0\varepsilon_a ExEy^* \qquad \text{Equation 3.58}$$

These equations will serve as the governing equations for the SOS effect throughout all the simulations under steady-state condition.

The SOS equations can be solved numerically for various parameter values by using a fourth-order Runge-Kutta routine. The parameters are chosen to correspond to the

experiment done by Khoo [Khoo 1995] in order to have a comparison between the theoretical analysis and experimental data. The material parameters of liquid crystal E7 are: refractive indices n_e=1.75, n_o=1.54, bending elastic constant K_2 = 3.0x10^{-12} N, and the viscosity coefficient η = 0.07 Poise. The sample thickness is 400 μm and the laser used is an Argon laser (0.5 μm). The laser is focused to on the NLC film with a diameter ~ 30 μm.

As noted in Equations 3.56 – 58, there are 4 variables E_x, E_y, θ, Ω and 3 equations. In order to get a solution, it is necessary to fix one of the variables. Closer study reveals that Ω is an independent variable and it in fact determines which frequency component of noise will get amplified by achieving the optimum gain and winning the competition against other noise components. As predicted in [Tabiryan 1986], the maximum gain occurs when

$$\Omega = K_2 q^2 / \eta \qquad \text{Equation 3.59}$$

This conclusion was derived at the small amplified signal situation but is valid for all of the SOS analyses. At the early stages of the SOS effect, only the noise signal satisfieing Equation 3.59 will have the maximum gain and get amplified. As long as this specific noise gets amplified, it continuously grabs energy from the pump beam and gets amplified. For the above parameters, the maximum gain of the stimulated wave is found at a frequency difference $\Omega = \omega_x - \omega_y = 31\,\text{Hz}$. The simulation result is shown in Figure 3.2 . Compared with Khoo's experimental result Figure 3.3 [Khoo 1999], there is a good agreement in the exponential gain after the input laser power exceeds the

threshold value. As denoted in Figure 3.3, the generated o-wave continues to grow to be even larger than the transmitted e-wave, which can not be explained under the non-pump-depletion assumption and has been successfully demonstrated in our complete analysis as shown in the simulation curve, Figure 3.2.

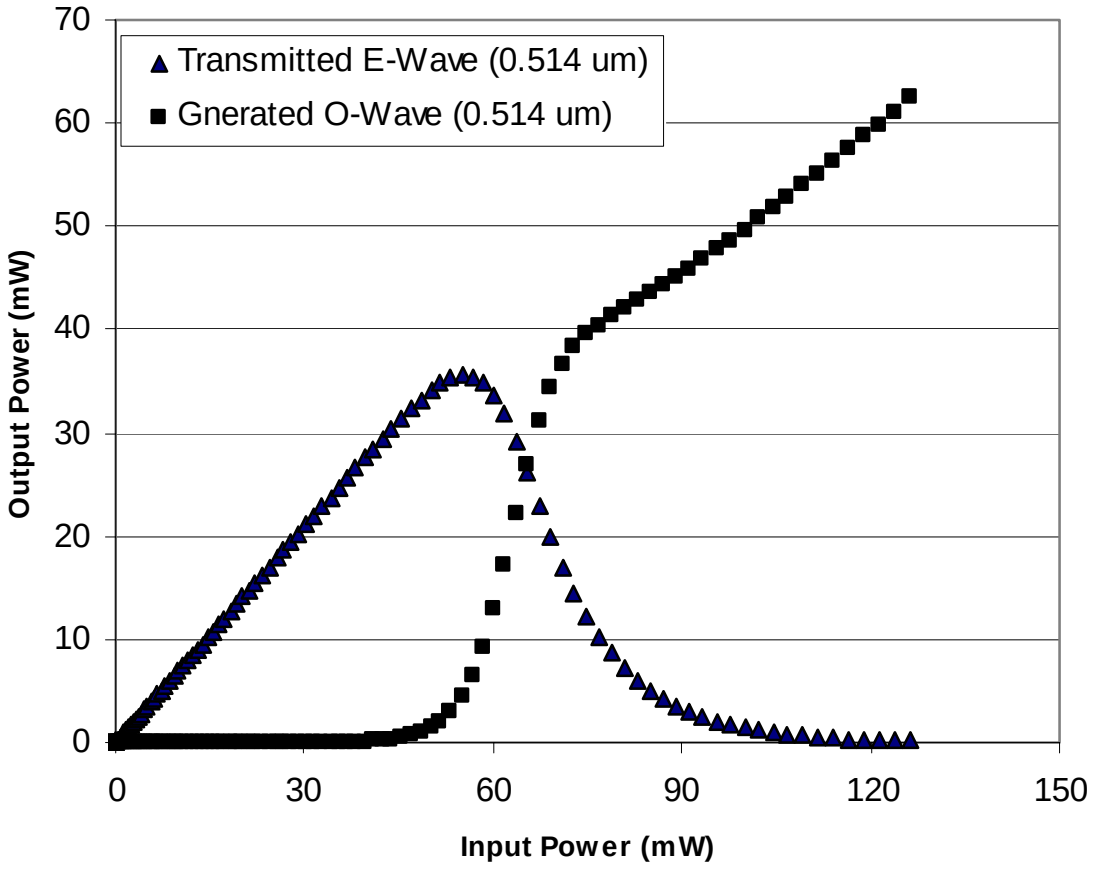

Figure 3.2: Simulated curve of the SOS effect in the visible regime. (Laser: 0.514 μm, focal spot diameter: 40 μm, cell thickness 250 μm.)

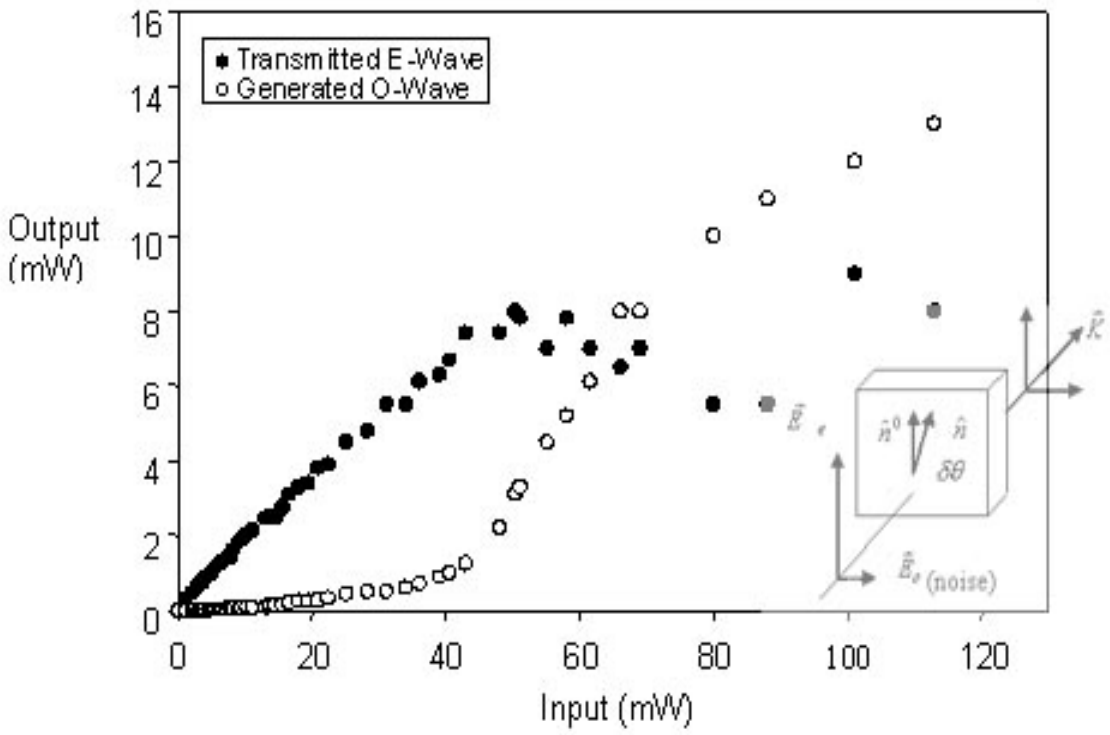

Figure 3.3: Experimental result of the SOS effect in the visible regime. (Laser: 0.514 μm, focal spot diameter: 40 μm, cell thickness 250 μm.)

As shown in the numerically simulated director reorientation plot, Figure 3.4, the maximum of the reorientation angle is indeed very small (~0.2 degrees). For a 250 μm thick NLC film, the peak of the reorientation angle does not appear in the middle which is due to the absorption of the NLC medium.

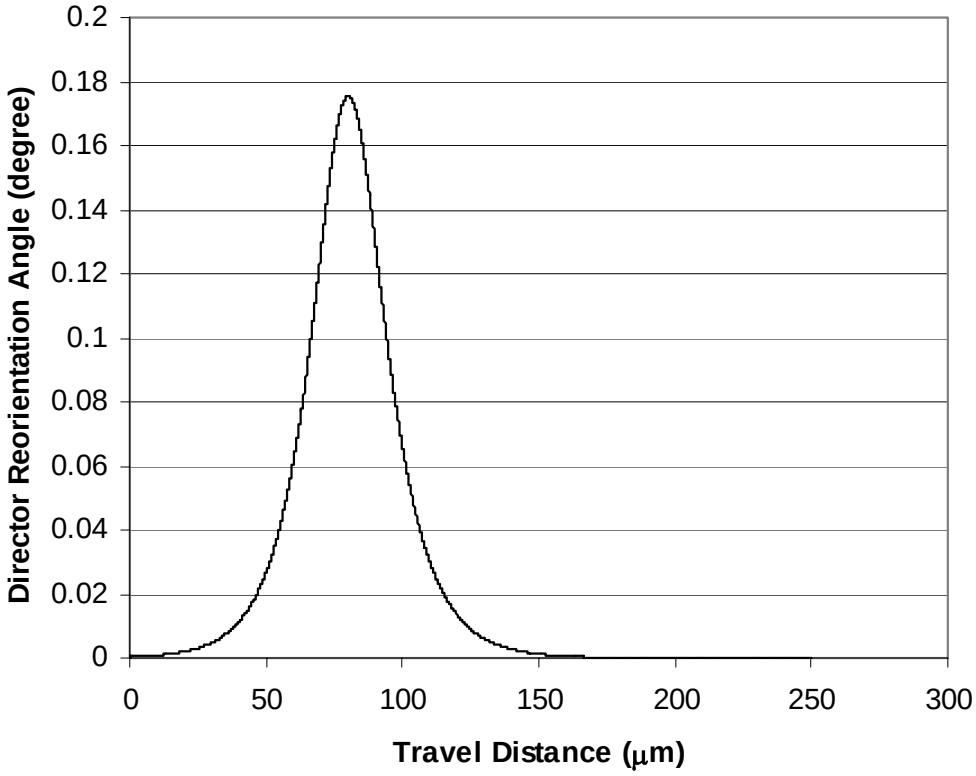

Figure 3.4: Director reorientation angle versus the distance into the NLC film. (Laser: 0.514 μm, focal spot diameter: 40 μm, cell thickness 250 μm.)

It has also been shown in numerical simulations that the threshold value of the input laser power can be decreased by choosing the liquid crystals with smaller elastic constant K_2 and smaller viscosity η. The comparison of theoretical simulations between different K_2 is shown in Figure 3.5**.** The threshold point is defined as the input pump beam power at which the stimulated beam starts the exponential growth while the polarization conversion point is defined as the input pump beam power at which the stimulated noise beam is stronger than the transmitted beam. The comparison of the threshold and the polarization conversion for different η values is shown in Figure 3.6

while the other parameters are remained the same. The reason of the threshold decrease is that smaller elastic constant or viscosity means the NLC molecules can be more easily reoriented. Thus a scattered beam with the same intensity will have a larger impact on the reorientation of the NLC director at smaller K_2 and η. It makes the energy transfer between E_x and E_y easier and in turn lowers the threshold power requirement for the SOS effect.

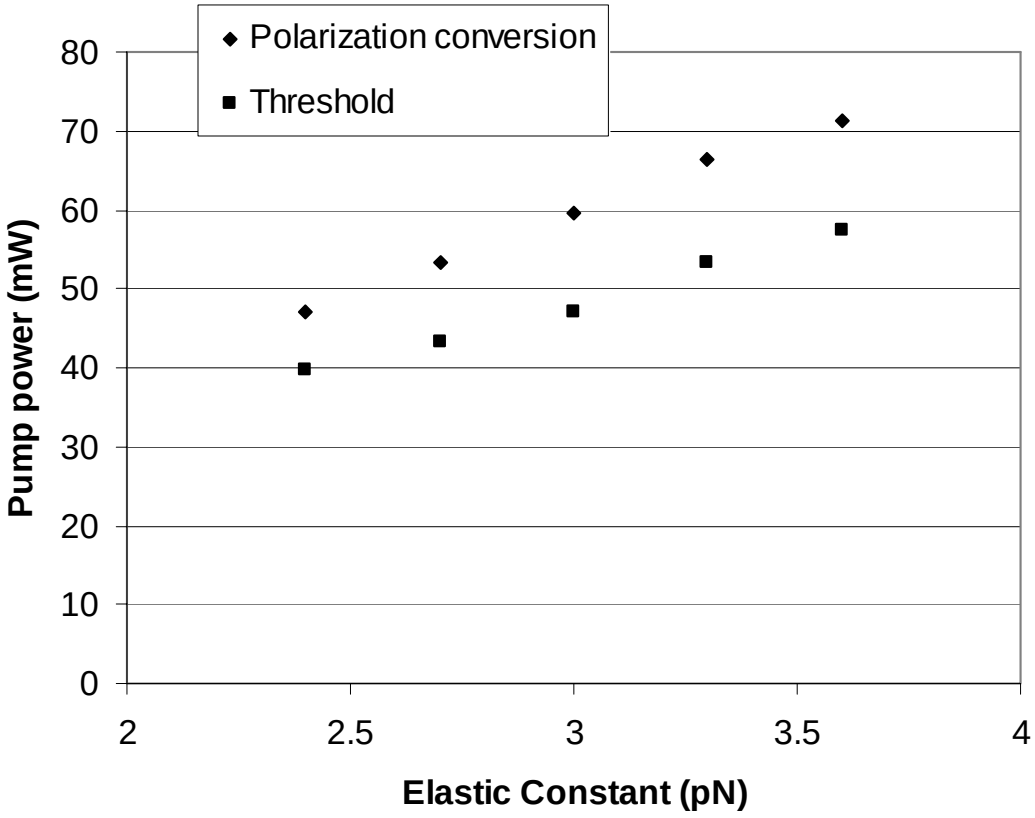

Figure 3.5: The SOS simulation curve for different elastic constant. (Laser 532nm, sample thickness 250 μm, focal diameter 50 μm.)

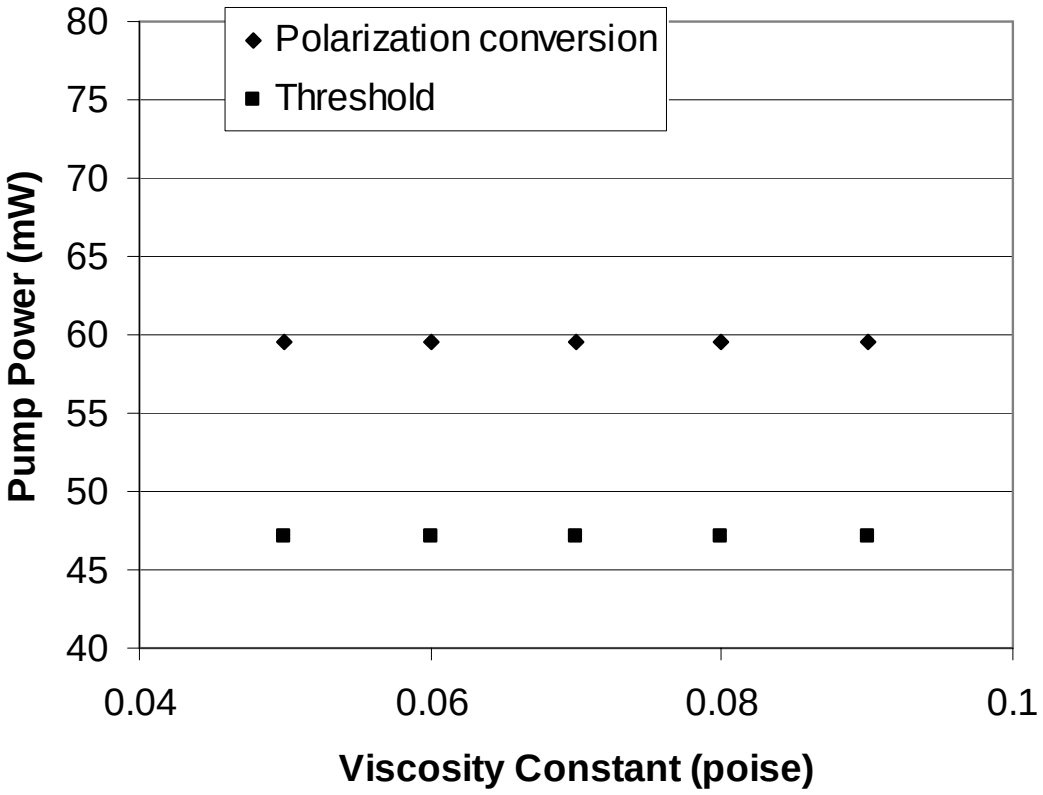

Figure 3.6: SOS simulation curve for different viscosity constant. (Laser 532nm, sample thickness 250 μm, focal diameter 50 μm.)

3.4 Implementation of SOS in the Communication Bandwidth

The good agreement between our theoretical analysis and the experimental SOS effect greatly encouraged the further pursuit toward other wavelengths since liquid crystals have good transparency and large anisotropy over a very wide range of wavelength regimes. From Equation 3.1, the differential scattering cross section is dependent on the input light's frequency as $\frac{d\sigma}{d\Omega} \propto \omega^4$. Thus in the near infrared regime,

particularly the communication wavelength (1.55 μm), the scattering loss is an order of magnitude smaller than in the visible region because of the smaller light frequency. As shown in the previous section, the small signal gain coefficient involved in the two-wave mixing process leading to polarization conversion is only weakly dependent on the laser wavelength. Since the SOS effect is non-resonant and does not rely on specific energy levels of liquid crystal molecules, one should also be able to observe the SOS effect in other wavelengths. In fact, due to the smaller scattering loss, the effect should be more significant in the infrared regimes. For comparison, the stimulated orientational scattering is simulated in the Figure 3.7 for various wavelengths. The following parameters are used: refractive indices n_e=1.75, n_o=1.54, bending elastic constant K_2 = 3.0x10^{-12} N, and the viscosity coefficient η = 0.07 Poise, sample thickness 250 μm, laser focal spot diameter 50 μm. As shown in Figure 3.7, the pump beam power at the polarization conversion decreases with the increase in the pump beam wavelength.

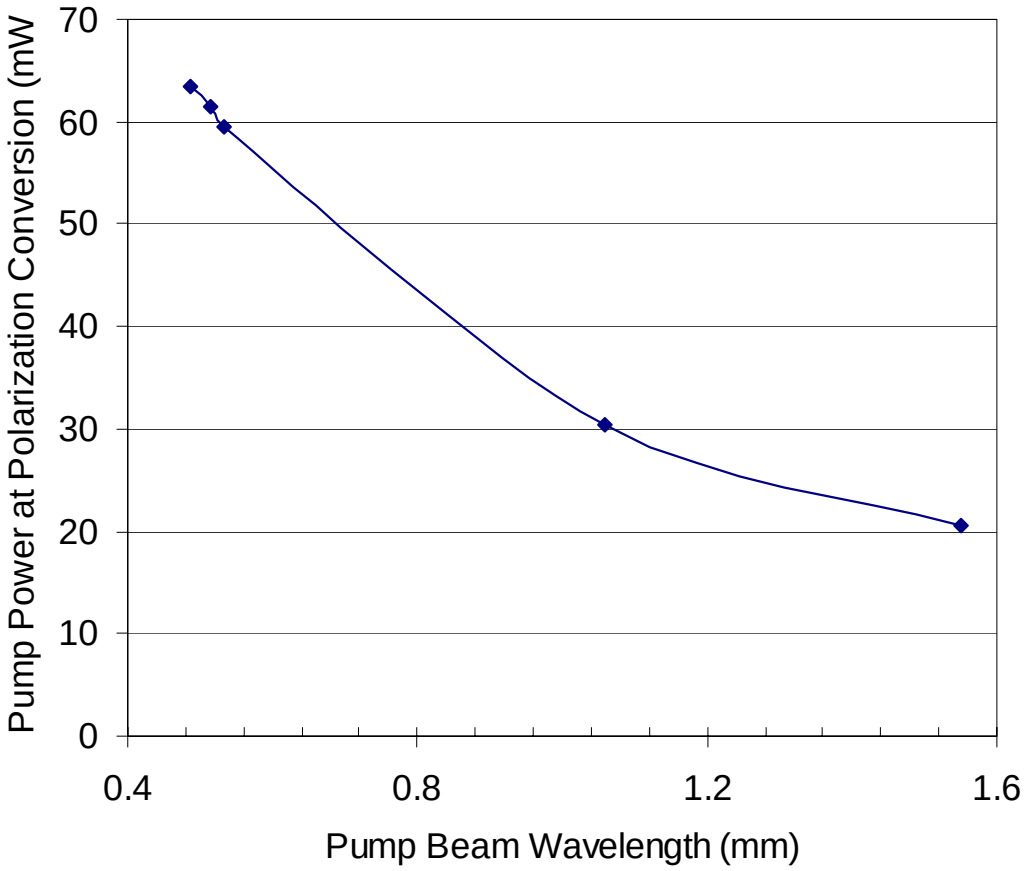

Figure 3.7: (a) Simulated stimulated orientational scattering in 1.55 μm. (b) The comparison of polarization conversion point for various pump lasers.

The experimental setup for the SOS effect at 1.55 μm is shown in Figure 3.8. A linearly polarized laser is normally incident on a homogeneously aligned nematic liquid crystal film as an e- or o- wave, i.e., with the optical electric field parallel or perpendicular to the director axis of the liquid crystal, respectively. In this research work, the coordinate system is defined as: the initial NLC director lies in the *x*-direction, the beams are propagating in the *z*-direction. For the e-beam, the electrical field lies in the *x*-direction while the electric filed of the o-beam lies in the *y*-direction. The output beams

are sent through a polarizing beam splitter to separate the e- and o- components. The liquid crystal used is pure E7 (EM chemicals). The laser used is an Erbium Doped Fiber Laser form IPG Photonics capable of 2 W unpolarized output.

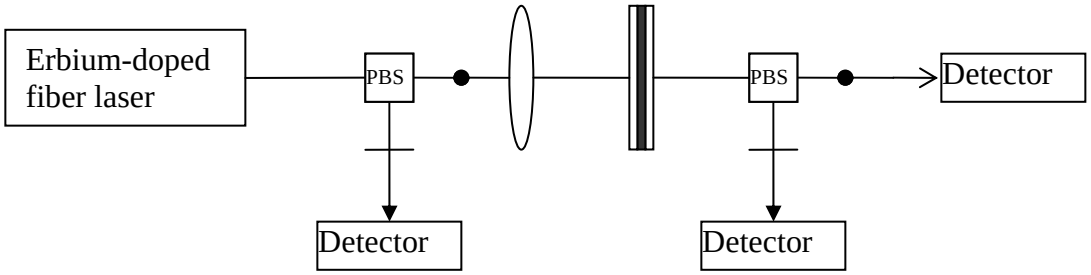

Figure 3.8: Experimental setup for the SOS effect in the infrared wavelength regime.

The experiment was conducted at room temperature and the NLC cell used was 400 μm thick. Figure 3.9 and 3.10 shows the simulated and measured transmitted e- and o- waves as a function of the input laser power for different input beam focus diameters. The input e-wave increases linearly at low input power, and begins to show sign of depletion as soon as the o-wave power is substantial, eventually dropping to an almost diminishing value. In the numerical simulations shown in Figure 3.9(a) and 3.10(a), complete conversion is achieved at an input power level of 30 mW for a laser of 40 μm focal diameter whereas at 120 mW for a laser with 80 μm focal diameter. These results compare favorably with experimental observations as shown in Figure 3.9(b) and 3.10(b), taking into account the simplifying assumptions (plane wave, one elastic constant, etc.) made in the theory. Almost complete conversion was observed for an input power around

50 mW for an input laser focused diameter of 40 μm, whereas the power required to achieve maximal (but not complete as in the 40 μm case) conversion is around 400 mW for a laser with larger focal diameter (80 μm). Because of the presence of multifrequency components and thermal fluctuations, considerable oscillatory behavior in the e- and o-wave outputs are observed, as shown in Fig 3.9(b). The dynamics of this stimulated orientational scattering effect will be discussed in details in the next chapter. At high pump laser intensity, we also observed considerable side scattering and defocusing of the output beams; these effects are likely the cause for the drop-off in the exit beam power after reaching the maximum.

The successful implementation of the SOS effect not only provided additional proof to our theoretical analysis but also demonstrated its potential in communication and other all-optical applications.

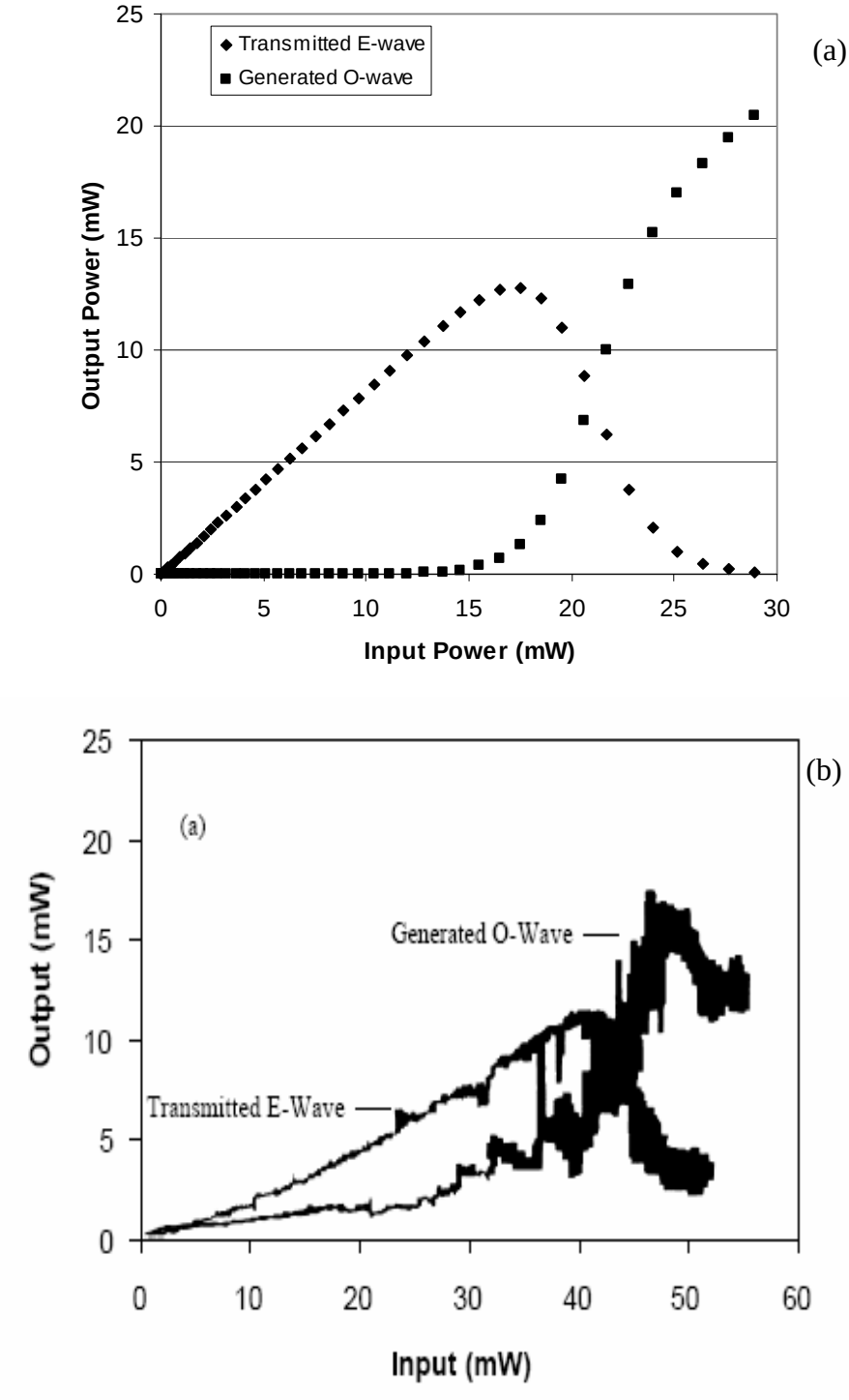

Figure 3.9: Output vs. input for the SOS effect in the infrared, input beam diameter 40 μm.

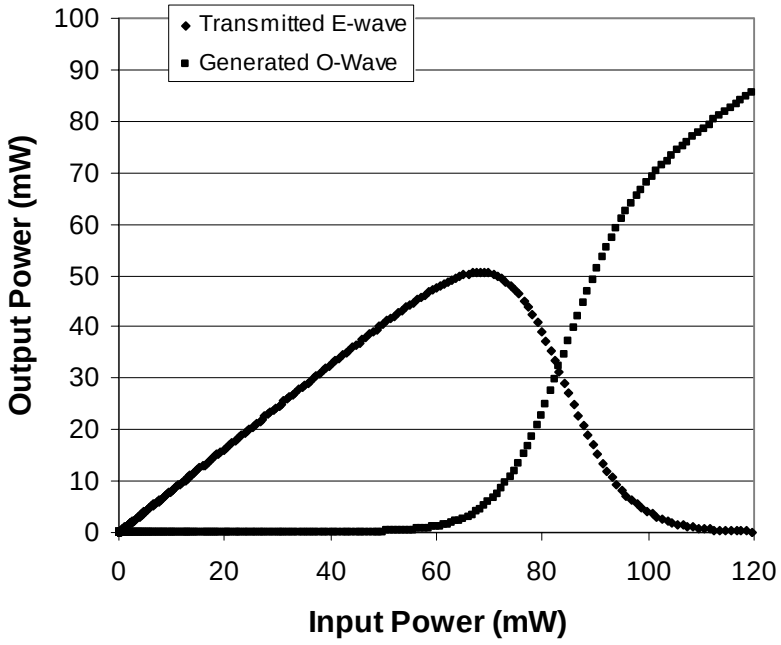

(a)

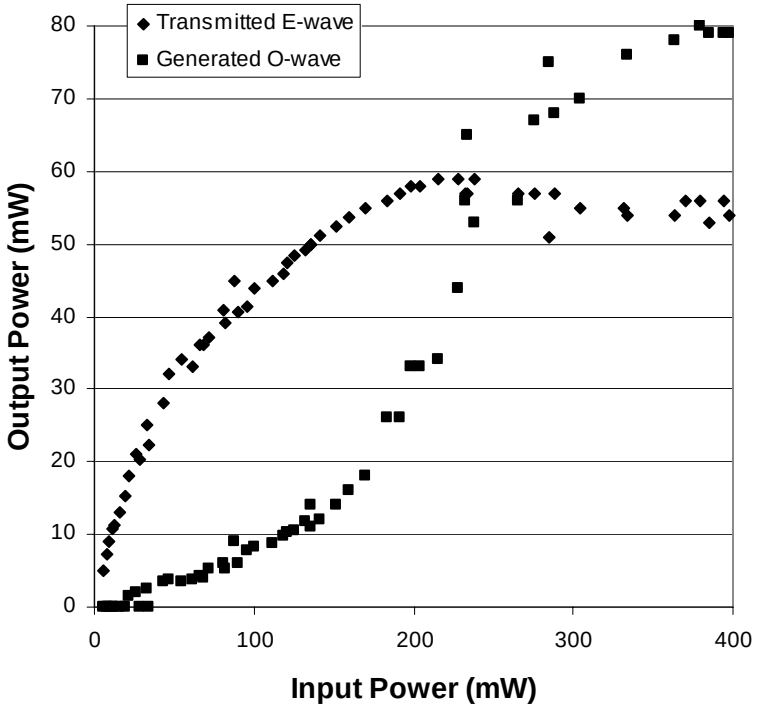

(b)

Figure 3.10: Output vs. input for the SOS effect in the infrared, input beam diameter 80 μm.

3.5 Influence of Carbon Nanotube Dopant

Recently, following its discovery in 1990 by Iijimo [Iijimo 1990], carbon nanotubes and especially single-wall carbon nanotubes (SWNT) have attracted much attention in optics [Xie 1997, Kataura 1999]. SWNTs have already been reported in applications such as optical limiting in carbon-black suspension [Mishra 2000, Vivien 2002] and photorefractivity of dye-doped NLC [Lee 2002], showing significantly enhanced nonlinearity. The novel properties of SWNTs, such as one-dimensional structure and increased nonlinearity, make them a very promising candidate to improve the orientational nonlinearity of NLCs. It has been shown that carbon nanotubes can be oriented parallel to the NLC director (where the director is defined as the local average NLC molecular direction) in a NLC solvent [Mrozek 2003]. This alignment of liquid crystals from carbon nanotubes implicates that there exists a strong coupling between NLC molecules and carbon nanotubes. This strong coupling may enable carbon nanotube to influence the mechanical properties of liquid crystals. Because of the low dissolvability of SWNT in NLC media, the added SWNT dopant does not degrade the optical quality of a NLC film, yet is sufficient to change the NLC's orientational properties. Our experiment has shown the film with SWNT dopants gives increased transmission compared to the pure NLC film under the same condition. Indeed, carbon nanotubes are perhaps one of the most interesting new materials emerged during the past decade. They exhibit unique electronic properties and can be tailored to become either metallic or semiconducting. As such, they have been considered as the basis for future nanoscale electronic devices. The complete knowledge of the interaction between NLC

molecules and carbon nanotubes and incorporating NLC techniques into nanoscale assembling, and processing, is still under consideration. In this section, we report the improved orientational nonlinearity in nematic liquid crystals with the SWNT dopants.

The experiment was done using an Argon laser at 488 nm and the setup is shown in Figure 3.11. The liquid crystal used is E7 (EM Industries), which has a negligibly small absorption at the laser wavelength. It has refractive indices of $\varepsilon_{\|}$=1.75 and ε=1.54 respectively for light polarized parallel and perpendicular to the NLC director axis, and a dielectric anisotropy of 13.8 at room temperature. It has a bending elastic constant K_2=3.0x10^{-12} N and viscosity coefficient of 0.07 Poise. The experiment was conducted at room temperature, which is far below E7's nematic-isotropic phase transition temperature 60.5 ^{o}C to minimize any thermal effects. The NLC sample was doped with 0.0001% (by weight) of purified SWNTs (SES Research). The sample was thoroughly sonificated at a temperature above the nematic-isotropic phase transition temperature. The SWNT-doped liquid crystal film is 250 μm thick and is homogenously aligned with the director axis of the NLC film lying in the plane of the cell window. Using a tight focusing lens (10mm focal length), a linearly polarized laser beam was focused at normal incidence onto the NLC film as an extraordinary wave (i.e., the laser polarization is parallel to the NLC director). A polarizing beam splitter at the output end was used to separate the transmitted extraordinary (e) and generated ordinary (o) waves.

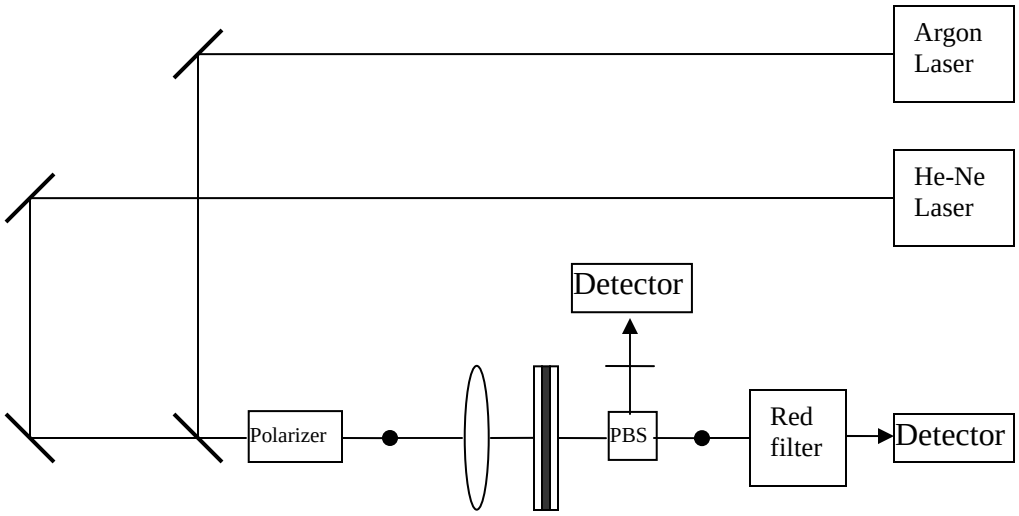

Figure 3.11: Experimental setup for the SOS effect in carbon-nanotube doped NLC

Figure 3.12 summarizes the experiment results obtained. The transmitted e wave and generated o wave are plotted as a function of the input laser power for both the pure E7 and the SWNT-doped E7 films. For both samples, output vs. input curves show typical SOS effect behavior. Below the threshold, both the transmitted (e) and generated (o) wave are linearly dependent on the input power. Above the threshold, the stimulated o wave grows dramatically, eventually surpassing the power of the transmitted e wave. The threshold for the E7 film doped with SWNTs is only 30mW compared to the threshold for the pure E7 film of about 55mW. That represents a 45% decrease in the threshold value. Similarly the input intensity for the polarization conversion (defined as the input

power at which the stimulated beam becomes stronger than the transmitted beam) has decreased from 78mW for the pure E7 film to 50mW for the E7 doped with SWNTs. Beside the decrease in threshold value, it has also been noticed that both e and o wave in the SWNT doped E7 film are stronger than those in the pure E7 film at the same input laser intensity.

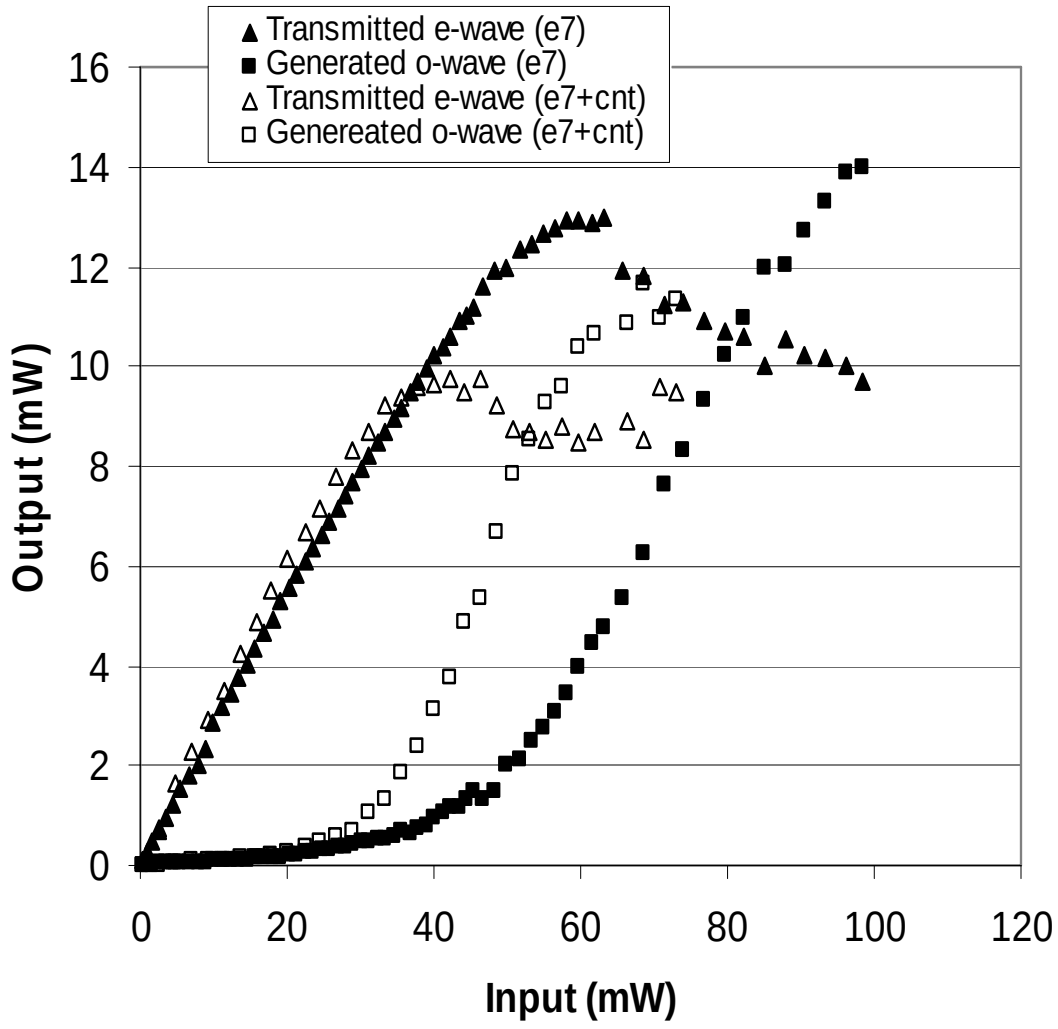

Figure 3.12: SOS curve in pure E7 and single-wall carbon nanotube doped E7 films

In order to clarify this increase in transmission, the total transmission as a function of input is plotted in Figure 3.13. In both samples, the transmission drops after the input laser intensity passes the polarization conversion point (50mW for the SWNT doped E7, 78mW for the pure E7 film). In general, the SWNT-doped E7 film gives 4-8% increase in transmission efficiency compared with the pure E7 film. This increase in the transmission implies that the added SWNT dopants increase the order parameter *S* and decreasie the scattering loss due to director orientation dispersion. In liquid crystals the elastic constant is related to the order parameter by:

$$K_2 = L_1 S \qquad \text{Equation 3.60}$$

Thus, the increased order parameter also implies an increase in elastic constant. The interpretation of our data in this manner is in good accordance with the report that carbon nanotubes cause increased order in liquid crystals [Mrozek 2003]. Different from the gradually decreasing transmission efficiency curve of the pure E7 film, there is a slight increase in transmission efficiency between the threshold (30mW) and the polarization conversion point (55mW) for the carbon nanotube doped E7 film. This increase in total transmission efficiency implies the decrease in scattering loss in the SWNT doped E7 film.

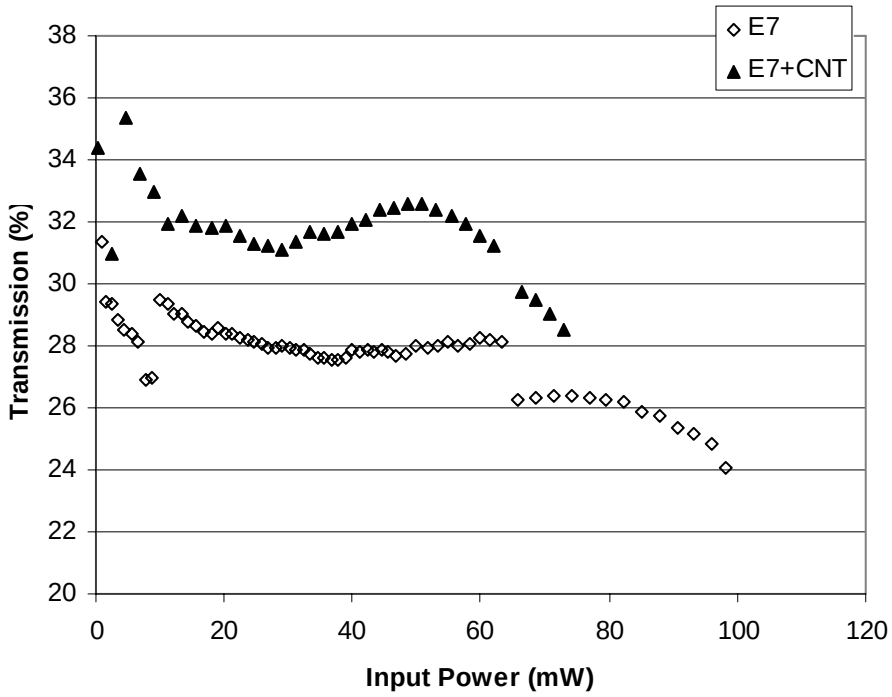

Figure 3.13: Total transmission vs. input for pure E7 film and SWNT-doped E7 film

In conclusion, we have reported the influence of SWNT dopants on nonlinear NLC films. We proposed that the added carbon nanotubes increase the orientational order and elastic constant of the NLC film and bring a significant enhancement to the SOS effect. The threshold and polarization conversion point for the input laser intensity were decreased from 55mW and 78mW to 30mW and 50mW respectively. In addition to the improvement in the orientational nonlinearity, the SWNT-doped NLC film showed a 4-8% increase in transmission. A more detailed analysis of the phenomenon requires an understanding of the microscopic interaction between carbon nanotubes and nematic liquid crystals as well as the macroscopic influence to NLC's mechanical, electrical and optical properties from the SWNT dopants. Furthermore, a thorough study of output

spectrum will help to understand the dynamical reorientational process of the NLC director.

3.6 External AC Control of the SOS Effect

After the realization of the SOS effect at the communication wavelength (1.55 μm), one of the primary quests is to decrease the laser power requirement for the SOS effect to make its applications more plausible. Because the SOS signal is initiated from the scattering due to the NLC director fluctuation, more intense oscillation would generate stronger noise. The stronger noise in turn would intensify the reorientation of the NLC director through the interaction with the pump beam. This positive-feedback loop would produce a stronger SOS signal for the same pump beam intensity. Consider the interaction geometry shown in Figure 3.14. A linearly polarized laser beam impinges normally on a NLC film, with electric field $\vec{E}_x = \hat{e}_x E_x e^{i(\vec{k}_x \cdot \vec{r} - \omega_x t)}$. The spontaneously scattered noise field at the y direction is $\vec{E}_y = \hat{e}_y E_y e^{i(\vec{k}_y \cdot \vec{r} - \omega_y t)}$. The NLC director reorientation occurs only in the x-y plane under these two electric fields and is described by

$$\vec{n} = [\cos\theta(z,t), \sin\theta(z,t), 0] \qquad \text{Equation 3.61}$$

where $\theta(z,t)$ denotes the reorientation angle of the NLC director.

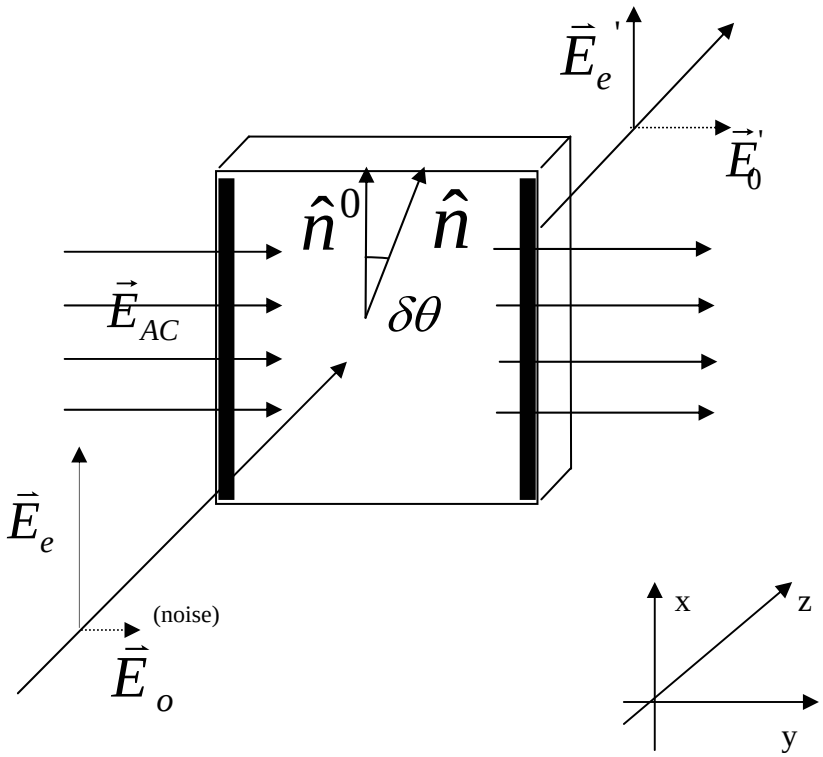

Figure 3.14: Interaction geometry of the SOS effect with an external applied AC field.

In order to intensify the NLC director's reorientation to achieve a lower SOS threshold, an external AC modulation field is applied on the *y*- direction whereas the NLC director lies originally in the *x*-direction and the input pump beam is parallel to the NLC director, i.e. e-wave input. The parameters of the liquid crystal used (E7) are: refractive indices $n_e = 1.75$, $n_o = 1.54$, elastic constant K_2 =3.0 x 10^{-12} N, and the viscosity 0.07 Poise. The sample thickness is 250 μm. The external AC field strength is 4×10^4V/m and modulation frequency is 30Hz. The laser wavelength is 532 nm and the focus spot diameter is about 30 μm. The initial noise intensity is assumed to be 0.0001%

of the input laser beam in the case of no AC modulation. The simulation curve is shown in Figure 3.15. With the application of an external AC field, the scattering becomes more intense, and the intensity of the scattered noise is assumed to be 0.0025%. (Although this estimate noise is 25 times larger than that in the absence of AC modulation, it is still a very tiny portion of the input laser intensity.)

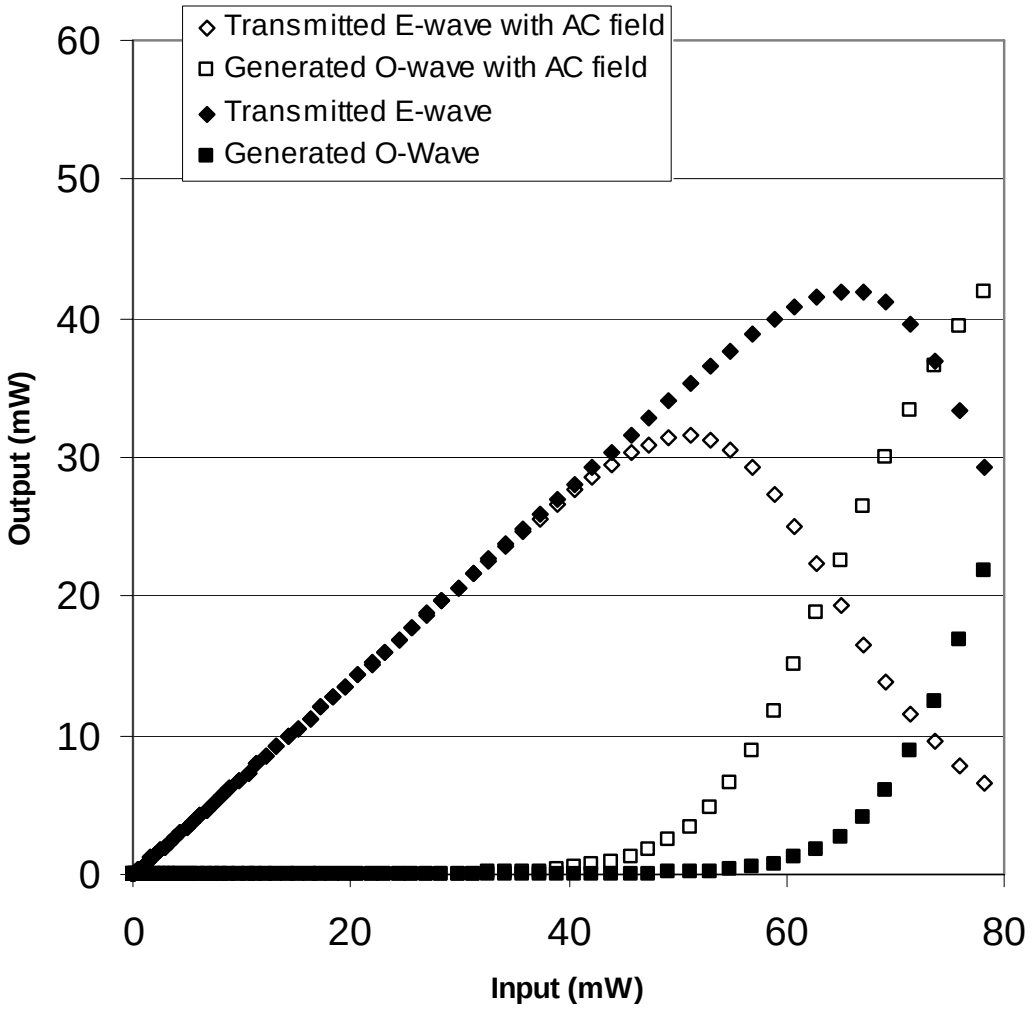

Figure 3.15: Simulation of the SOS effect with an external AC field

The numerical simulation in this case is shown in Figure 3.15 . It is very clear that the threshold for the SOS effect has decreased from 80mW to 55mW with the application of an external AC modulation field. Further increase in scattered noise would cause larger scattering loss which will hamper the SOS effect rather than lead to further enhancement.

The experiment setup is the same as the setup for the SOS experiment in dye-doped liquid crystals except for the use of different laser and cell preparation. The laser used is a Coherent Double-Pumped Solid State (DPSS) laser (λ=0.532 μm). The cell has two side electrodes attached to an external low frequency voltage source. After passing through an *x*-directed polarizer, the laser is focused by a tight-focus lens (f=10mm) onto a planar-aligned liquid crystal E7 (from EM Chemicals) film. The NLC director is initially in the *x*-direction and the laser impinges on the sample as an e-wave, i.e., with the electrical field of the laser beam parallel to the NLC director. After collimation by a large diameter lens, the output beams are sent through a polarizing beam-splitter to separate the transmitted e-wave and the generated o-wave. The collection optics is F4. As shown in Figure 3.16 , the experimental data agrees well with the theoretical prediction in demonstrating the decrease in the threshold of the SOS effect with the application of an external AC modulation field. Under the same experimental condition, the crossing-point of the transmitted e-wave and the generated o-wave changed from 60mW to 55mW when the AC field was applied.

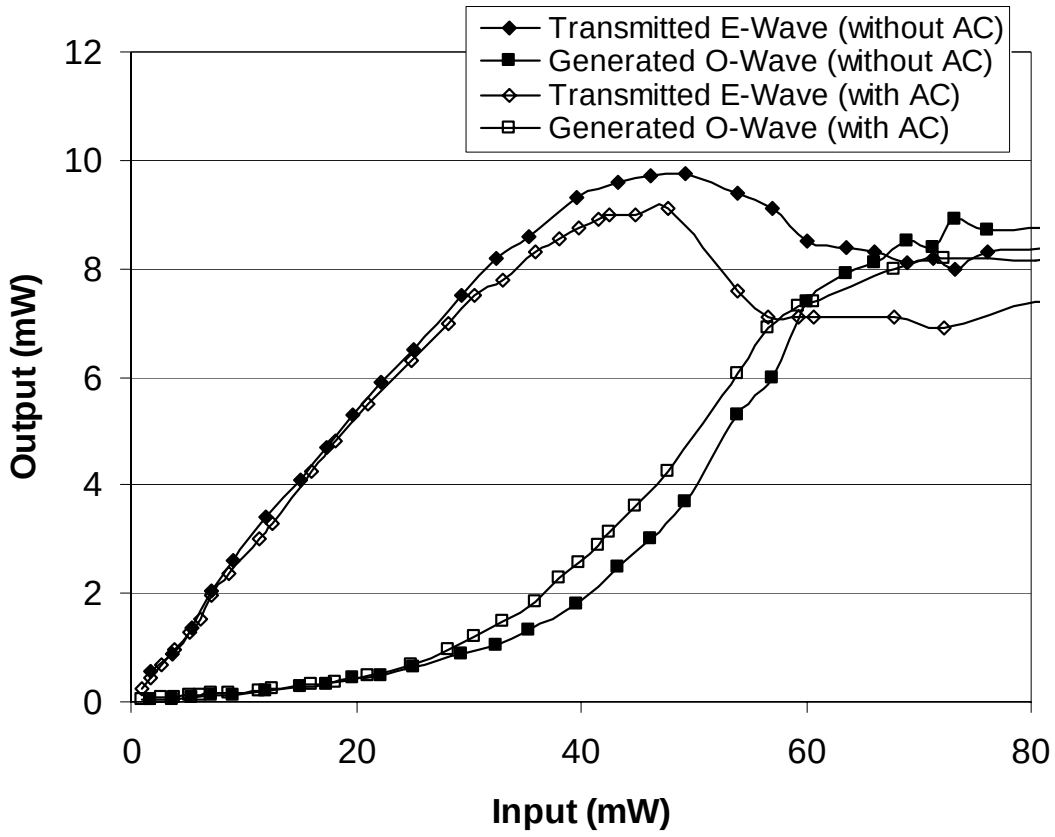

Figure 3.16: Experimental result of the SOS effect with and without an external AC field.

3.7 Polarization Conversion in Liquid Crystal Waveguide Structure

As shown in Figure 3.17, the input laser power requirement for the stimulated orientational scattering decreases with the increase of the NLC sample thickness. In other words, the increased interaction length decreases the power requirement for the SOS effect. Due to the rather weak inter-molecular forces, it is very hard to fabricate liquid crystal films that are thicker than 1 mm and maintain good crystalline structure at the

same time. Furthermore, the strong divergence of the input laser due to the tight-focus lens used limits the effective interaction length of a NLC film.

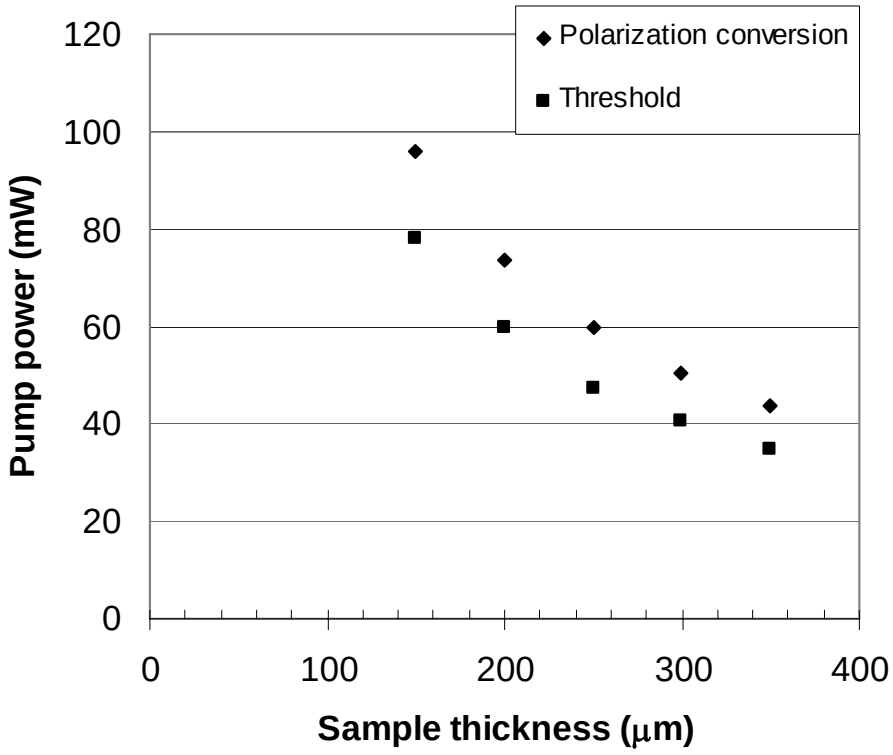

Figure 3.17: SOS simulation for different NLC film thicknesses. The polarization conversion point stands for the pump power at which the stimulated signal exceeds the transmitted signal. The threshold point stands for the pump power that the stimulated signal starts to grow exponentially.

In order to increase the effective interaction length in the stimulated orientational scattering and decrease the power requirement for the pump laser, a liquid crystal waveguide structure is proposed to overcome the above difficulties. Figure 3.18 illustrates the NLC waveguide structure. A single mode fiber with only inner cladding (diameter ~ 150 μm) is coupled into the NLC waveguide from the open window. The output beam from the NLC waveguide has very good optical quality as shown in Figure

3.19. By using a NLC waveguide structure, the light is confined within the waveguide and experiences a rather longer interaction length (~2mm).

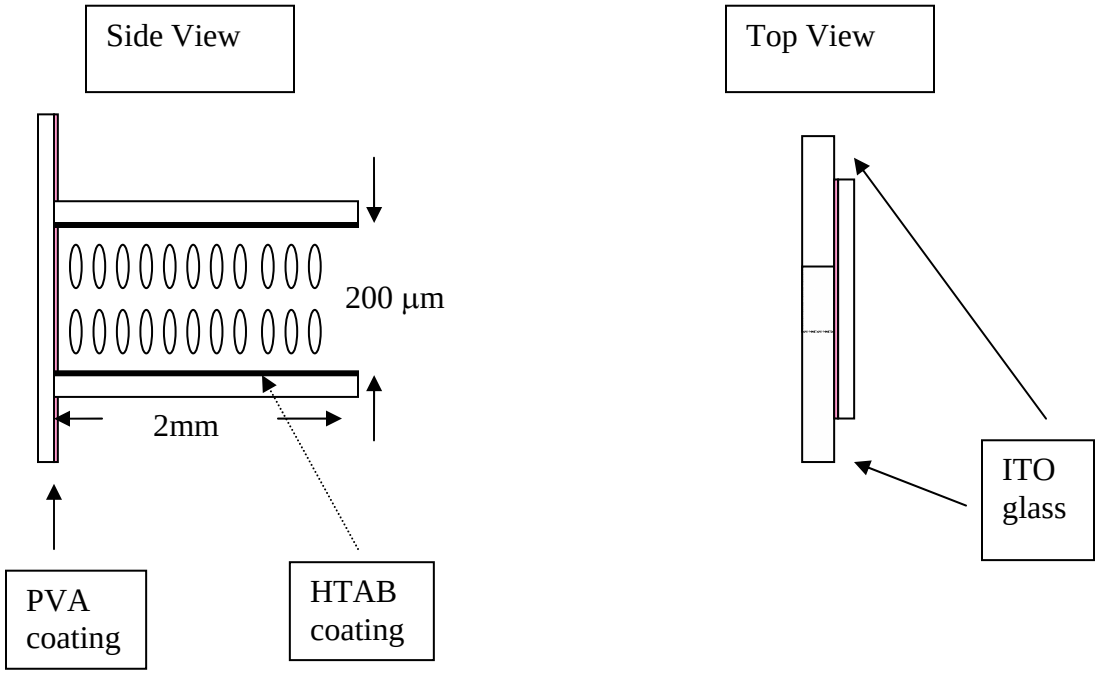

Figure 3.18: NLC waveguide structure illustration.

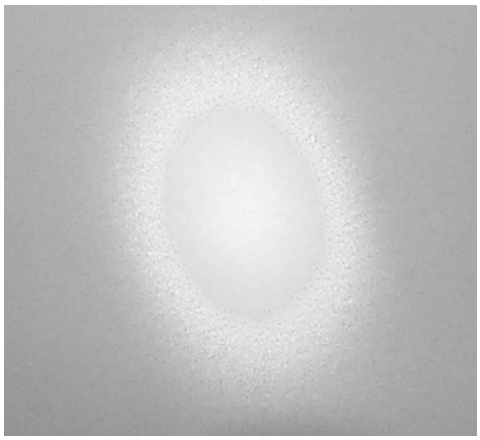

Figure 3.19: Output laser spatial profile after exiting from the NLC waveguide.

The experimental geometry is same as that shown in Figure 3.8 except that the laser after the tight-focus lens is coupled into the single mode fiber then fed into the NLC waveguide structure. The liquid crystal used is E7 and the laser is an Erbium doped infrared semiconductor laser (1.55 μm). The experimental result is shown in Figure 3.20. It is quite obvious that the increased interaction length of the waveguide structure has indeed decreased the power requirement for the threshold value.

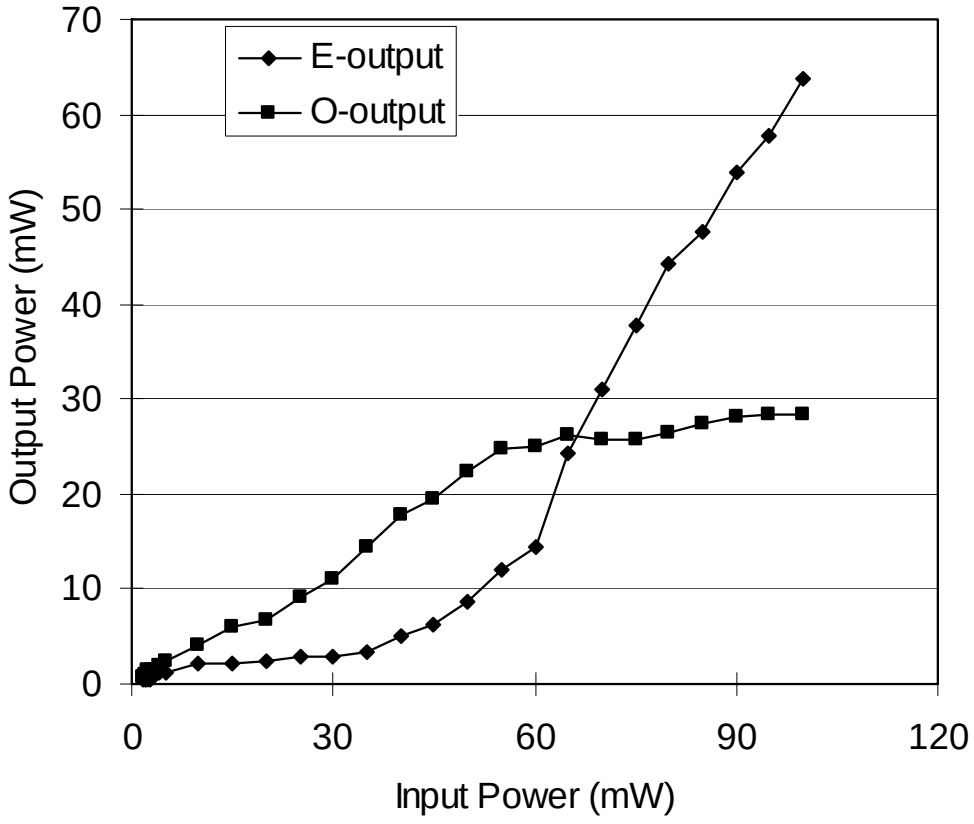

Figure 3.20: SOS curve of the NLC waveguide at the 1.55 μm wavelength.

3.8 Summary

Stemming from the intensive nonlinear interaction between liquid crystals and optical fields, stimulated orientational scattering serves as a powerful tool to probe the physical properties of liquid crystals for scientific research as well as a potential candidate for applications such as polarization switching and phase conjugation devices for adaptive optics. In the present work, we have theoretically and experimentally investigated this non-resonant stimulated scattering phenomenon. A complete theoretical analysis of steady-state stimulated orientational scattering without the non-pump-depletion approximation has been presented. A high percentage of polarization conversion has been observed as the original perpendicularly-polarized pump dies out and the horizontally-polarized stimulated scattering grows up to about 90% of the initial input. The numerical simulation shows a good agreement with the previous SOS experiment in the visible wavelength [Khoo 1994b]. Due to its non-resonant characteristic, the SOS effect is numerically simulated in the near infrared region (1.55 μm). The simulated curve showed similar polarization conversion behavior. Subsequent experiment using an Erbium doped semiconductor laser has indeed verified our theoretical prediction.

In an effort to decrease the power requirement for the input pump laser in order to make it more feasible for applications, the SWNT-doped NLC, the application of an external AC field and NLC waveguide structures have been considered in the SOS experiments. The added carbon nanotube dopants increased the orientational order and elastic constant of a NLC film and brought a significant enhancement to the SOS effect in

the NLC film. The threshold and polarization conversion point for the input laser intensity were decreased from 55mW and 78mW to 30mW and 50mW, respectively. It is also worth noting that SWNT dopants have a low solubility in liquid crystals and do not deteriorate the optical quality of NLC films. The application of an external modulation field provides more control of the SOS effect. As shown in Figure 3.16, the applied low frequency AC field decreased the laser power from 68 mW to 56 mW at the polarization conversion point. Finally the SOS effect was implemented in a NLC waveguide structure. The increased interaction length decreased the power requirement for the pump laser. All of these approaches to improve the SOS performance make this unique all-optical non-resonant effect more attractive for both scientific researches and potential applications.

Chapter 4

Dynamics of Stimulated Orientational Scattering in Liquid Crystal Films

Self-organization and collective phenomena have been studied extensively in various material and optical systems [Peccianti 2002, Sandfuchs 2001 Jenekhe 1998] These studies provide fundamental insights into how seemingly incoherent individual molecules or noises would self-select or self-organize by mutual interactions into a crystalline or coherent form/signal, with or without an external driving field. In these contexts, nematic liquid crystals that exhibit collective molecular processes are particularly intriguing. As a result of their unique physical properties not available in crystals or fluids, liquid crystal optical materials have found widespread applications in linear and nonlinear optical systems. In particular, the collective dynamics of the director axis of liquid crystals can bring forth an extremely nonlinear response, capable of photorefractive effects and grating formation [Khoo 1994b, Khoo 1998], self-starting optical phase conjugation [Khoo 2000, Zeldovich 1985], polarization rotation and beam control, stimulated scatterings [Khoo 2002], and optically-induced complex dynamics [Carbone 2001] in spatial as well as temporal frequency domains. The time scale of these laser induced director axis reorientation (~ms) allows simple experimental monitoring and visualization of the dynamical processes. In this chapter, the dynamics of the liquid crystal director reorientation will be studied in the context of stimulated orientational scattering.

4.1 Introduction to the Director Reorientation Dynamics

In the investigation of stimulated orientational scattering, an important point to note is that although the driving or pump beam is a continuous-wave (CW) source, the output waves are found to exhibit various dynamical and oscillatory phenomena, as a result of the underlying complex nonlinear nature of the field(s) driving director axis reorientation process. Strong oscillations and exchange of energy between the various interacting waves occur as a result of the frequency and phase shifts created in such multi-wave mixing processes.

As illustrated in Figure 4.1, the linearly-polarized input pump beam will cause various scattered beams ($E_i(z,t),\omega_i,\vec{k}_i$) in a homogeneously aligned NLC film. Among multi-frequency scattering noise components, only the one satisfying the phase-matching conditions will be able to coherently interact with the pump beam as shown in Figure 4.2. In order to study the NLC director reorientation dynamics, the time-varying stimulated orientational scattering equations (Equation 3.52 – 54) have to be considered. The NLC director $\hat{n}$ is expressed as $\hat{n}=\cos\theta(z,t)\hat{x}+\sin\theta(z,t)\hat{y}$ and the total coherent electric fields (*x*-directed pump beam and *y*-directed scattering beam) inside the cell are $\vec{E}=E_x e^{i(k_x z-\omega_x t)}\hat{x}+E_y e^{i(k_y z-\omega_y t)}\hat{y}$. Also, the NLC director reorientation angle θ is expressed as $\theta(z,t)=\frac{1}{2}\left[\theta(z,t)e^{i(qz-\Omega t)}+c.c.\right]$. Under the slowly-varying-envelop-approximation (SVEA), i.e. $\partial^2\theta(z,t)/\partial z^2$ and $q\partial\theta(z,t)/\partial z$ are negligible compared to $q^2\theta(z,t)$, $\omega_y{}^2>>\Omega\omega_y>>\Omega^2$, the time-dependent SOS equations can be simplified as:

$$\eta\frac{d\theta}{dt}-K_2\frac{\partial^2\theta(z,t)}{\partial z^2}=\frac{\varepsilon_a}{2}\left[\begin{array}{l}\sin(2\theta)\left(\left|E_y\right|^2-\left|E_x\right|^2\right)\\+\cos(2\theta)\left(E_xE_y^{\ *}e^{i(qz-\Omega t)}+E_x^{\ *}E_ye^{-i(qz-\Omega t)}\right)\end{array}\right] \qquad \text{Equation 4.1}$$

$$\frac{\partial E_x}{dz}=-i\frac{\varepsilon_a k_x}{4\varepsilon_x}\left|\theta_s\right|^2E_x+i\frac{\mu\varepsilon_a\omega_y^{\ 2}}{4k_x}\theta_sE_y \qquad \text{Equation 4.2}$$

$$\frac{\partial E_y}{dz}=i\frac{\varepsilon_a k_y}{4\varepsilon_y}\left|\theta_s\right|^2E_y+i\frac{\mu\varepsilon_a\omega_x^{\ 2}}{4k_y}\theta_s^{\ *}E_x \qquad \text{Equation 4.3}$$

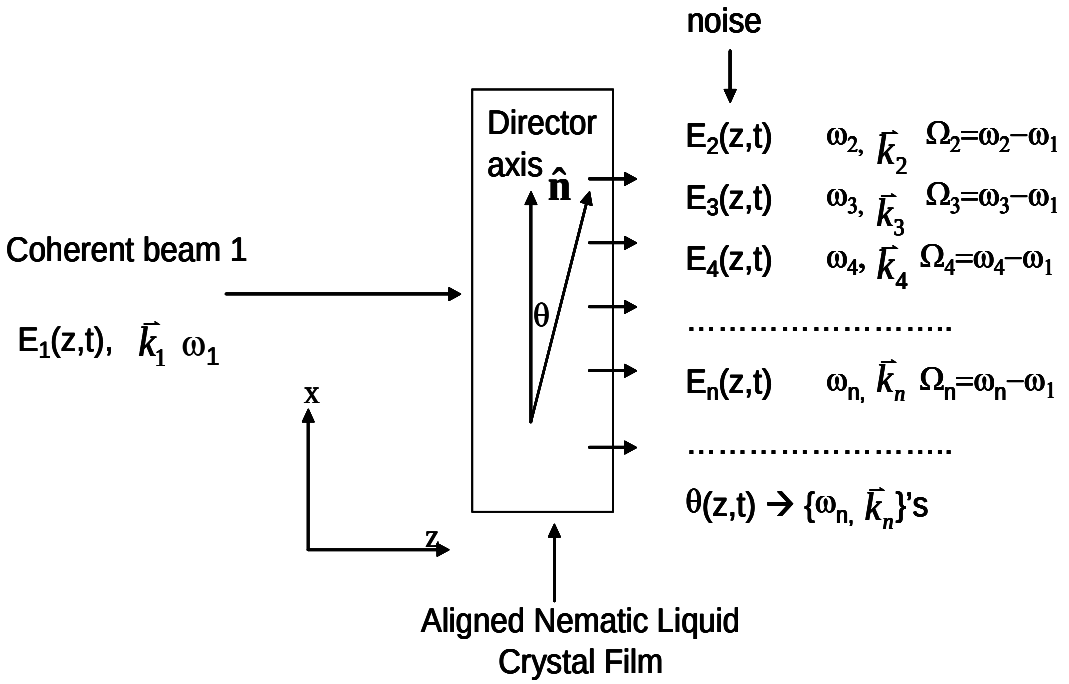

Figure 4.1: Schematic depiction of multi-frequency scattering noise components by a linearly polarized laser incident on a nematic liquid crystal film.

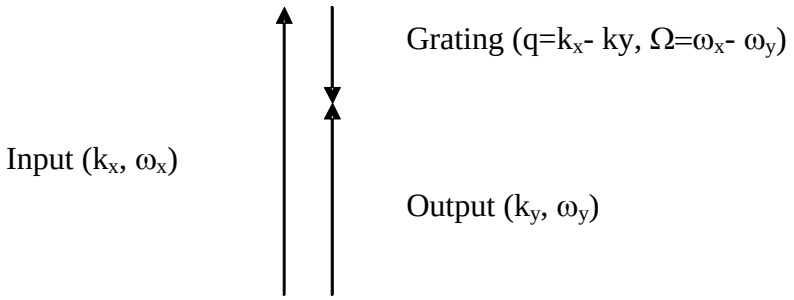

Figure 4.2: A particular vector matching condition for the optical waves and the grating wave vector in the forward direction.

The strong coupling among the input and generated waves and the director axis reorientation are clearly evident in Equations 4.1- 3. The "driving" fields on the R.H.S. of these equations consist of "static" terms (e.g. $\left|E_{x,y}\right|^2$) as well as moving grating terms ($\sim e^{i(qz-\Omega t)}$) caused by the interference of the pump and scattered waves. The frequencies Ω_n of these moving gratings span the spectrum of the director axis fluctuations, usually up to a few KHz [Khoo 1994a]. However, only the noise component that experiences the maximum gain will be the first to evolve from noise to coherent beam and substantially drain energy from the pump wave E_x. In the steady-state small-signal gain regime [Khoo 2000, Khoo 1998], i.e. at the onset of stimulated orientational scattering, the gain constant is given by $G = f(\Omega)\pi\varepsilon_a{}^2 / 2cn_e\lambda K_2 q^2$ where $f(\Omega) = (2\Omega/\Gamma)/(1+\Omega^2/\Gamma^2)$ [Tabiryan 1986]. In these expressions, $\Omega = \omega_x - \omega_y$ is the frequency difference, K_2 is the elastic constant and η is the viscosity of the nematic liquid crystal, q is the grating wave vector $\vec{q} = \vec{k}_x - \vec{k}_y$ and $\Gamma = K_2 q^2/\eta = 1/\tau$ is the characteristic frequency of the director

axis fluctuations (the inverse of the characteristic relaxation time constant τ). Note that the maximal gain occurs at $\Omega = \Omega_{max} = \Gamma$, the characteristic director relaxation frequency. As it will be shown in the following section, this characteristic frequency appears prominently in the spectrum of the observed intensity oscillations above the stimulated scattering threshold.

4.2 Experimental Results

The experiment set up used is shown in Figure 4.3. The sample is made by sandwiching liquid crystal E7 between two uni-directionally rubbed PVA [Polyvinyl Alcohol] coated glass slides. The sample thickness, as defined by the plastic spacer used, is 250 μm. The liquid crystal is homogeneously aligned in the *x*-direction, i.e. with the director axis lying parallel to the cell windows. An important advantage of stimulated orientation scattering in nematic liquid crystals is its non-resonant nature; the gain and other wave mixing parameters are only weakly dependent on the wavelength, allowing one to realize the effect in any desirable wavelength regime of interest. We have performed complete sets of experiments using both visible and infrared lasers. For the visible regime, we employ a Diode-Pumped-Solid-State (DPSS) laser that emits at 532 nm. For the infrared, an Erbium Doped Fiber Laser emitting at 1550 nm is used.

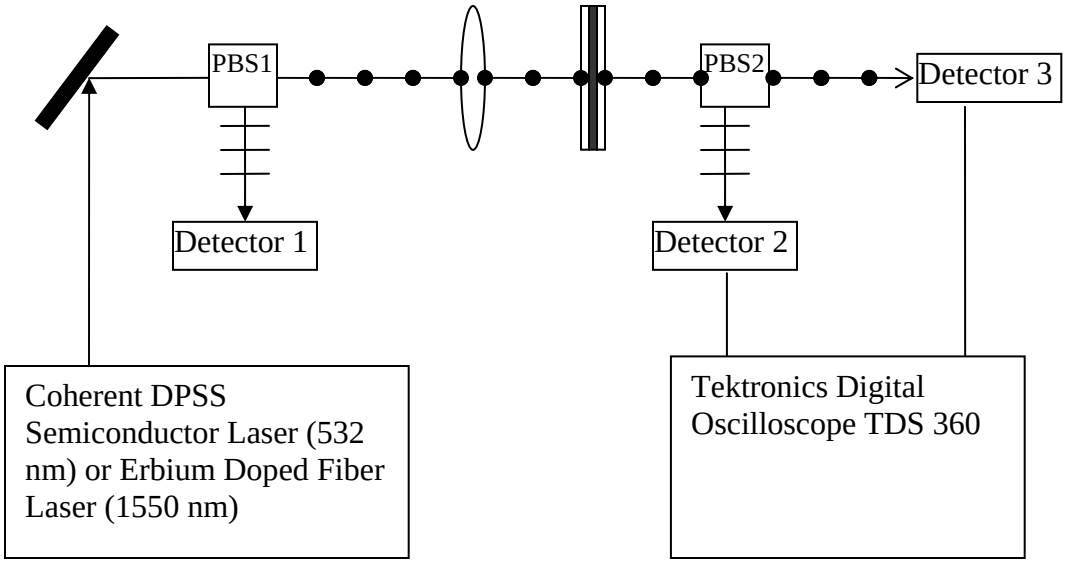

Figure 4.3: Experimental set up for the stimulated orientation scattering effect. PBS: polarizing beam splitter.

The input unpolarized laser is separated into two beams after passing through a polarizing beam splitter (PBS1). One beam is monitored as the reference for the input beam intensity. The other linearly polarized input pump beam is focused as an e-wave onto a homogeneously-aligned NLC film by a 10 mm focal lens. The output from the NLC film is separated by a polarizing beam splitter (PBS2) into two different polarizations. The generated o-beam and the transmitted e beam are then sent into a digital oscilloscope (Tektronics TDS360) for real-time data collection and Fourier spectrum analysis. The transmission of the e-wave through the rather thick cell (250 μm) is actually quite good. For the 1550 nm laser, the transmission is measured to be over 85%, with the air-glass interface reflection contributing to the most of the losses.

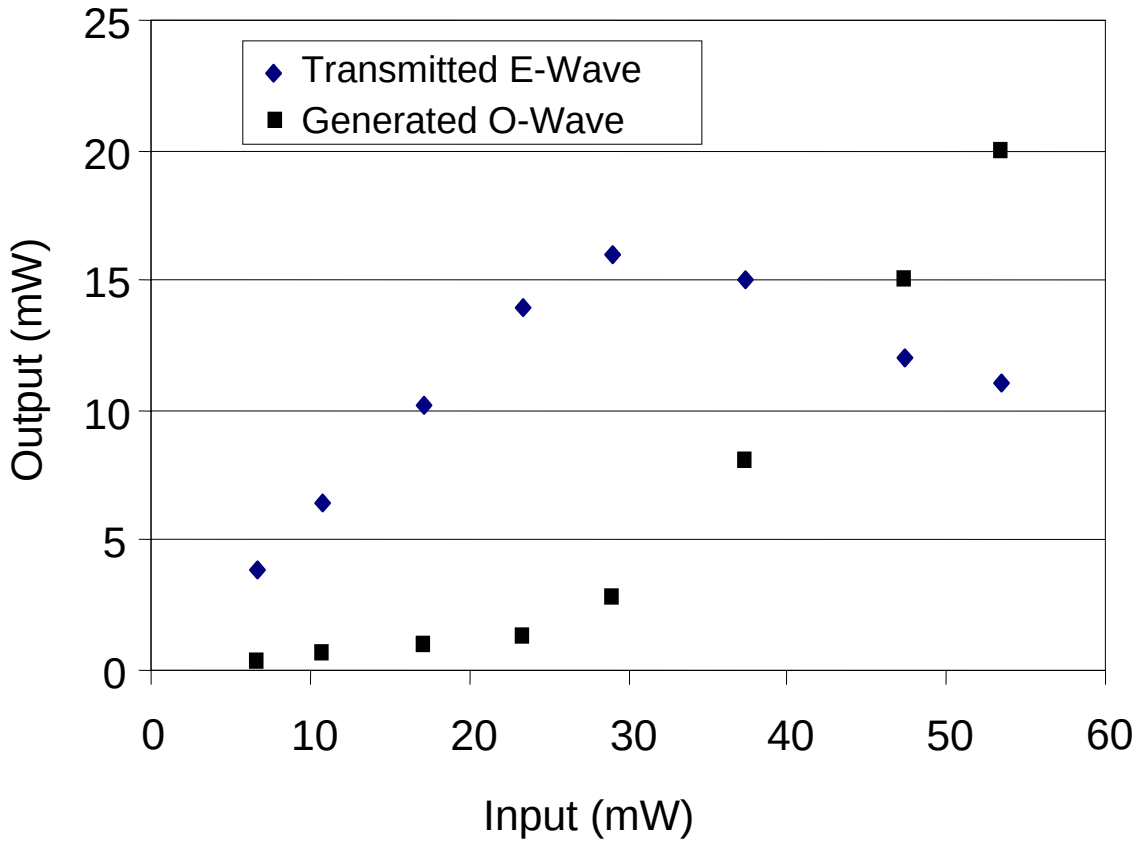

Figure 4.4 (a): A typical measured dependence of the (average) output pump and generated waves versus the input power. Sample thickness: 250 μm; Laser wavelength: 532 nm; Focal spot diameter: 40 μm.

Figure 4.4 (a) shows the dependence of the measured (average) transmitted and generated waves versus the input power. Figure 4.4 (b) shows the chart record of the output beams versus the input beam intensity. Both the transmitted e-wave pump beam and the (very weak) o-wave "noise" initially grow linearly with the input power. Typically for a mW-power pump beam, the total (within the same beam divergence cone as the pump beam) scattered noise is on the order of 10's of μWs. Above the stimulated scattering threshold pump power of around 30 mW (intensity of ~ 2.5 KW/cm^2 for a

focused laser spot diameter of 40 μm) the o-wave noise component increases exponentially. Above the threshold power, both the transmitted and the generated waves are observed to fluctuate dramatically as shown in Figure 4.4(b).

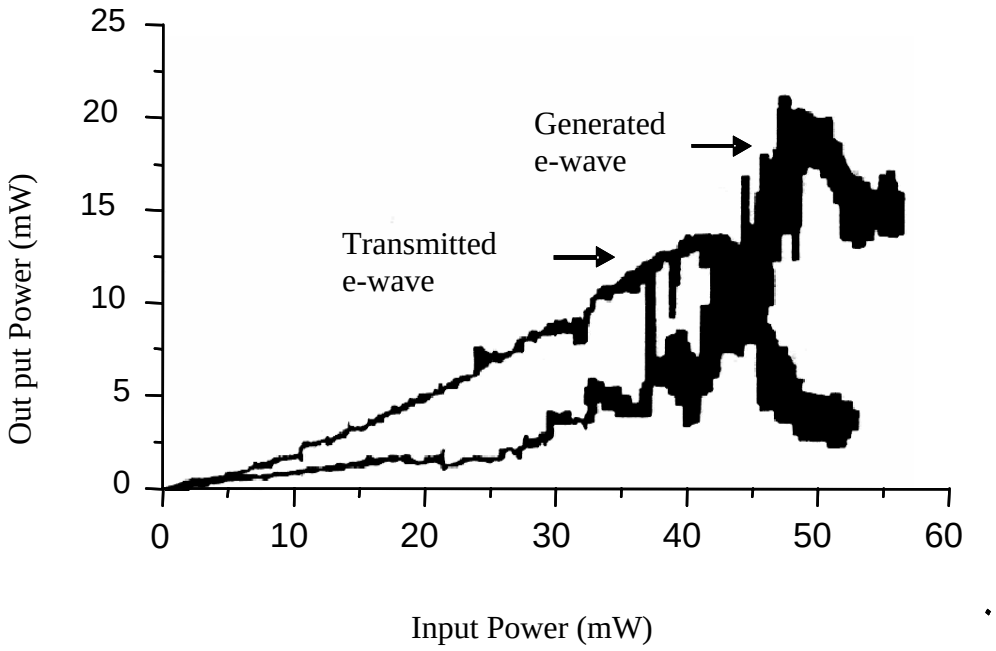

Figure 4.4 (b): Chart recorder traces of the output pump and generated waves versus the input power showing oscillatory intensities at a fixed input intensity. Sample thickness: 250 μm; Laser wavelength: 1550 nm; Focal spot diameter: 40 μm.

The time-dependency of both the transmitted and generated beams is plotted in Figure 4.5. The energy transfer between the transmitted and the generated beams is obvious in that as one beam increases the other decreases correspondingly while both are fluctuating in the time domain.

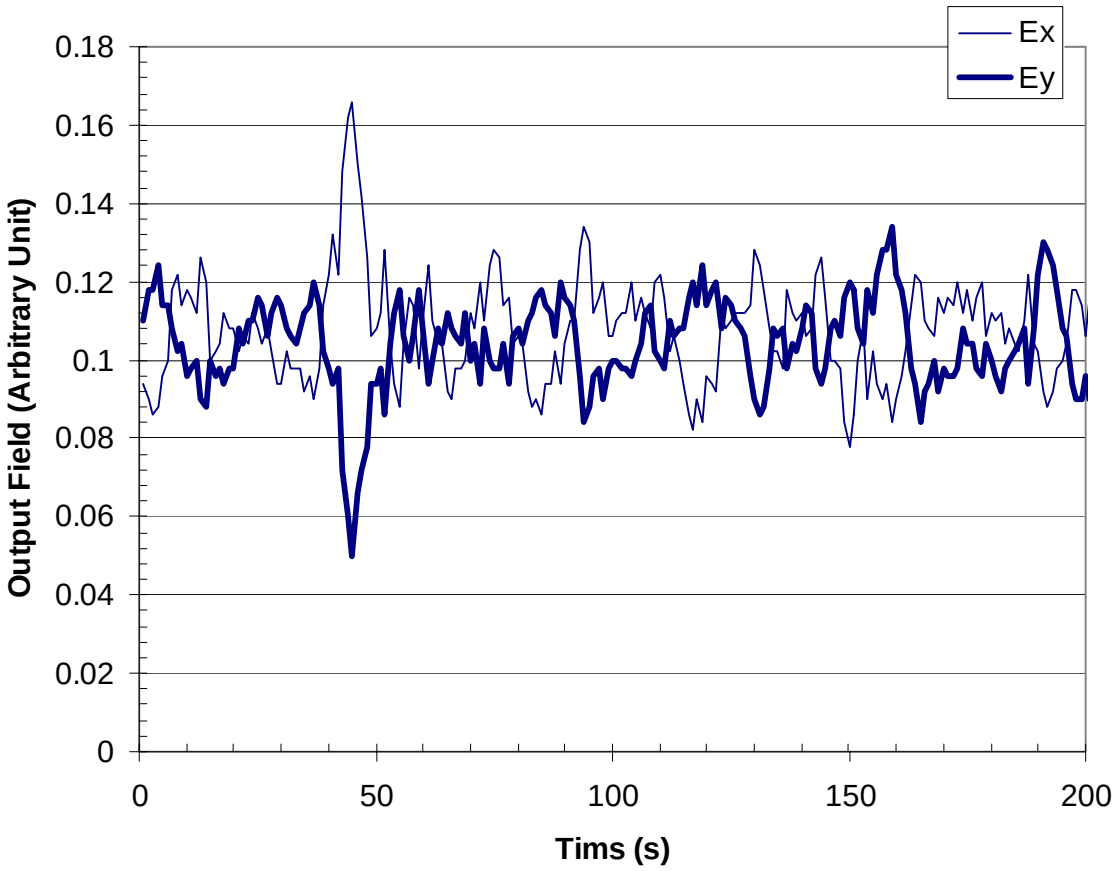

Figure 4.5: Simultaneous oscilloscope traces of the transmitted and generated waves showing the oscillatory energy exchanges between the two beams. Pump laser power: 60 mW; Laser wavelength: 532 nm; sample thickness: 250 μm; Laser spot diameter: 40 μm.

However, the total power of the transmitted and generated beams remains essentially constant as shown in Figure 4.6 even as each of them fluctuates dramatically in time. This observation indeed verifies that the generated signal drains energy from the pump beam. The regime where oscillations are observed lasts from just above the threshold to well over the half-way point of the polarization conversion (at which the scattered o-wave is greater than the transmitted e- beam).

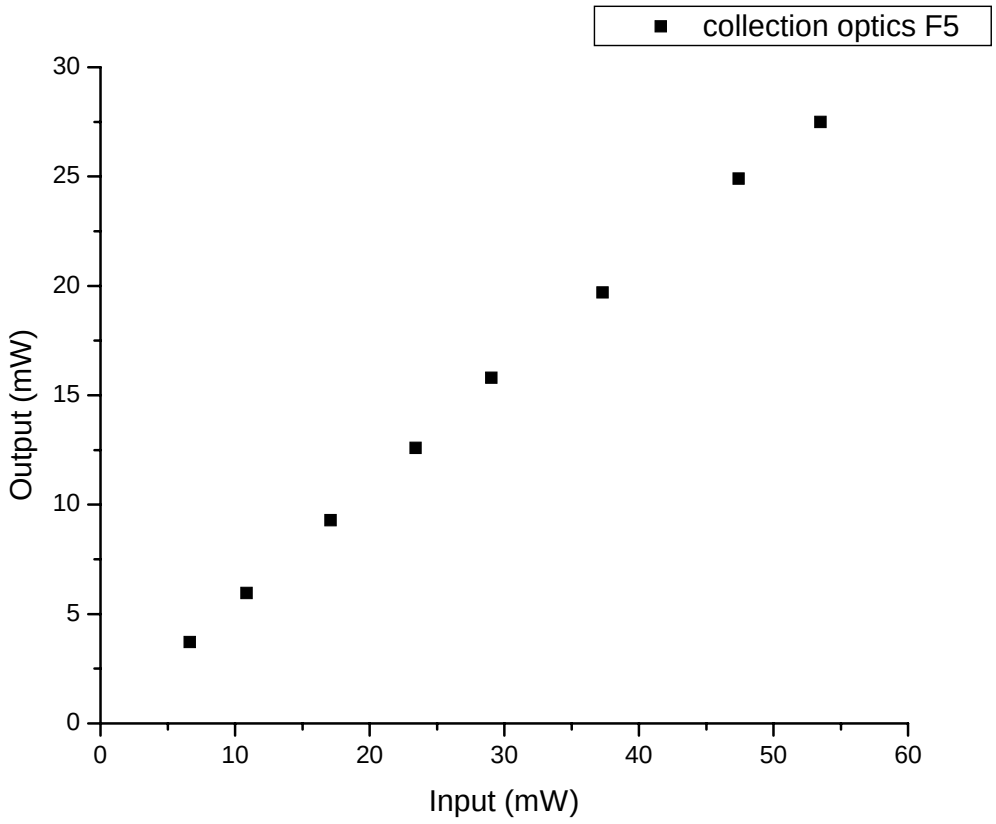

Figure 4.6: Total output power, measured with the output polarizing beam splitter removed, showing the linear dependence with input power.

These intensity oscillations observed just above the stimulated scattering threshold are reminiscent of director motion above the optically induced Freedericksz threshold in previous studies [Carbone 2001] in nematic liquid crystals. Even though the oscillation of the director axis is extremely small, there is an effective periodic transfer of energy (while the total energy remains constant) between the e- and o-waves through the sample.

We have carried out detailed measurements of the Fourier spectra of the oscillations at various fixed input power above the threshold, using both visible and

infrared lasers. In general, the observed spectra are very complex. However, the spectra all exhibit common features that are in good agreement with the theoretical expectations. In particular, the characteristic director relaxation frequency Γ is featured prominently in all the spectra of the generated o-wave. Figure 4.7 depicts a typical spectrum obtained with a DPSS (532 nm) laser, with a very well defined "peak" at 32 Hz that is in excellent agreement with the theoretical expectations as $\Gamma = K_2 q^2 / \eta = 1/\tau = 32$ for the NLC E7 and the laser wavelength of 532 nm.

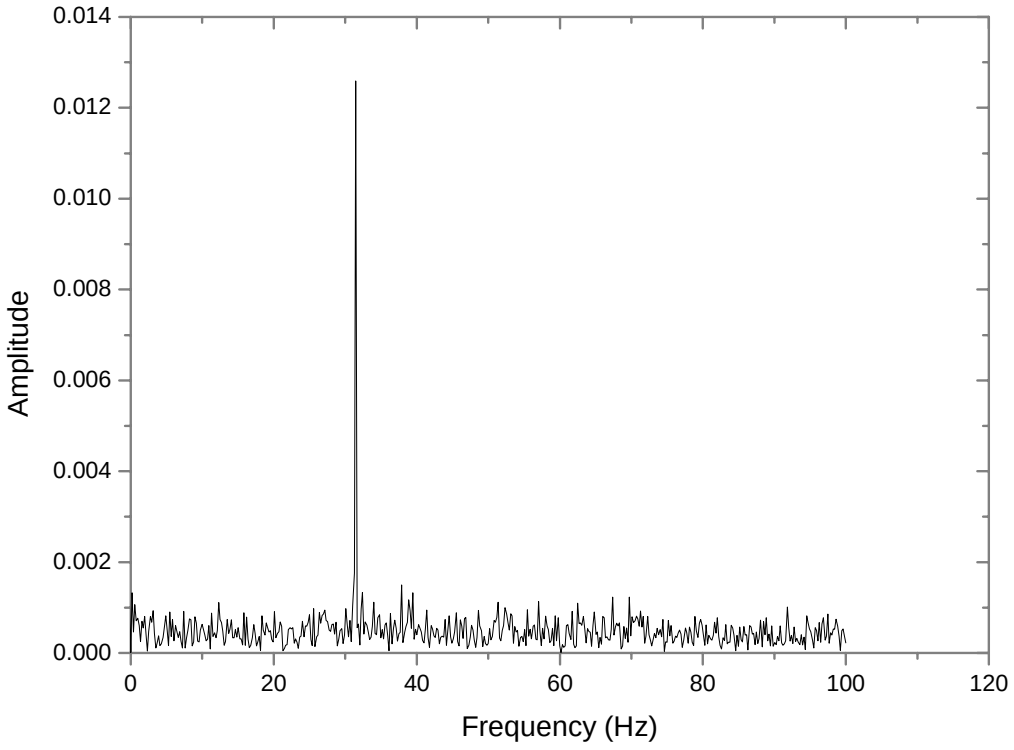

Figure 4.7: Measured Fourier spectrum of the output e-wave showing a sharp spike at the characteristic frequency Γ = 32 Hz. Pump laser power: 60 mW; Laser wavelength: 532 nm; sample thickness: 250 μm; Laser spot diameter: 40 μm.

The characteristic frequency and other features in the spectrum such as the number and locations of “peaks” in the spectra and their power dependence are also borne out in the study conducted with an infrared Erbium doped fiber laser (1550 nm). Figure 4.8 shows the spectrum of the intensity oscillation of the stimulated o-wave for example. A distinct peak occurs at 4 Hz, which is in very good agreement with the characteristic frequency calculated for this wavelength and the NLC E7. The spike is slightly wider than the one observed with the 532 nm laser, and it is attributed to the (less stable) nature of the pump laser used. At higher input power, these intensity oscillations begin to pick up higher harmonics and more frequency components as shown in Figure 4.8-10.

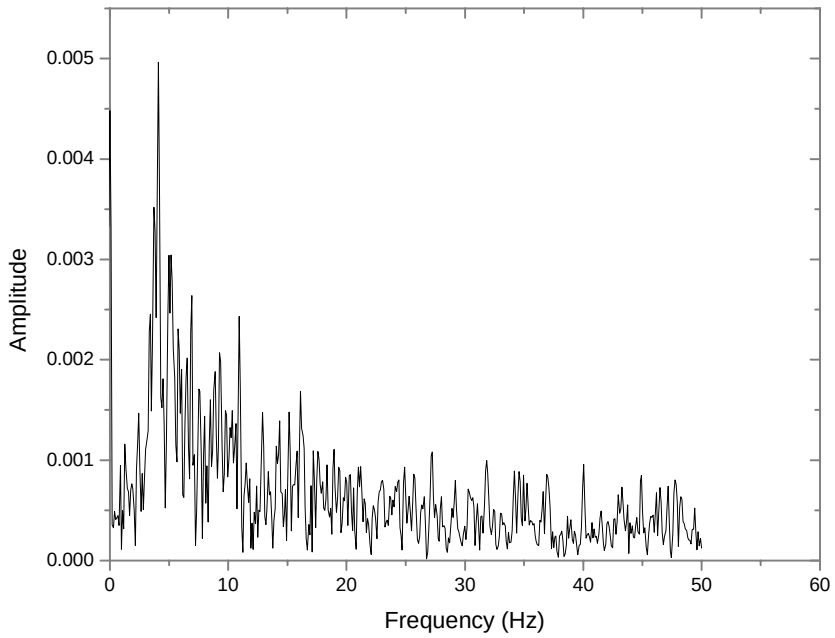

Figure 4.8: Fourier spectrum of the output e-wave showing a spike at the expected characteristic frequency Γ = 4 Hz. Pump laser power: 180 mW; Laser wavelength: 1550 nm; sample thickness: 250 μm; Laser spot diameter: 100 μm.

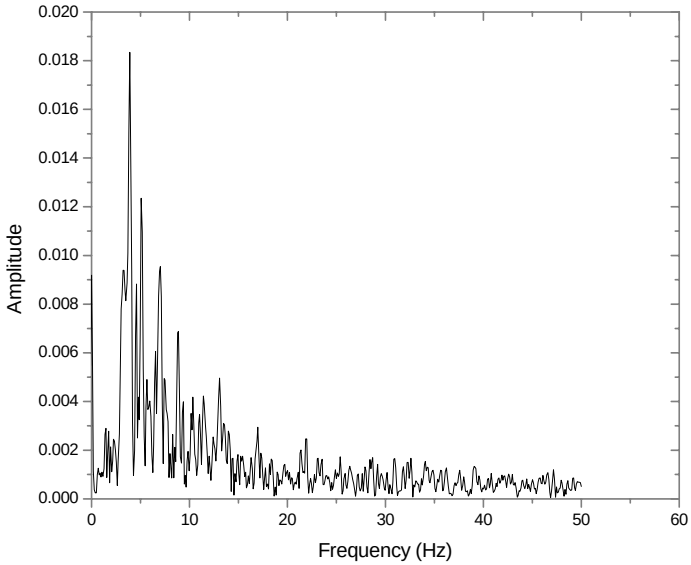

Figure 4.9: Fourier spectrum of the output e-wave showing a spike at the expected characteristic frequency Γ = 4 Hz. Pump laser power: 270 mW; Laser wavelength: 1550 nm; sample thickness: 250 μm; Laser spot diameter: 100 μm.

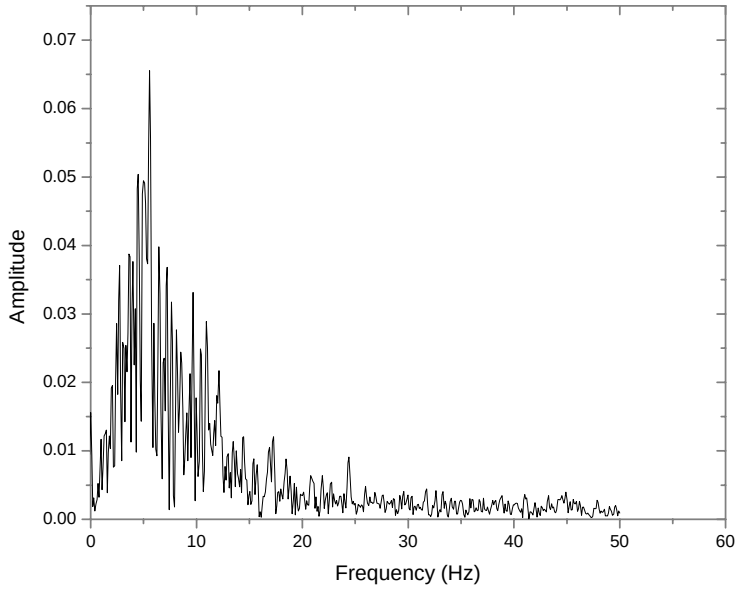

Figure 4.10: Fourier spectrum of the output e-wave showing a spike at the expected characteristic frequency Γ = 4 Hz. Pump laser power: 410 mW; Laser wavelength: 1550 nm; sample thickness: 250 μm; Laser spot diameter: 100 μm.

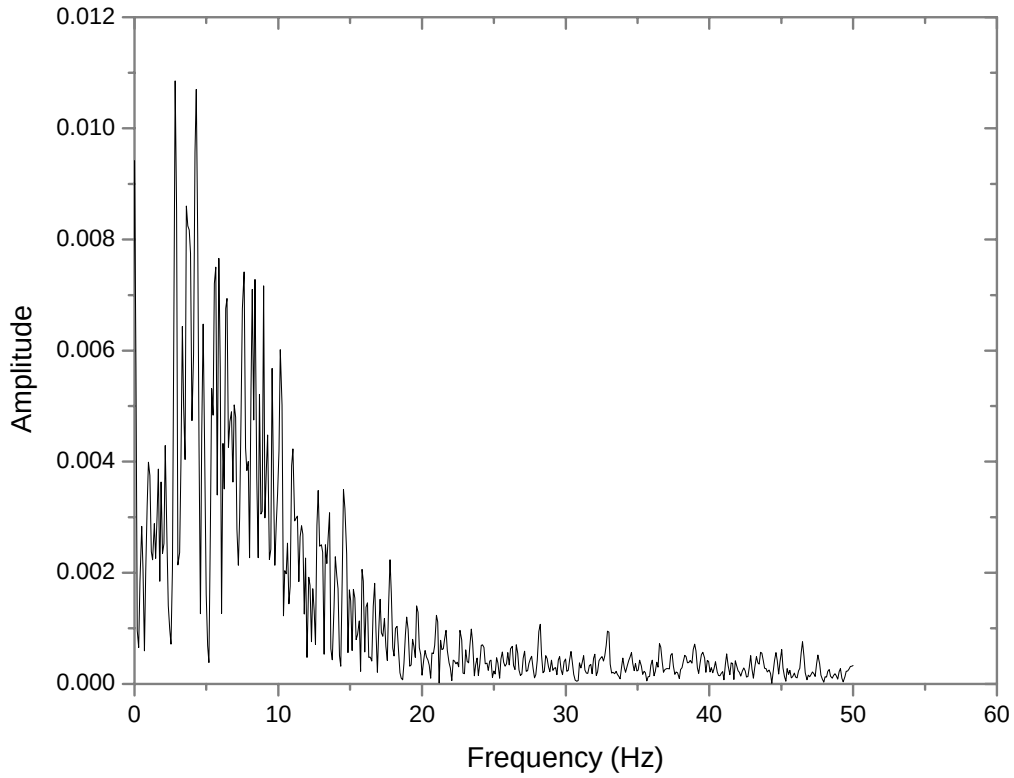

Figure 4.11: Fourier spectrum of the output e-wave showing a spike at the expected characteristic frequency Γ = 4 Hz. Pump laser power: 680 mW; Laser wavelength: 1550 nm; sample thickness: 250 μm; Laser spot diameter: 100 μm.

4.3 AC Modulation of the Time-varying SOS Effect

The influence of a low-frequency external AC field to the steady-state SOS effect has already been presented in the previous chapter. As discussed in the previous section, the oscillation of the induced NLC director reorientation grating is centered around the

characteristic frequency which is defined as $\Gamma = K_2 q^2 / \eta = 1/\tau$. For a common NLC like E7, this characteristic frequency is about 4 -32 Hz for different pump beam wavelengths (4 Hz for 1.55 μm and 32 Hz for 0.532 μm). Since the orientation of the NLC director can be influenced by an external electric field, the application of an external low-frequency AC field will interact with the reorientation of the NLC director and influence the dynamics of this reorientation process.

As we can infer from the dynamical equations (Equation 4.1-3) governing the director axis reorientation, the applied low frequency field would contribute to the process when its magnitude is comparable to the optical threshold field, i.e. field strength of kV/cm. In the experiment, two aluminum electrodes are mounted on the side of a 250 μm thick E7 nematic film and an AC voltage of varying frequency is applied in the transverse [*y*-] direction. The separation between the electrodes is 2 mm and the voltage used is 200 Volts, i.e. the ac field amplitude is 1 kV/cm. Figure 4.12(a) shows the Fourier spectrum of the generated signal at an input visible (0.532 μm) pump laser power of 20mW when there is no external AC modulation field. The pump beam power is just below the threshold and there is no significant stimulated scattering signal. The Fourier spectrum shows no prominent peak. With the application of an external low-frequency AC field, the phase-matched scattering signal is able to grow into a coherent laser and there is a prominent peak at the characteristic frequency of the NLC director reorientation as shown in Figure 4.12(b).

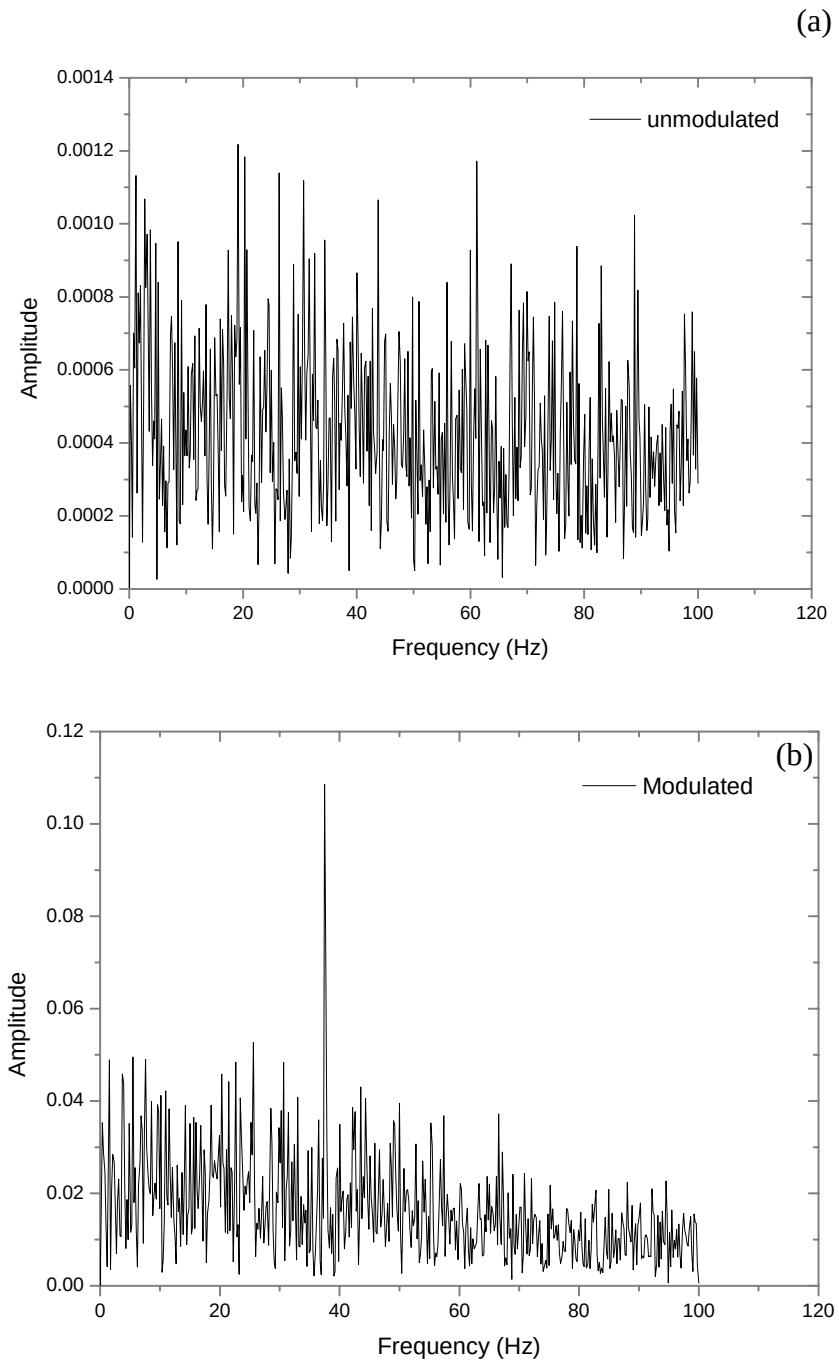

Figure 4.12: (a) Fourier spectrum of the stimulated signal without the external AC modulation field; (b) Fourier spectrum with the external AC modulation field. Laser wavelength: 532 nm; Sample thickness: 250 μm; input laser power: 28.9 mW; Laser focal spot diameter: 40 μm; AC field strength 1kV/cm.

By changing the amplitude of the external modulation field, the power of the output beams changes accordingly as shown in the Figure 4.13. Without the low-frequency modulation field (V=0), the ratio of the stimulated signal to the transmitted signal is about 0.55. This ratio decreases to about 0.4 when the voltage is increased to 50V for a NLC film of 250 μm thick. After that, the ratio of the stimulated signal to the transmitted signal increases almost linearly with the increase in the amplitude of the external modulation AC field.

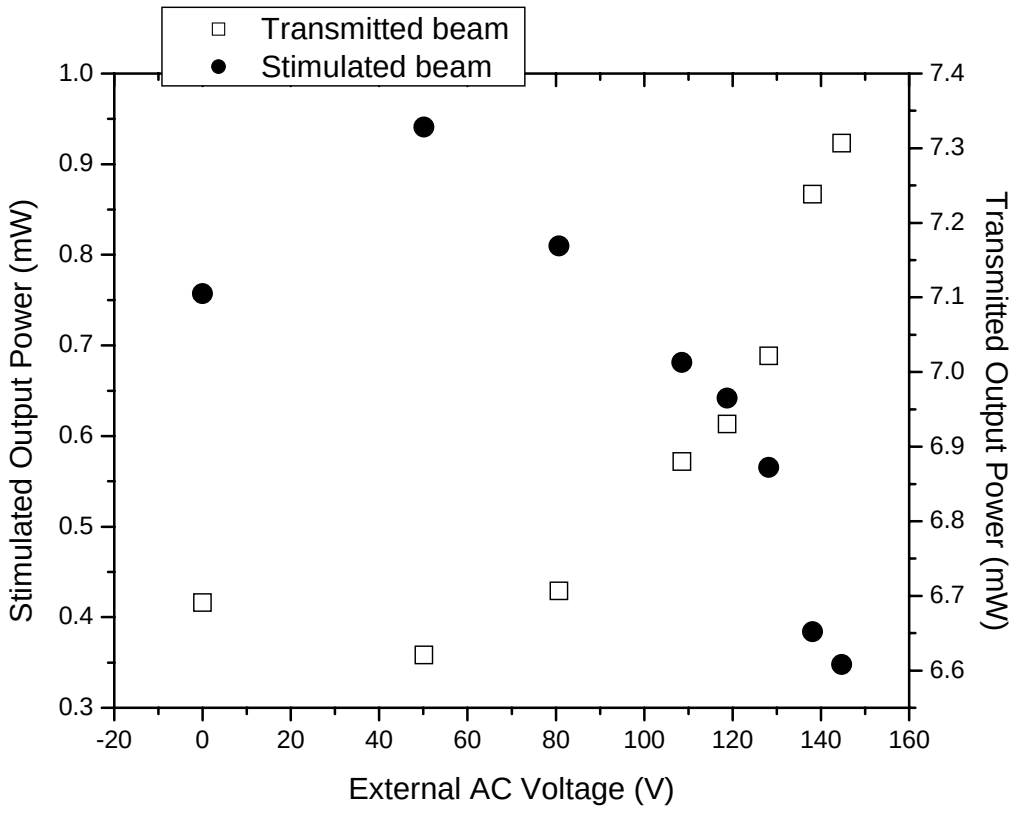

Figure 4.13: The power of the stimulated and transmitted beams vs. the amplitude of the external AC modulation field. Laser wavelength: 532 nm; Sample thickness: 250 μm; input laser power: 28.9 mW; Laser focal spot diameter: 40 μm.

In addition to the influence due to the amplitude of the external low-frequency AC modulation field, the response of the generated signal to the change of the modulation field frequency is also investigated as shown in Figure 4.14. With the application of an external modulation field, the power of the generated beam has significantly increased.

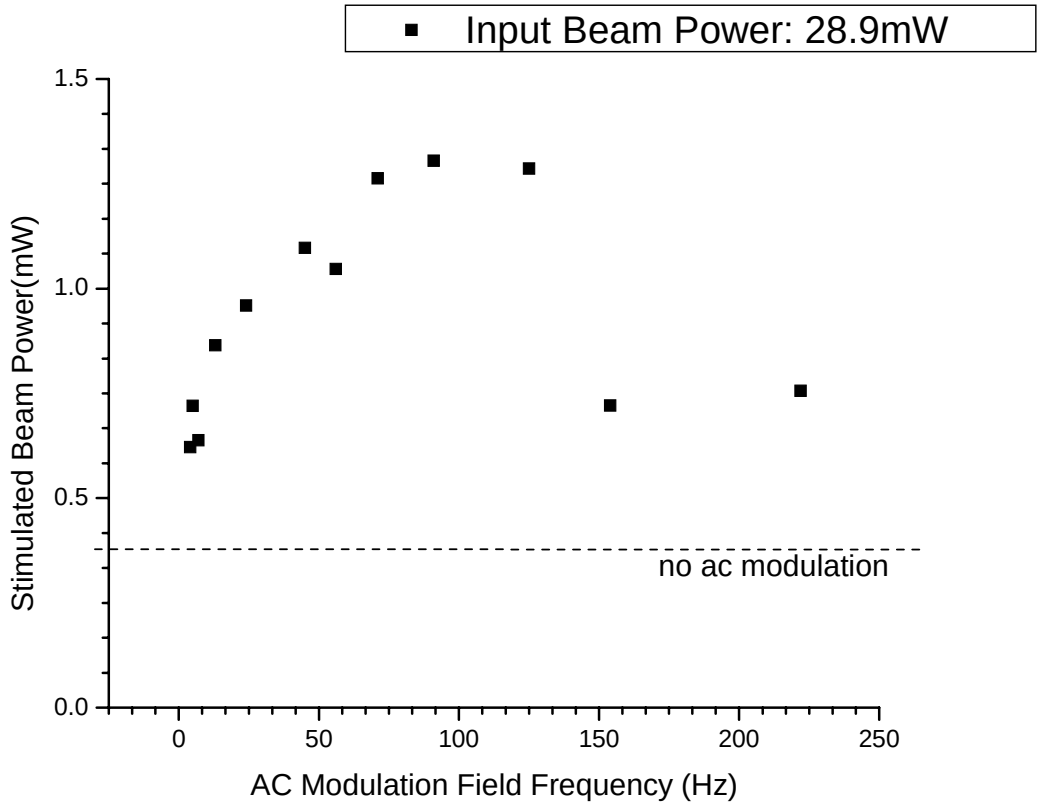

Figure 4.14: Observed average generated output power dependence on the applied ac modulation frequency showing enhanced stimulated scattering efficiency when the applied ac field amplitude is comparable to the optical field. Laser wavelength: 532 nm; Sample thickness: 250 μm; input laser power: 28.9 mW; Laser focal spot diameter: 40 μm.

With the application of a low-frequency AC field, in general, the stimulated scattering efficiency is enhanced, as demonstrated by Figure 4.13-14 and new oscillation components are created, c.f. Figure 4.15-17. For example, with a 35 Hz modulated applied AC voltage, “peaks” are observed in the Fourier spectrum at 35 Hz and its harmonics of 70 Hz, and also at the characteristic frequency of 32 Hz and its harmonic of 64 Hz, c.f. Figure 4.15. This is perhaps the first instance where an applied ac field could influence laser induced stimulated scattering. It is simply due to the rather low optical threshold field [~ kV/cm] for stimulated scattering in nematic liquid crystals, in contrast to other nonlinear materials [Zeldovich 1985] that require orders of magnitude higher threshold field.

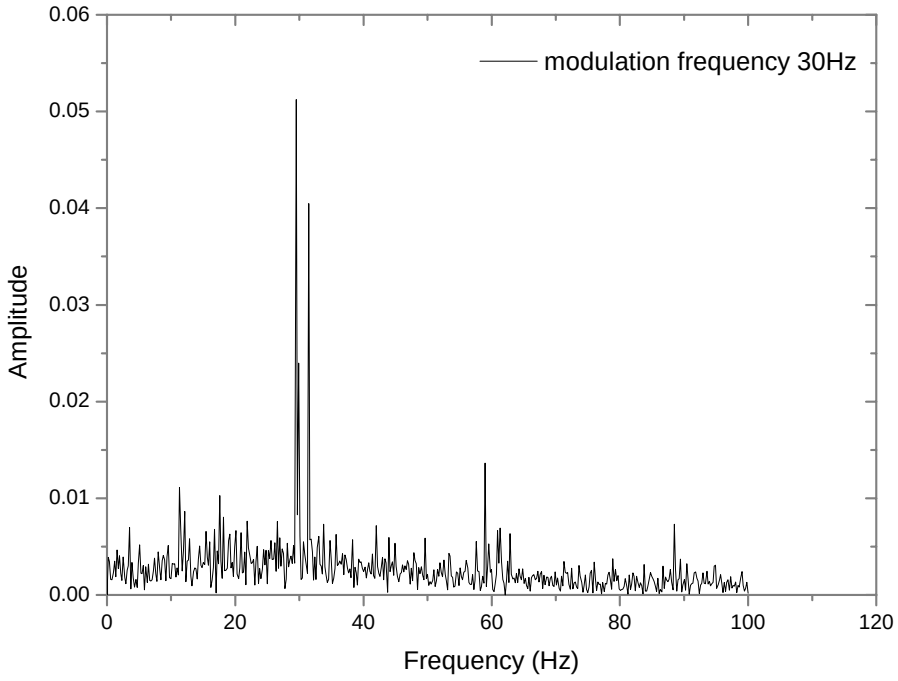

Figure 4.15: Modulation ac frequency: 30 Hz. Distinctive peaks occur at the harmonics of the AC frequency:30, 60, and 90 Hz and at the characteristic frequency of 32 Hz

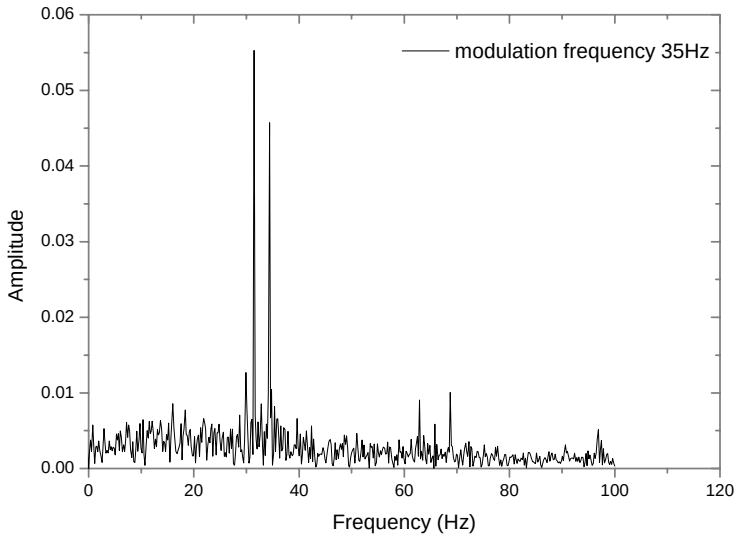

Figure 4.16: Modulation ac frequency: 35 Hz. Distinctive peaks occur at the harmonics of the AC frequency: 35 and 70 and at the characteristic frequency of 32 Hz and its harmonic of 64 Hz..

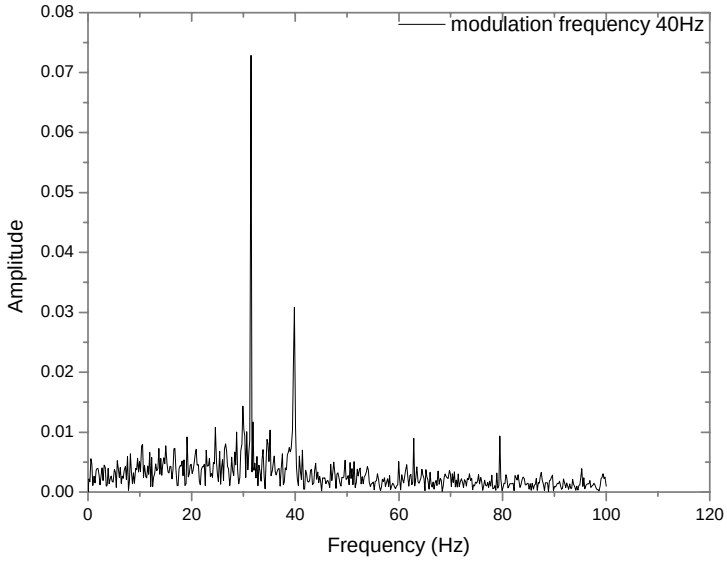

Figure 4.17: Modulation ac frequency: 40 Hz. Distinctive peaks occur at the harmonics of the AC frequency:40 and 80 and at the characteristic frequency of 32 Hz and its harmonic of 64 Hz.

As shown in Figure 4.18, the response time of this director orientational phenomenon to an external AC modulation electric field is in the order of seconds. In accordance with the previous experimental reports, the application of an external AC modulation field increases the amplitude of the stimulated signal while the stimulated noise signal remains oscillating. After the removal of the AC modulation field, the stimulated signal decays in about 1 second.

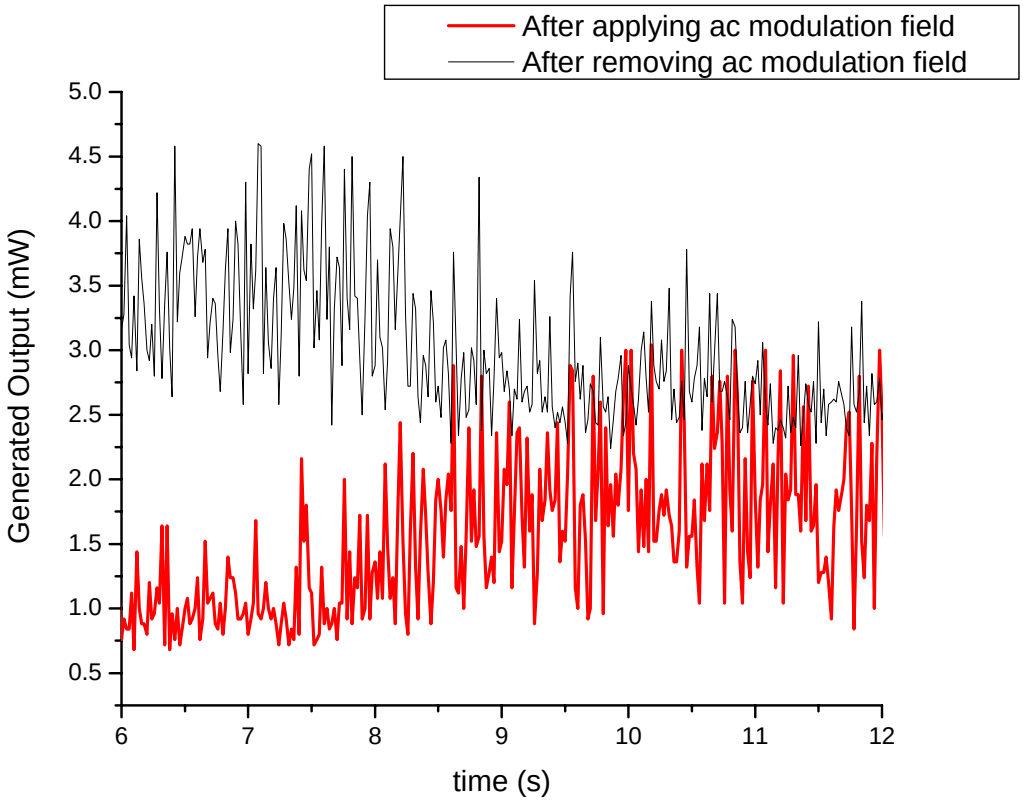

Figure 4.18: Temporal response of the stimulated signal with the addition/removal of the external AC modulation field.

4.4 Conclusion

A concise account of our experimental studies of dynamical behaviors of laser induced stimulated orientation scattering in nematic liquid crystal is presented in this chapter. The observed energy exchange between the driving and generated waves, frequency spectra of their intensity oscillations associated with the evolution of scattered noise to coherent beams, and other temporal and parametric dependencies are consistent with theoretical expectations. The enhancement to the SOS effect and the appearance of frequency harmonics, with the application of an external low-frequency modulating AC field, provide another means of control of the stimulated scattering process/devices. In addition, the control from the external modulation field provides a new ground for further fundamental pursuits similar to previous studies on route to chaos and control of nonlinear dynamics [Carbone 2001, Russo 2000]. These observations are reminiscent of "stochastic" oscillations that were observed in stimulated back scattering in photorefractive crystals [Odoulov 1996]. The driven coupled oscillators model and the build up of noise to a coherent signal also resembles the coupled-oscillators-neural-network model which shows how arbitrary, randomly assembled oscillators can establish a desired "coherent" configuration [Hoppensteadt 1999]. In these regards, nematic liquid crystals remain an interesting and low-power nonlinear material for practical simulations and understanding of fundamental processes in many disciplines [Khoo 2005].

Chapter 5

Photorefractivity in Nematic Liquid Crystalline Materials

The photorefractive (PR) effect refers to the spatial modulation of the refractive index generated by the light-induced space charge field in a material in which the refractive index depends upon electric field(s). The PR effect has many important applications including high density optical data storage, image processing (correlation, pattern recognition), spatial light modulation, phase conjugation, optical limiting, simulations of neural networks and associative memories, and programmable optical interconnection [Brown 2002, Gooneseker 2000, Gunter 1989].

In the pursuit of improved photorefractive materials, liquid crystals were found to be a very good candidate because they provide much larger nonlinearity (implying larger diffraction efficiency, thus stronger photorefractive effect) than traditional organic photorefractive crystals, due to their large anisotropy and director reorientational characteristics [Khoo 1994a, Khoo 1994b].

5.1 General Description of Photorefractivity

The photorefractive effect in some electro-optic materials, such as $LiNbO_3$, SBN, dye-doped liquid crystals, can lead to large optical gains through optical wave-mixing, as well as large refractive index changes without requiring high-power lasers [Fazio 2003].

As a result, photorefractive materials are becoming increasingly important in the field of nonlinear optics.

It is generally believed that the photorefractive effect arises from photon-generated charge carriers which migrate and redistribute when the material is illuminated by a spatially-varying optical field with sufficient energy. Migration of the generated charge carriers and differences in the drift and diffusion coefficients for positive and negative charges produce a space-charge separation, which then gives rise to a strong space-charge field. Such a field in turn induces a refractive index change in the medium. There is an important difference between liquid crystals and other usual photorefractive crystals (such as $LiNbO_3$) in how the refractive index arises. In usual photorefractive crystals the refractive index change is induced by the space-charge via the Pockel's effect, which means the refractive index is proportional to the magnitude of the space-charge field. In contrast, the refractive index change in liquid crystals is associated with the reorientation of the liquid crystal director and is quadratically dependent on the applied field. This latter mechanism may be termed as a Kerr response.

The mechanism underlining the photorefractive effect is best illustrated by the band transport model as shown in Figure 5.1. According to this model, a photorefractive material contains deep and shallow traps of opposite sign. These traps will be identified by impurities or defects in photorefractive materials. Assuming the deep traps are donors, the shallow traps are acceptors and the charge carriers are electrons, the concentration of donors is greater than that of acceptors and hence the shallow acceptors are completely filled by electrons in the photorefractive effect. The shallow traps function to produce empty sites in deep donors so that electrons can move among those empty sites by

ionization or recombination. In the case of very deep donor levels, thermal excitation is negligibly small. The photorefractive effect is induced by a non-uniform light illumination. Free charge carriers are produced by the photo-ionization from the deep traps to the conduction band in bright regions. They then transport to the dark regions, where the free electron concentration is smaller, by diffusion and drift. The free carriers recombine with ionized deep traps in the dark regions. At equilibrium, a space charge field is formed to balance the diffusion from the charge carrier concentration gradient and the drift from the electric field. This space charge field then changes the refractive index by the electro-optic effects.

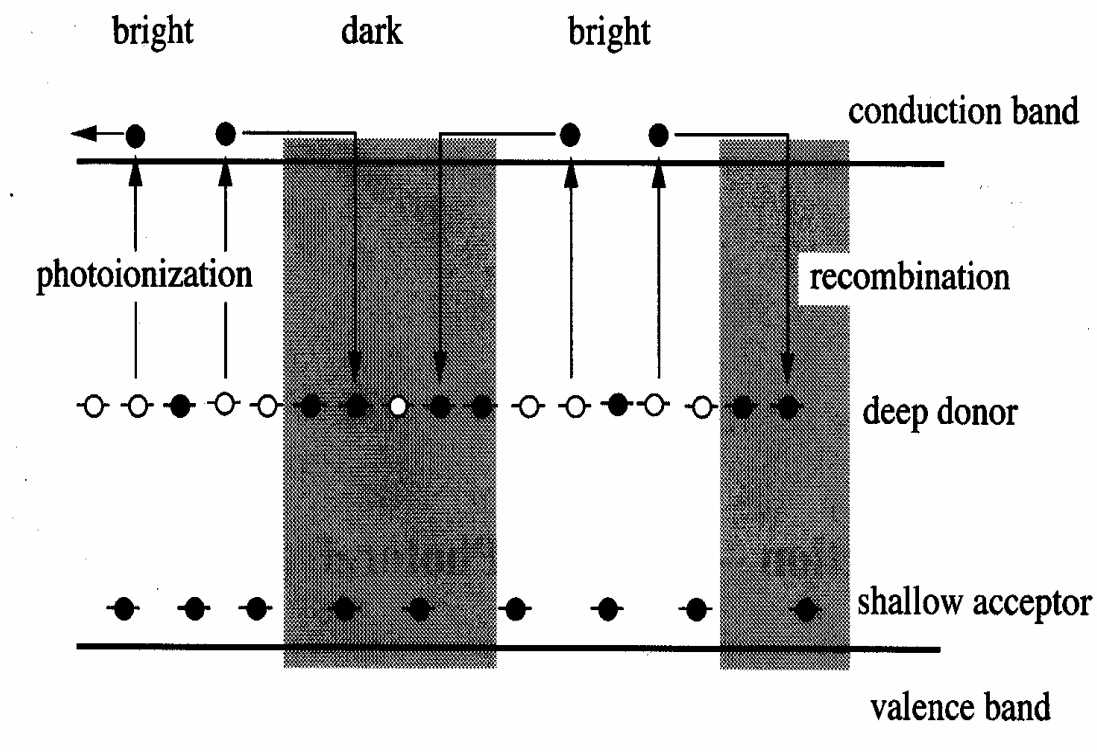

Figure 5.1: Band transport model of the photorefractive effect.

Both linear and quadratic electro-optic effects are able to induce the photorefractive effect. Experiments have shown that an external electric field is necessary to form diffraction gratings when the quadratic electro-optic effect is utilized. As mentioned above, nematic liquid crystals utilize the quadratic electro-optic effect to achieve photorefractivity and this phenomenon will be discussed in details in the following sections. For the linear electro-optic effect, the index change is given by:

$$\Delta n = \frac{1}{2} n^3 r_{eff} E_{sc} \qquad \text{Equation 5.1}$$

where n is the average refractive index, r_{eff} is the effective linear electro-optic coefficient which depends on the orientation of the crystal and the polarization of the light, and E_{sc} is the space charge field generated.

5.2 Theoretical Analysis of Photorefractivity in Dye Doped NLCs

The analysis of photorefractivity in dye-doped NLCs consists of two parts: generation of the space charge field and the reorientation of the NLC director under the influence of the space charge field. As shown in Figure 5.2**,** under the illumination of a non-uniform optical field, the photo-sensitive dyes in liquid crystals will generate non-uniform charge distribution within the medium. Due to the disparity in diffusion and drift coefficients, the generated positive and negative charges will separate and form a non-uniform space charge field when they reach the equilibrium state. As described before, the NLC director would reorientate subjecting to an electrical or magnetic field. This induced non-uniform space charge field will tend to align the NLC director locally and

change the local refractive index of the NLC medium, due to the anisotropy of liquid crystals. The large anisotropy (~0.2) of liquid crystals makes them great candidates for highly effective photorefractive devices.

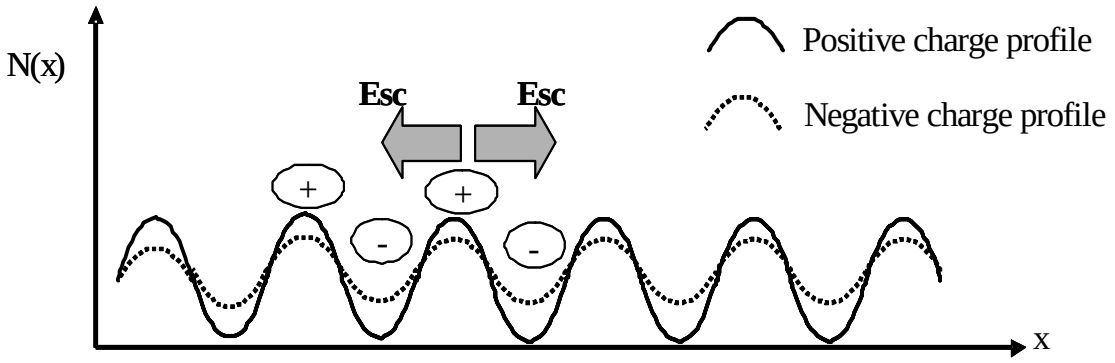

Figure 5.2: Intensity profile of the illumination field and the resulting space charge formation.

5.2.1 Space Charge Field

Assuming a photorefractive material is illuminated by an optical field with sinusoidally modulated intensity profile:

$$I = I_0(1 + m\sin qx)\exp(-\beta z) \qquad \text{Equation 5.2}$$

where $q = 2\pi/\Lambda$ is the grating vector and *m* is the modulation depth. Based on the band transport model mentioned in section 5.1, the continuity equation inside the medium is:

$$\frac{\partial n^{\pm}}{\partial t} = \alpha I(x) - \frac{n^{\pm}}{\tau} + D^{\pm}\frac{\partial^2 n^{\pm}}{\partial x^2} \mp \mu^{\pm}\frac{\partial (En^{\pm})}{\partial x} \qquad \text{Equation 5.3}$$

where $n^{\pm}$ are the positive and negative charge carrier densities respectively, $D^{\pm}$ are the diffusion constants of positive and negative carriers, $\mu^{\pm}$ are the drift coefficients of positive and negative carriers, τ is the carrier life time, E is the external applied electric field along the *x* direction, $I(x)$ is the illumination field, and α is the photo-ionization constant of the medium. At the steady state, the continuity equation is simplified to:

$$0 = \alpha I(x) - \frac{n^{\pm}}{\tau} + D^{\pm}\frac{\partial^2 n^{\pm}}{\partial x^2} \mp \mu^{\pm}\frac{\partial (En^{\pm})}{\partial x} \qquad \text{Equation 5.4}$$

Because there is no external electric field along the *x* direction, there is no drift movement along *x* direction. So the equation is further simplified as:

$$0 = \alpha I(x) - \frac{n^{\pm}}{\tau} + D^{\pm}\frac{\partial^2 n^{\pm}}{\partial x^2} \qquad \text{Equation 5.5}$$

It is natural to assume both positive and negative carriers follow the spatial pattern of the illuminating optical field as:

$$n^{\pm} = [n_0^{\pm} + n_1^{\pm}\sin(qx)]\exp(-\beta z) \qquad \text{Equation 5.6}$$

In this case the continuity equation is expressed as:

$$0 = \alpha I_0 + \alpha I_0 m\sin(qx) - \frac{n_0^{\pm}}{\tau} - \frac{n_1^{\pm}}{\tau}\sin(qx) - D^{\pm}q^2\sin(qx) \qquad \text{Equation 5.7}$$

After separating the terms with and without sinusoidal spatial modulation ($\sin qx$), the above equation can be simplified into two equations:

$$\alpha I_0 = \frac{1}{\tau}n_0^{\pm} \qquad \text{Equation 5.8}$$

$$\alpha I_0 m\sin(qx) = (\frac{1}{\tau} + D^{\pm}q^2)n_1^{\pm}\sin(qx) \qquad \text{Equation 5.9}$$

Then the space charge density can be analytically solved as:

$$\begin{aligned} n^{\pm} &= [n_0^{\pm} + n_1^{\pm} \sin qx]\exp(-\beta z) \\ &= \alpha I_0[\tau + \frac{m\tau}{1+\tau D^{\pm} q^2}\sin(qx)]\exp(-\beta z) \end{aligned} \qquad \text{Equation 5.10}$$

Thus the net charge distribution is:

$$\begin{aligned} \rho(x) &= en^{+} - en^{-} \\ &= e[\frac{\alpha I_0 m\tau}{1+\tau D^{+} q^2} - \frac{\alpha I_0 m\tau}{1+\tau D^{-} q^2}]\sin(qx)\exp(-\beta z) \\ &= \frac{e\alpha I_0 m\tau (D^{-} - D^{+}) q^2}{(1+\tau D^{+} q^2)(1+\tau D^{-} q^2)}\sin(qx)\exp(-\beta z) \end{aligned} \qquad \text{Equation 5.11}$$

This sinusoidal charge distribution still obeys the charge neutrality because the total charge within each grating period is 0, which is in a good agreement with the original condition of no external electric field. However there is an induced space-charge field within each grating period by integrating the Gauss's Law

$$\nabla \cdot \vec{E} = \rho / \varepsilon \qquad \text{Equation 5.12}$$

The space charge field has the form:

$$\begin{aligned} E_{sc}(x) &= \frac{e\alpha I_0 m\tau (D^{+} - D^{-}) q}{\varepsilon(1+\tau D^{+} q^2)(1+\tau D^{-} q^2)}\cos(qx)\exp(-\beta z) \\ &= E_{sc}\cos(qx)\exp(-\beta z) \end{aligned} \qquad \text{Equation 5.13}$$

The magnitude of this space charge field is noted as:

$$E_{sc} = \frac{e\alpha I_0 m\tau (D^{-} - D^{+}) q}{\varepsilon(1+\tau D^{+} q^2)(1+\tau D^{-} q^2)} \qquad \text{Equation 5.14}$$

It is no surprise that the space-charge field equals zero when the diffusion constants are the same for positive and negative charge carriers, because no charge separation would occur when the positive and negative charge carriers move in the same speed. Without

charge separation, the medium is neutral everywhere. It is also worth-noting that the generated space charge field is π/2 shifted from the illuminating interference grating in phase. This phase shift is the origin of the two-wave amplification as discussed in these literatures. The space charge field is proportional to the material's photo-sensitivity α, modulation depth and intensity of the input optical field. The maximum of the space charge field occurs when

$$\frac{1}{q^2} = \frac{1}{2}\tau(\sqrt{D^{+2} + D^{-2} + 14D^{+}D^{-}} - (D^{+} + D^{-})) \qquad \text{Equation 5.15}$$

5.2.2 Director Reorientation due to the Space Charge Field

As discussed in the precious chapters, an electric field will reorientate the NLC director to minimize the free energy of the system. The generated space charge field in photorefractive liquid crystals will introduce local reorientation of the NLC director. This director reorientation will in turn cause change to the local refractive index distribution. Illustration of how the NLC director reorients is shown in Figure 5.3. The analysis of this space charge field induced refractive index grating in photorefractive liquid crystals requires the knowledge of the NLC director reorientation under electrical fields.

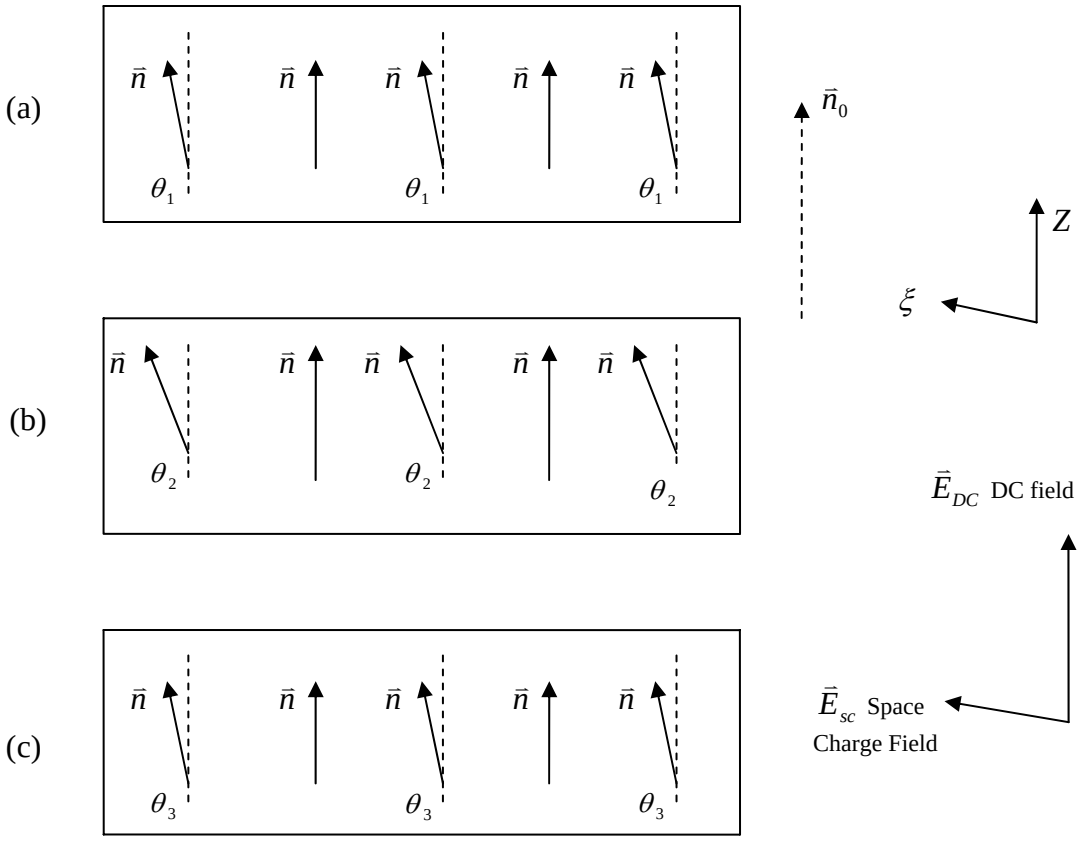

Figure 5.3: NLC director reorientation under the space charge field and the applied DC field.

To simplify the discussion, consider the interaction geometry as shown in Figure 5.4. Two coherent laser beams are obliquely incident on a NLC film confined within two pieces of ITO coated glass, which are connected to an external DC voltage source. In order to achieve photorefractivity, the addition of an external DC voltage across the sample (along *z*-axis) is necessary as reported in the previous research works [Khoo 1995]. This DC field will work together with the space charge field to achieve

appropriate NLC director reorientation distribution. However, the DC field would generate heat in the medium and even destroy the crystalline structure when the voltage is high enough. This limitation restrains the highest DC voltage that can be applied.

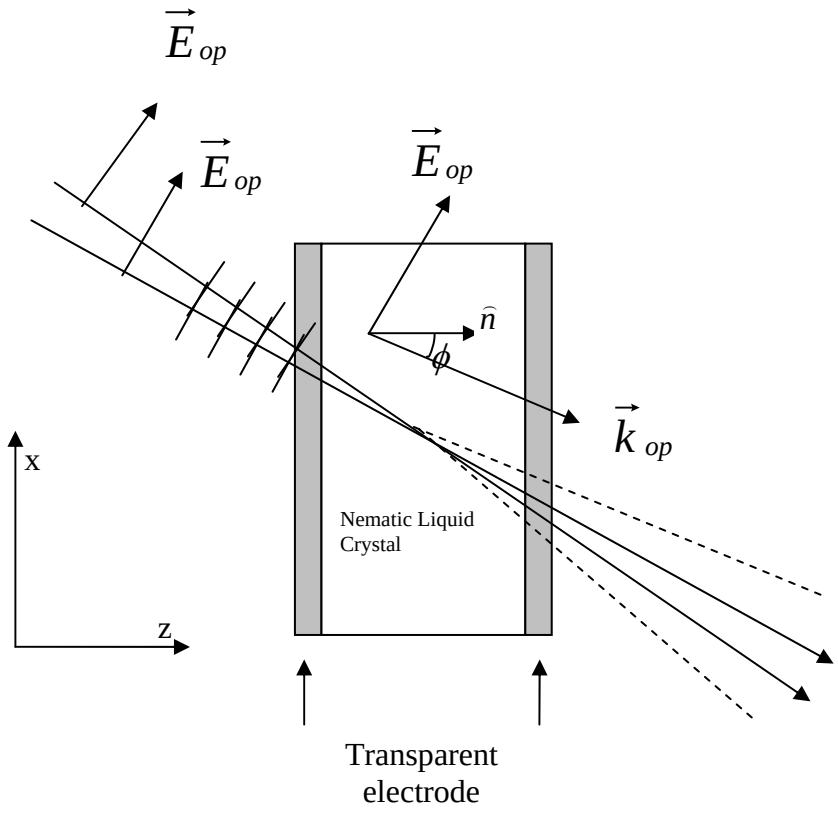

Figure 5.4: Interaction geometry for photorefractive NLC film

Immediately after the *x*-directed light-induced space charge field causes director reorientation in the *x*-*z* plane, there is a transverse field $\vec{E}_{\Delta\varepsilon}$ due to the dielectric anisotropy of liquid crystals as Equation 5.16 [Khoo 1996]:

$$\vec{E}_{\Delta\varepsilon} = -\frac{[\varepsilon_a \sin\theta\cos\theta]}{[\varepsilon_{\parallel}\sin^2\theta + \varepsilon_{\perp}\cos^2\theta]} E_{DC}\hat{x} \qquad \text{Equation 5.16}$$

The dielectric anisotropy induced electric field will generate a new space charge field $\vec{E}_{\Delta\sigma}$ due to the conductivity anisotropy until the resulting transverse fields stop the transverse currents as:

$$\vec{E}_{\Delta\sigma} = \frac{[\sigma_a \sin\theta\cos\theta]}{[\sigma_{\parallel}\sin^2\theta + \sigma_{\perp}\cos^2\theta]} E_{DC}\hat{x} \qquad \text{Equation 5.17}$$

where $\sigma_a = \sigma_{\parallel} - \sigma_{\perp}$ is the conductivity anisotropy of the liquid crystal and $\varepsilon_a = \varepsilon_{\parallel} - \varepsilon_{\perp}$ is the dielectric anisotropy, and θ is the reorientational angle. The conductivities $\sigma_{\parallel}$, $\sigma_{\perp}$ and the corresponding conductivity anisotropy are functions of the illuminating laser intensity as well. Notice for small θ, $\vec{E}_{\Delta\sigma}$ and $\vec{E}_{\Delta\varepsilon}$ can be simplified as:

$$\vec{E}_{\Delta\varepsilon} \approx -\frac{\varepsilon_a}{\varepsilon_{\perp}}\theta E_{DC}\hat{x}$$
$$\vec{E}_{\Delta\sigma} \approx +\frac{\sigma_a}{\sigma_{\perp}}\theta E_{DC}\hat{x} \qquad \text{Equation 5.18}$$

Assuming the interference pattern formed by the two coherent lasers is along the glass surface (*x*-direction). Then the generated space charge field is along the *x*-direction too with the effective grating constant $q_{eff} = q\cos\phi$. The total electric field is:

$$\vec{E} = E_x\hat{x} + E_z\hat{z} \qquad \text{Equation 5.19}$$

where

$$E_x = E_{sc}\cos(q_{eff}x)\exp(-\beta z) + E_{\Delta\sigma} + E_{\Delta\varepsilon} \qquad \text{Equation 5.20}$$

is the generated space charge field and

$$E_z = \frac{V_{DC}}{d} \qquad \text{Equation 5.21}$$

is the external DC field across the sample, V_{DC} is the applied DC voltage, d is the sample thickness.

This reorientation process of the NLC director has no difference to the director reorientation process in the SOS effect. The establishment of the equilibrium state is described by the same ELR equation:

$$\frac{\partial}{\partial x_j}\frac{\delta f}{\delta(\partial U_m/\partial x_j)} - \frac{\delta f}{\delta U_m} - \frac{\delta R}{\delta \dot{U}_m} = 0 \qquad \text{Equation 5.22}$$

As mentioned before, there are two typical alignments of NLC cells for photorefractivity: homeotropic or homogeneous. In this report, we limit our investigation on homeotropic samples. But in general, both alignments are capable of generating director reorientation under the induced space charge field and the external DC field. The analysis here for homeotropic NLC film is also suitable to homogeneous film. In a homeotropic cell, the initial NLC director is $\vec{n}_0 = \{0,0,1\}$ as the director axis lies in *z*-direction without external perturbation. Under the influence of the total electric field $\vec{E}$ bearing the form of Equation 5.19 , the NLC director will only reorientate in the *x*-*z* plane. Assuming the reorientation angle is θ, then the new NLC director can be expressed as:

$$\vec{n} = \{\sin\theta(x,z,t), 0, \cos\theta(x,z,t)\} \qquad \text{Equation 5.23}$$

The dissipative function density can be simplified as:

$$
\begin{aligned}
R &= \frac{1}{2}\eta\dot{\vec{n}}^2 \\
&= \frac{1}{2}\eta\dot{\vec{n}}\cdot\dot{\vec{n}} \\
&= \frac{1}{2}\eta\left[\frac{d}{dt}\{\sin\theta,0,\cos\theta\}\cdot\frac{d}{dt}\{\sin\theta,0,\cos\theta\}\right] \\
&= \frac{1}{2}\eta\left[\frac{d\theta}{dt}\{\cos\theta,0,-\sin\theta\}\cdot\frac{d\theta}{dt}\{\cos\theta,0,-\sin\theta\}\right] \\
&= \frac{1}{2}\eta\dot{\theta}^2
\end{aligned}
$$

Equation 5.24

The dielectric tensor changes accordingly to:

$$
\varepsilon = \begin{pmatrix}
\varepsilon_\perp + \varepsilon_a \sin^2\theta(x,z,t) & 0 & \varepsilon_a \cos\theta(x,z,t)\sin\theta(x,z,t) \\
0 & \varepsilon_\perp & 0 \\
\varepsilon_a \cos\theta(x,z,t)\sin\theta(x,z,t) & 0 & \varepsilon_\perp + \varepsilon_a \cos^2\theta(x,z,t)
\end{pmatrix}
$$

Equation 5.25

The resulting elastic free energy is:

$$
\begin{aligned}
f_{elastic} &= \frac{1}{2}K_1(\nabla\bullet\vec{n})^2 + \frac{1}{2}K_2(\vec{n}\bullet(\nabla\times\vec{n}))^2 + \frac{1}{2}K_3(\vec{n}\times(\nabla\times\vec{n}))^2 \\
&= \frac{1}{2}K_1\left(\frac{d\theta}{dx}\right)^2\cos^2\theta + \frac{1}{2}K_3\left(\frac{d\theta}{dx}\right)^2\{0,-\cos\theta\sin\theta,\sin^2\theta\}^2 \\
&= \frac{1}{2}K_1\left(\frac{d\theta}{dx}\right)^2\cos^2\theta + \frac{1}{2}K_3\left(\frac{d\theta}{dx}\right)^2\sin^2\theta
\end{aligned}
$$

Equation 5.26

The free energy due to the electric field is:

$$
\begin{aligned}
f_{elastic} &= -\frac{1}{2}\varepsilon_{ij}E_iE_j \\
&= -\frac{1}{2}\varepsilon_0[(\varepsilon_\perp + \varepsilon_a\sin^2\theta(x,t))\left|E_x\right|^2 + \varepsilon_a\sin\theta(x,t)\cos\theta(x,t) \\
&\quad (E_xE_z^{\ *} + E_x^{\ *}E_z) + (\varepsilon_\perp + \varepsilon_a\cos^2\theta(x,t))\left|E_z\right|^2]
\end{aligned}
$$

Equation 5.27

Choosing the director reorientational angle θ as the independent variable and plugging the expression of the free energy and dissipative function into the ELR equation, the first term in ELR equations can be expressed as:

$$\begin{aligned}\frac{\partial}{\partial x_j}\frac{\delta f}{(\partial U_m/\partial x_j)} &= \frac{\partial}{\partial x}\left[\frac{\delta f}{\delta(d\theta/dx)}\right]+\frac{\partial}{\partial z}\left[\frac{\delta f}{\delta(d\theta/dz)}\right] \\ &= [K_1\sin^2\theta + K_3\cos^2\theta]\frac{d^2\theta}{dz^2}+[K_1-K_3]\sin 2\theta\left(\frac{d\theta}{dz}\right)^2 \\ &+[K_1\cos^2\theta + K_3\sin^2\theta]\frac{d^2\theta}{dx^2}+[K_3-K_1]\sin 2\theta\left(\frac{d\theta}{dx}\right)^2 \\ &-[K_1-K_3]\sin 2\theta\frac{d^2\theta}{dxdz}-2[K_1-K_3]\cos 2\theta\frac{d\theta}{dx}\frac{d\theta}{dz}\end{aligned} \qquad \text{Equation 5.28}$$

Following a similar procedure, the second term in the ELR equation can also be analytically solved:

$$\begin{aligned}-\frac{\delta f}{\delta U_m} &= -\frac{\delta f}{\delta\theta} \\ &= \varepsilon_0\varepsilon_a[E_{sc}(x)\cos\theta + E_{DC}(\frac{\sigma_a}{\sigma_\perp}-\frac{\varepsilon_a}{\varepsilon_\perp})\theta\cos\theta - E_{DC}\sin\theta] \\ &[E_{sc}(x)\sin\theta + E_{DC}(\frac{\sigma_a}{\sigma_\perp}-\frac{\varepsilon_a}{\varepsilon_\perp})\theta\sin\theta + E_{DC}\cos\theta]+ \\ &\varepsilon_0\varepsilon_o[E_{sc}(x)\cos\theta + E_{DC}(\frac{\sigma_a}{\sigma_\perp}-\frac{\varepsilon_a}{\varepsilon_\perp})\theta\cos\theta - E_{DC}\sin\theta] \\ &E_{DC}(\frac{\sigma_a}{\sigma_\perp}-\frac{\varepsilon_a}{\varepsilon_\perp})\cos\theta + \varepsilon_0\varepsilon_e[E_{sc}(x)\sin\theta + \\ &E_{DC}(\frac{\sigma_a}{\sigma_\perp}-\frac{\varepsilon_a}{\varepsilon_\perp})\theta\sin\theta + E_{DC}\cos\theta]E_{DC}(\frac{\sigma_a}{\sigma_\perp}-\frac{\varepsilon_a}{\varepsilon_\perp})\sin\theta \\ &+\frac{1}{2}[K_1-K_3]\sin 2\theta\left(\frac{d\theta}{dx}\right)^2+\frac{1}{2}[K_3-K_1]\sin 2\theta\left(\frac{d\theta}{dz}\right)^2 \\ &+(K_1-K_3)\cos 2\theta\left(\frac{d\theta}{dx}\right)\left(\frac{d\theta}{dz}\right)\end{aligned} \qquad \text{Equation 5.29}$$

Putting together all three terms in the ELR equation and plugging in the expression of the space charge field, we get the following expression:

$$\begin{aligned}
\eta\dot{\theta} &= \varepsilon_0\varepsilon_a[E_{sc}\cos qx\cos\theta + E_{DC}(\frac{\sigma_a}{\sigma_\perp}-\frac{\varepsilon_a}{\varepsilon_\perp})\theta\cos\theta - E_{DC}\sin\theta] \\
&[E_{sc}\cos qx\sin\theta + E_{DC}(\frac{\sigma_a}{\sigma_\perp}-\frac{\varepsilon_a}{\varepsilon_\perp})\theta\sin\theta + E_{DC}\cos\theta] + \\
&\varepsilon_0\varepsilon_o[E_{sc}\cos qx\cos\theta + E_{DC}(\frac{\sigma_a}{\sigma_\perp}-\frac{\varepsilon_a}{\varepsilon_\perp})\theta\cos\theta - E_{DC}\sin\theta] \\
&E_{DC}(\frac{\sigma_a}{\sigma_\perp}-\frac{\varepsilon_a}{\varepsilon_\perp})\cos\theta + \varepsilon_0\varepsilon_e[E_{sc}\cos qx\sin\theta + E_{DC}(\frac{\sigma_a}{\sigma_\perp}-\frac{\varepsilon_a}{\varepsilon_\perp})\theta\sin\theta \\
&+ E_{DC}\cos\theta]E_{DC}(\frac{\sigma_a}{\sigma_\perp}-\frac{\varepsilon_a}{\varepsilon_\perp})\sin\theta[K_1\sin^2\theta + K_3\cos^2\theta]\frac{d^2\theta}{dz^2} \\
&+\frac{1}{2}[K_1-K_3]\sin 2\theta\left(\frac{d\theta}{dz}\right)^2 + [K_1\cos^2\theta + K_3\sin^2\theta]\frac{d^2\theta}{dx^2} \\
&+\frac{1}{2}[K_3-K_1]\sin 2\theta\left(\frac{d\theta}{dx}\right)^2 - [K_1-K_3]\sin 2\theta\frac{d^2\theta}{dxdz} \\
&-[K_1-K_3]\cos 2\theta\frac{d\theta}{dx}\frac{d\theta}{dz}
\end{aligned}$$

Equation 5.30

With the external applied DC voltage in the *z*-direction and the space charge field in the *x*-direction, there would be flow in the liquid crystal film. The flow torque τ_{flow} can be expressed as:

$$\begin{aligned}\tau_{flow} &= (\kappa_1 \cos^2\theta + \kappa_2 \sin^2\theta)S \\ &= -\frac{dv_x}{dx}(\kappa_1 \cos^2\theta + \kappa_2 \sin^2\theta) \\ &= -\frac{(\varepsilon_{\parallel} \cos^2\theta + \varepsilon_{\perp} \sin^2\theta)E_x E_z}{\eta}(\kappa_1 \cos^2\theta + \kappa_2 \sin^2\theta) \\ &= -\frac{(\varepsilon_{\parallel} \cos^2\theta + \varepsilon_{\perp} \sin^2\theta)(\kappa_1 \cos^2\theta + \kappa_2 \sin^2\theta)}{\eta} E_{DC} \cdot \\ &\left(E_{sc}(x) + E_{DC}(\frac{\sigma_a}{\sigma_{\perp}} - \frac{\varepsilon_a}{\varepsilon_{\perp}})\theta \right) \\ &\approx -\frac{\varepsilon_{\parallel}\kappa_1}{\eta} E_{DC}\left(E_{sc}(x) + E_{DC}(\frac{\sigma_a}{\sigma_{\perp}} - \frac{\varepsilon_a}{\varepsilon_{\perp}})\theta \right)\end{aligned} \qquad \text{Equation 5.31}$$

Using the small director reorientational angle approximation, $\sin\theta \approx \theta$, $\cos\theta \approx 1$ and higher order terms of θ can be neglected. With the consideration of the flow-induced torque, the director reorientation equation is simplified as:

$$\begin{aligned}\eta\dot{\theta} &= \varepsilon_0 E_{DC} E_{sc} \cos q_{eff} x \exp(-\beta z)[\varepsilon_a - \frac{\varepsilon_{\perp}\kappa_1}{\eta} + \varepsilon_o(\frac{\sigma_a}{\sigma_{\perp}} - \frac{\varepsilon_a}{\varepsilon_{\perp}})] \\ &+ \varepsilon_0\theta[\frac{1}{2}\varepsilon_a({E_{sc}}^2(x)\exp(-2\beta z) - {E_{DC}}^2)\cos^2 q_{eff} x \\ &+ \varepsilon_o {E_{DC}}^2(\frac{\sigma_a}{\sigma_{\perp}} - \frac{\varepsilon_a}{\varepsilon_{\perp}})^2 - \frac{\varepsilon_{\perp}\kappa_1}{\eta}{E_{DC}}^2(\frac{\sigma_a}{\sigma_{\perp}} - \frac{\varepsilon_a}{\varepsilon_{\perp}})] \\ &+ K_3\frac{d^2\theta}{dz^2} + K_1\frac{d^2\theta}{dx^2}\end{aligned} \qquad \text{Equation 5.32}$$

In steady state ($\dot{\theta} = 0$), neglecting the non-contributing higher spatially varying terms, the director equation is simplified as:

$$\begin{aligned}0 &= \varepsilon_0 E_{DC} E_{sc} \cos q_{eff} x \exp(-\beta z)[\varepsilon_a - \frac{\varepsilon_{\perp}\kappa_1}{\eta} + \varepsilon_o(\frac{\sigma_a}{\sigma_{\perp}} - \frac{\varepsilon_a}{\varepsilon_{\perp}})] + \\ &\varepsilon_0\theta{E_{DC}}^2[\varepsilon_o(\frac{\sigma_a}{\sigma_{\perp}} - \frac{\varepsilon_a}{\varepsilon_{\perp}})^2 - \frac{\varepsilon_{\perp}\kappa_1}{\eta}(\frac{\sigma_a}{\sigma_{\perp}} - \frac{\varepsilon_a}{\varepsilon_{\perp}})] + K_3\frac{d^2\theta}{dz^2} + K_1\frac{d^2\theta}{dx^2}\end{aligned} \qquad \text{Equation 5.33}$$

By assuming uniform elasticity ($K = K_1 = K_3$), the director reorientation due to the bulk-activated torques can be solved using the mathematical technique used in [Tabiryan 1998] as:

$$\begin{aligned}\theta &= \frac{\varepsilon_0[\varepsilon_a + \varepsilon_o(\frac{\sigma_a}{\sigma_\perp} + \frac{\varepsilon_a}{\varepsilon_\perp})]}{K\left(q'^2 - \beta^2\right)}[\frac{\sinh q'z}{\sinh q'd}[\exp(-q'd) - \exp(-\beta d)] \\ &+ \exp(-\beta z) - \exp(-q'z)]E_{DC}E_{sc}\cos qx \\ &= \theta_{bulk}\cos qx\end{aligned} \qquad \text{Equation 5.34}$$

where

$$q'^2 = {q_{eff}}^2 + \frac{\varepsilon_0 {E_{DC}}^2}{K}[\varepsilon_o(\frac{\sigma_a}{\sigma_\perp} - \frac{\varepsilon_a}{\varepsilon_\perp})^2 - \frac{\varepsilon_\perp \kappa_1}{\eta}(\frac{\sigma_a}{\sigma_\perp} - \frac{\varepsilon_a}{\varepsilon_\perp})] \qquad \text{Equation 5.35}$$

This solution of the director reorientation distribution clearly satisfies the hard-boundary condition as $\theta(0) = \theta(d) = 0$. The director reorientational grating shows similar sinusoidal spatial distribution but with $\pi/2$ phase shift with respect to the sinusoidally varying illuminating optical field.

5.2.3 Induced Refractive Index Grating

NLC is an anisotropic material with extraordinary refractive index n_e and ordinary refractive index n_o. For an incident extraordinary wave with an angle β to the NLC director in the *x*-*z* plane, the effective refractive index is:

$$n(\phi) = \sqrt{n_e^2 \cos^2\phi + n_o^2 \sin^2\phi} \qquad \text{Equation 5.36}$$

After the director reorientation, the new effective refractive index is:

$$n(\phi+\theta)=\sqrt{n_e^2\cos^2(\phi+\theta)+n_o^2\sin^2(\phi+\theta)} \qquad \text{Equation 5.37}$$

Thus the effective refractive index change due the space charge field induced director reorientation is:

$$\begin{aligned}\Delta n &= n(\phi+\theta)-n(\phi)\\ &=\sqrt{n_e{}^2\cos^2(\phi+\theta)+n_o{}^2\sin^2(\phi+\theta)}-\sqrt{n_e{}^2\cos^2\phi+n_o{}^2\sin^2\phi}\\ &\approx\sqrt{n_e{}^2\cos^2\phi+n_o{}^2\sin^2\phi-2\theta\sin 2\phi(n_e{}^2-n_o{}^2)}\\ &\quad-\sqrt{n_e{}^2\cos^2\phi+n_o{}^2\sin^2\phi}\\ &\approx\frac{\sin 2\phi(n_e{}^2-n_o{}^2)}{\sqrt{n_e{}^2\cos^2\phi+n_o{}^2\sin^2\phi}}\theta\\ &=\frac{\sin 2\phi(n_e{}^2-n_o{}^2)}{\sqrt{n_e{}^2\cos^2\phi+n_o{}^2\sin^2\phi}}\theta_{bulk}\cos qx\end{aligned} \qquad \text{Equation 5.38}$$

The spatial variation of the refractive index in a NLC film inherits the sinusoidal form of the illuminating field. It is proportional both to the magnitude of the space charge field and the applied DC field. In the small signal limit, the diffraction efficiency is:

$$\begin{aligned}\eta &= \frac{\pi\Delta n_0 d}{\lambda}\\ &=\frac{\pi d}{\lambda}\frac{\sin 2\phi(n_e{}^2-n_o{}^2)}{\sqrt{n_e{}^2\cos^2\phi+n_o{}^2\sin^2\phi}}\Delta\theta_{bulk}\end{aligned} \qquad \text{Equation 5.39}$$

The effective nonlinear index n_2 indicates the degree of materials' nonlinearity and is expressed as:

$$\Delta n_0 = n_2 I_0 \qquad \text{Equation 5.40}$$

With the measurement of the first-order diffraction efficiency, the illuminating laser intensity, the effective nonlinear index can be easily calculated with the knowledge of the illuminating laser wavelength and the film thickness by the following expression:

$$
\begin{aligned}
n_2 &= \Delta n_0 / I_0 \\
&= \frac{\sin 2\phi (n_e^{\,2} - n_o^{\,2})}{\sqrt{n_e^{\,2}\cos^2\phi + n_o^{\,2}\sin^2\phi}} \frac{\theta_{bulk}}{I_0} \\
&= \frac{\sin 2\beta (n_e^{\,2} - n_o^{\,2})}{\sqrt{n_e^{\,2}\cos^2\beta + n_o^{\,2}\sin^2\beta}} \frac{\varepsilon_0[\varepsilon_a + \varepsilon_o(\frac{\sigma_a}{\sigma_\perp} + \frac{\varepsilon_a}{\varepsilon_\perp})]}{K\left(q'^2 - \beta^2\right)} \\
&\quad [\frac{\sinh q'z}{\sinh q'd}[\exp(-q'd) - \exp(-\beta d)] + \exp(-\beta z) - \exp(-q'z)]\frac{E_{DC}E_{sc}}{I_0}
\end{aligned}
\qquad \text{Equation 5.41}
$$

5.3 Experimental Manifestation of Photorefractivity in Carbon Nanotube Doped NLCs

Multiple-wall carbon nanotubes have recently been reported as photo-sensitive dopants for photorefractive liquid crystals [Lee 2000, Lee 2001, Lee 2002]. From the structure point of view, single-wall carbon nanotube is an elongated version of C_{60}. As C_{60} has been reported [Khoo 1995] to generate photo charges and introduce photorefractive effect when doped in liquid crystals, we expect single-wall carbon nanotubes will also be able to induce the space charge field and the photorefractive effect when doped in liquid crystals. In addition, single-wall carbon nanotubes are expected to yield larger diffraction efficiency because the interaction between them and liquid crystal molecules [Mrozek 2003].

The experimental configuration is illustrated in Figure 5.4. Two coherent linearly polarized laser beams impinge onto a homeotropically aligned dye-doped nematic liquid crystal film at the incident angle ϕ. The two coherent beams are in the same incident plane with two degrees of angle difference. An Argon-Ion laser is used to generate 0.488 μm CW coherent laser beams. The input beams are polarized in the *x*-direction and the liquid crystal film is aligned in the *z*-direction. As discussed in the previous section, the input laser will induce a refractive index grating in *x*-*z* plane. This grating will in turn diffract the input laser beams to generate a series of diffracted beams in a certain pattern depending on the grating constant and the input laser wavelength. The ratio between the intensity of the first-order diffraction beam and that of the 0^{th} order beam is called the diffraction efficiency, a very important parameter used to measure the nonlinearity of photorefractive materials.

The liquid crystal used is E7, in which a small amounts of SWNTs (diameter ~1.2–1.4 nm, length 4–100 nm) and/or C_{60} are dissolved; the concentration is ~0.05%. Typical absorption constants α of these samples vary from 5 to 10 cm^{-1}, depending on the concentration. The cell thickness is 25 μm. The incident laser power used ranges from 25 to 500 μW (beam diameter of 5 mm). This corresponds to an intensity range of 100 $\mu W/cm^2$ to 2 mW/cm^2, similar to those used in the spatial light modulators. The wave-mixing angle is about 2°, corresponding to an intensity grating constant inside the NLC film of ~ 23 μm. The angle of incidence β of the writing beam in air is 45° with respect to the normal.

In the experiments, side diffractions become visible when the applied DC voltage is above 3 V. Figure 5.5 shows the observed nonlinear dependence of the diffraction on the optical writing beam intensity for a SWNT-doped sample (α=4 cm^{-1}). The diffraction efficiency is also nonlinearly dependent on the applied DC voltage, as shown in Figure 5.6, where the first-order diffraction efficiency η=8% is obtained with a writing beam intensity of 2 mW/cm^2 [500 μW; 5-mm beam diameter], for a sample with an absorption constant α=4 cm^{-1}. Since $\eta = (\pi \Delta n d/\lambda)^2$, we get $\Delta n = 1.6 \times 10^{-3}$, and therefore an effective nonlinear index coefficient n_2=0.8 cm^2/W. This value of n_2 is already 10 times the one reported for MWNT-doped films, and about 1000 times larger than C_{60}-doped liquid crystal studied previously. The enhanced response is due to a combination of higher photorefractive response of single-walled carbon nanotubes and the higher DC applied voltage that these samples can hold before dynamic scattering sets in. The latter is further confirmed by measurements from a C_{60}-doped nematic film (α=4 cm^{-1}). We observed a diffraction efficiency of 5% at an applied voltage of 3.7 V, and an n_2 value of 0.6 cm^2/W. This is 300 times larger than previous values obtained in samples, in which the dynamic scattering threshold voltage is 2.5 V.

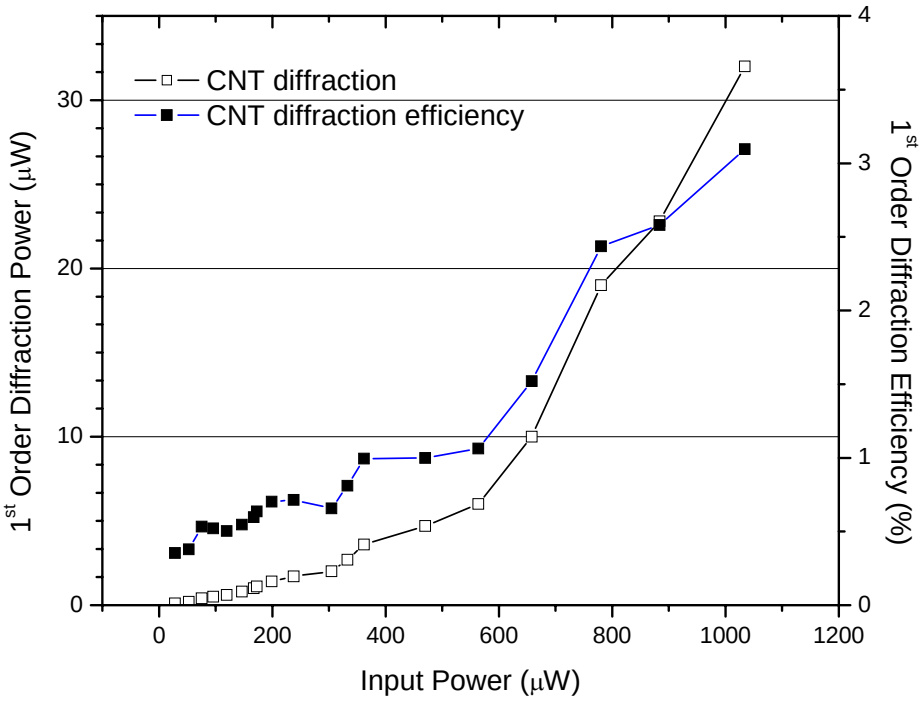

Figure 5.5: Diffraction as a function of the optical writing intensity for a SWNT-doped sample (α=4 cm^{-1}).

From Figure 5.5, it can be concluded that the first order diffraction efficiency is approximately linearly proportional to the input writing beam power. It is in good accordance with Equation 5.39 which shows that the diffraction efficiency has a linear relationship with the intensity of the illuminating optical field when other parameters are unchanged. Since the diffraction efficiency is calculated as $\eta = I_1 / I_0$, the power of the first order diffracted beam is quadratically dependent on the input laser power as shown in Figure 5.5. Variance in the absorption constant represents the concentration difference of SWNT dopants in liquid crystals. Higher absorption means that more active photo-

sensitive SWNTs are dissolved in the solution and larger photo-sensitivity of the film. In Equation 5.39, the diffraction efficiency is proportional to the photo-sensitivity of the medium. The experimental results in Figure 5.6 verified the previous prediction that liquid crystals with higher SWNT dopant concentration yield higher diffraction efficiency at the same condition.

It has also been noticed that the relationship between the diffraction efficiency and the applied DC voltage is not exactly linear as shown in Figure 5.6. This reveals the limitation of our previous analysis that the above derived photorefractive theory in dye-doped nematic liquid crystal medium is based on the bulk while the anchoring force from the boundary has been intentionally neglected in order to simplify the analysis. In all the photorefractive experiments in dye-doped nematic liquid crystal solution, the thickness of the film is only about 20 – 50 μm. If the applied DC voltage is below the Fredericks transition threshold value, there is hardly any NLC director reorientation in the bulk. That is why photorefractivity in dye-doped NLC film only occurs when the applied DC voltage exceeds a certain value. After the photorefractivity begins to take place, the diffraction efficiency shows an obvious linear dependency on the magnitude of the DC voltage as predicted in the previous derivation.

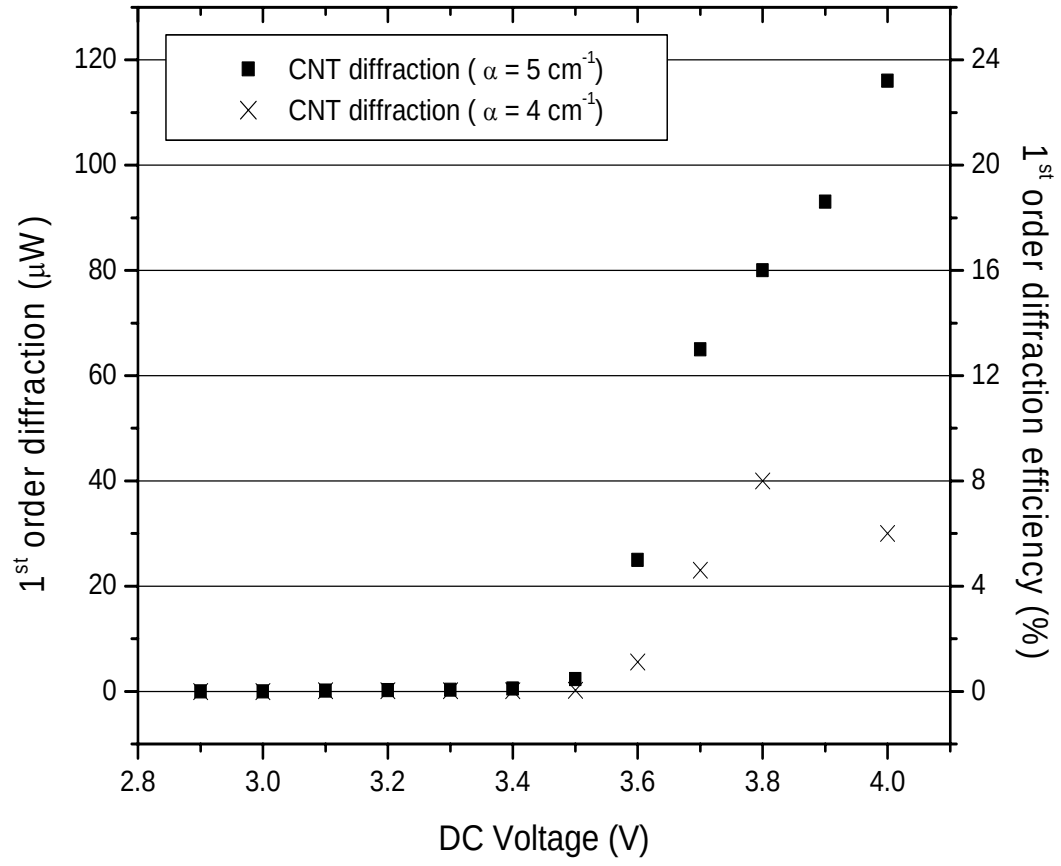

Figure 5.6: Diffraction as a function of dc voltage for the SWNT-doped sample (squares: α=5 cm^{-1}; crosses: (α=4 cm^{-1}).

With slightly higher dopant concentration, the optical nonlinearity improves considerably, as depicted in Figure 5.6, 5.7 and 5.8 for SWNT-, and SWNT+C_{60}-doped samples (absorption constants of 8, and 7 cm^{-1}, respectively). Upon continuous optical illumination and the application of DC bias field, all three samples exhibit similar diffraction efficiency. The corresponding n_2 values obtained are 1.4, 1.3, and 1.4cm^2/W. As remarked earlier, for C_{60}+SWNT doped films, the ‘‘threshold’’ for dynamic scattering is generally higher, ranging from about 5 to 11 V when continuously applied. Dynamic

scattering can be inhibited if the DC voltage is applied for a short duration. This actually provides a means of extracting larger nonlinearity and faster response times. For example, with the application of a 1 second duration DC voltage of 20 V on the C_{60} +SWNT doped sample, we have observed a diffraction efficiency η=1% under a writing-beam power of 40 μW. This diffraction efficiency corresponds to an effective coefficient n_2 =7 cm^2/W. The buildup and decay times are on the order of tens of milliseconds to 100 ms, which are clearly more desirable than their extremely slow counterparts.

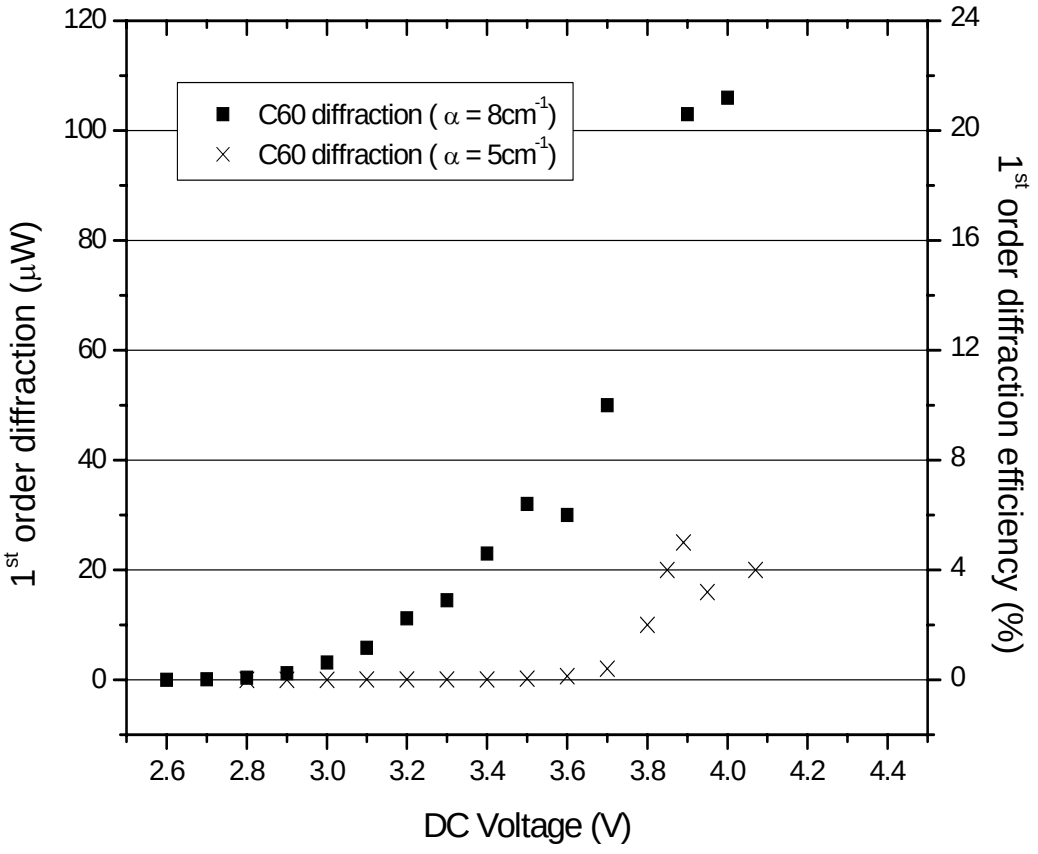

Figure 5.7: Diffraction as a function of the Applied DC field for a C_{60}-doped sample (squares: α=8 cm^{-1}; crosses: α=5 cm^{-1}).

In the C_{60} doped liquid crystal photorefractivity experiment, the relationship between the diffraction efficiency and the applied DC voltage is also nearly linear in the photorefractive domain for different C_{60} concentrations as shown in Figure 5.7. But different from the results of SWNT doped NLC films, the increase in C_{60} concentration decreased the threshold DC voltage for the occurrence of photorefractivity. This decrease may have something to do with the interaction between ions from photo-excited C_{60} and the coated polymer alignment layer on the glass surface and need further investigation.

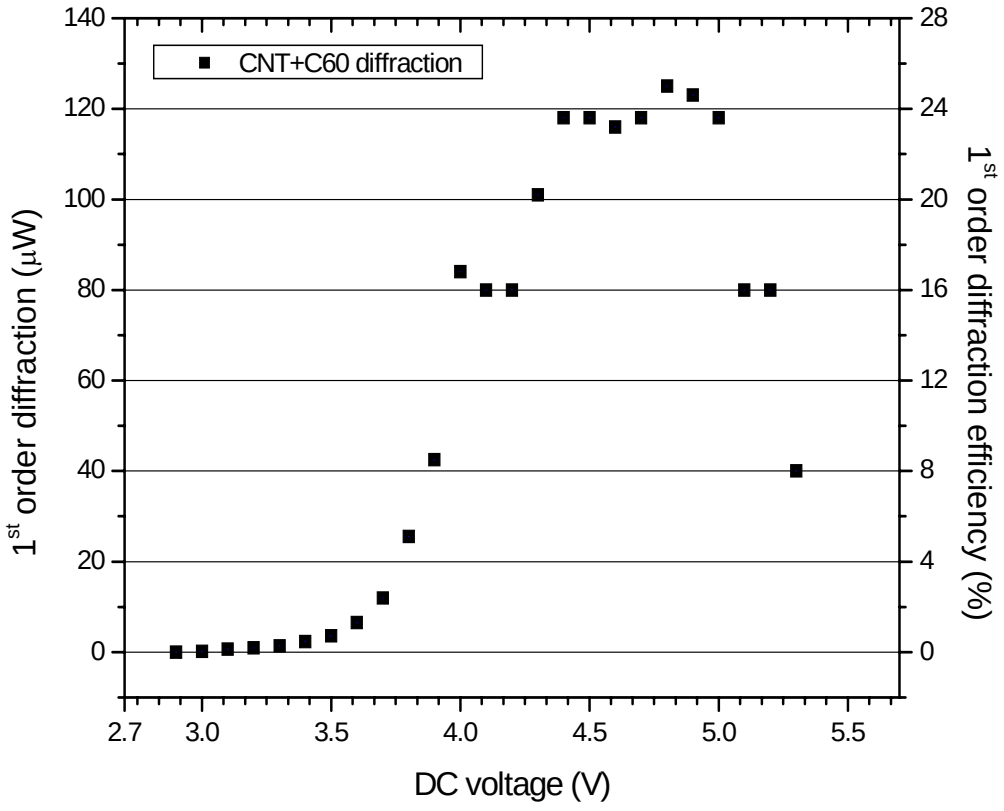

Figure 5.8: Diffraction as a function of DC voltage for a SWNT+C_{60}-doped sample (α=7 cm^{-1}).

The relationship between the diffraction efficiency and the applied DC voltage is rather complicated as shown in Figure 5.7. When the applied DC voltage is between 3.6 and 4.4 V, the diffraction efficiency is linearly proportional to the applied DC voltage. Between 4.4 and 5.0 V, the diffraction efficiency saturates at around 24% and quickly drops when the applied field is above 5.0V. As discussed before, the higher the DC voltage is applied, the larger the heat that will be generated inside the liquid crystal film. The accumulated heat would cause phase transition in the bulk and disturb the induced refractive index grating. In turn, the diffraction efficiency would deteriorate. When the applied the DC voltage is too large (5.0V in this case), the accumulated heat destroys the refractive index grating resulting in the significant drop in the diffraction efficiency.

5.4 Surface-Induced Photorefractive-like Effect in Liquid Crystal Films

Studies in the photorefractivity of Methyl-red doped liquid crystals have shown very large optical nonlinearity with effective refractive index coefficient of ~10. In the mean time, there is no sign of two beam amplification which is a signature phenomenon of the photorefractive effect. Recent experimental demonstrations of diffractive gratings in pure nematic liquid crystal films have generated enormous amount of interest in the surface-activated photorefractivity. The grating in pure liquid crystals films also shows no sign of two beam amplification while it still needs an external DC field to trigger the effect. There is no commonly accepted theoretical explanation to date. In this section, a theoretical explanation based on the surface-induced torque is derived to account for the

diffractive gratings generated in pure and Methyl-red doped liquid crystals and the lack of the two-beam amplification.

For a pure liquid crystal film, the rather small ion density and the absence of charge trap center make it impossible to generate space charge field strong enough to induce director reorientation in the film. The generation of diffractive grating is attributed to the surface torque induced by the external electric DC field and the inhomogeneous laser illumination. With the application of an external DC field, there is charge accumulation along the interface between the liquid crystal and the alignment chemical surfactant. Under an illumination of inhomogeneous optical field, the charge at the surface will redistribute and induce a surface torque carrying the same spatial distribution as the illuminating optical field. In the case of Methyl-red doped liquid crystal, the surface torque is speculated to be induced to the surface photo-chemical reaction and possible trans-cis photo-isomerization. Assuming the incoming laser has a periodic spatial distribution as:

$$I = I_0 (1 + m \sin qx) \exp(-\beta z) \qquad \text{Equation 5.42}$$

where m is the modulation depth, q is the grating constant of the interference grating in the film, and β is the absorption constant of the liquid crystal film. For the surface-activated photorefractive effect, this inhomogeneous laser will induce a surface torque as:

$$\tau = \tau_0 \exp(-z / z_0) \sin qx \qquad \text{Equation 5.43}$$

where τ_0 is the amplitude of the surface torque, and z_0 represents the distance that the surface torque can penetrate. With this surface torque, the director reorientation equation can be readily expressed as:

$$\eta\dot{\theta} = \tau_0 \exp(-z/z_0)\sin qx + K_3\frac{d^2\theta}{dx^2} + K_1\frac{d^2\theta}{dz^2} \qquad \text{Equation 5.44}$$

Assuming uniform elasticity in the liquid crystal film ($K = K_3 = K_1$), the director reorientation induced by the surface torque can be analytically solved as:

$$\begin{aligned}\theta &= \frac{\tau_0}{K\left(q^2 - z_0^{-2}\right)}\sin qx \\ &\left[\frac{\sinh qz}{\sinh qd}[\exp(-qd) - \exp(-d/z_0)] + \exp(-z/z_0) - \exp(-qz)\right] \\ &= \theta_{surface}\sin qx\end{aligned} \qquad \text{Equation 5.45}$$

Not surprisingly, the director reorientation shows the same sinusoidal distribution as the surface torque and the illuminating optical field. The zero phase-shift explains why there is no observation of the two beam amplification in the surface- activated photorefractivity such as seen in pure liquid crystals or Methyl-red doped liquid crystals.

5.5 Summary

In this chapter, detailed analysis of the space charge field formation in a photo-sensitive medium has been presented using the band transport model. The generated space charge field changes the local orientation of the NLC director and produces the variation in the refractive index distribution. The creation of a periodic refractive index grating under a sinusoidal illuminating field is thoroughly analyzed through the

orientational dynamics of the NLC director staring from the Euler-Lagrange-Rayleigh equation. The analytical expressions of the reorientational angle distribution, refractive index distribution, and diffraction efficiency were obtained. The effective nonlinear index is proportional to the applied DC field, and input lasers' modulation depth. The NLC's physical parameters such as conductivity difference, absorption constant, and birefringence play important roles in this nonlinear orientational effect. We have also observed a large electrically assisted nonlinear photorefractive response in SWNT- and C_{60}-doped nematic liquid crystals. Supra-nonlinearities are found in these solutions, which enable the use of optical intensity in the 100 $\mu W/cm^2$ level for various holographic and image processing applications. The generation of diffractive gratings in pure and Methyl-red doped liquid crystal is also explained based on the induced surface torque and the absence of the two-beam amplification is accounted as well.

Chapter 6

Conclusions and Future Work

6.1 Conclusions

In this thesis, optical wave-mixing and photorefractivity in nematic liquid crystals (NLC) have been theoretically and experimentally investigated in the contexts of stimulated orientational scattering and photorefractivity in liquid crystals. Due to their large optical anisotropy, NLC media have been demonstrated to exhibit superior optical

nonlinearities in optical wave-mixing phenomena. In what follows, I will briefly summarize this research work.

1. A theory to describe the steady-state stimulated orientational scattering in NLC film has been successfully developed, for the first time, without the non-pump-depletion approximation. This approximation becomes invalid when the stimulated output grows comparable to the transmitted output. The numerical simulation at visible wavelength showed a very good agreement with the previously reported experimental results using an Argon laser.

2. The first stimulated orientational scattering (SOS) effect in 1.55 μm wavelength using an Erbium-doped semiconductor laser was observed and a polarization conversion of more than 60% was achieved. This finding makes NLC films potential candidates as polarization switchers in fiber communication and integrated photonics. The SOS effect is a non-resonant effect even though the power requirement for the polarization conversion varies for different pump laser wavelengths. The experimental results in the infrared regime are in a good agreement with the numerical simulation based on the developed steady-state model.

3. The influence of an external AC field to the SOS effect has also been evaluated. It has been shown that the power requirement for the polarization conversion can be decreased with the application of an external low-frequency AC modulating field.

4. The dynamics of the liquid crystal director reorientation process has been experimentally investigated. The characteristic frequency of the NLC director

orientation grating has been observed in the Fourier frequency spectrum of the stimulated output beam and its value agrees with the theoretical calculation. The influence of an external low-frequency AC modulation field to the SOS dynamics has also been studied using the Fourier frequency spectrum of the output beams.

5. The photorefractivity in a photo-sensitive dye doped NLC film has been theoretically studied. The distribution of photo charges and the subsequent space charge field has been derived using the transport band model. Due to their weak inter-molecular forces, NLC molecules will reorient under the influence of the space charge field and the external DC field. The NLC director reorientation grating and the resulting refractive index grating have been analytically derived using the NLC director reorientation equations. The influence of various material parameters, such as NLC's physical parameters, photo-sensitivity of dye dopants, intensity and modulation depth of the illumination light, has also been evaluated.

6. The generation of the diffractive gratings in pure and Methyl-red doped liquid crystals has been theoretically explored. Different from photo-sensitive dye doped photorefractive liquid crystals, there has been no report of two-beam amplification in pure and Methyl-red doped liquid crystals. Surface torque has been proposed to explain the generation of diffractive gratings in pure and Methyl-red doped liquid crystals. The NLC director reorientational grating and the resulting refractive index grating have been analytically solved and the absence of the two-beam amplification has also been explained.

7. The supra photorefractivity has been observed in single-wall carbon nanotube (SWNT) doped NLC films. The SWNT-doped NLC films have an

effective nonlinear index 10 times larger than previously reported value of multiple-wall carbon nanotube-doped NLC films, and about 1000 times larger than that of C_{60}-doped liquid crystal films. The relationship between the diffractive index and the dopant concentration, the magnitude of the applied DC voltage has been experimentally investigated and it is in a good agreement with our theoretical analysis.

6.2 Future Work

Orientational nonlinearity is one of the most fundamental and unique properties of liquid crystals stemming from their crystalline structure and weak intermolecular force. Optical wave-mixing in liquid crystals has been utilized in a wide range of applications. The stimulated orientational scattering effect in NLC films not only has the potential for a lot of applications, such as polarization converter, and also has profound scientific impact in the study of dynamical process and chaotic behavior in liquid crystals. Photorefractive materials have already found their positions in applications such as spatial light modulators, and holographic storage. The improvement in the diffraction efficiency and effective nonlinear index in carbon nanotube doped NLC films lowers the power requirement for the photorefractive effect and expands its potential applications into integrated photonics, liquid crystal nano structures.

Orientational nonlinearity of liquid crystals, optical wave-mixing and energy transfer in liquid crystals, and refractive index grating formation in dye doped and pure liquid crystal films have been extensively explored in this thesis research. However, more

works (both theoretical and experimental) need to be performed to fully understand the dynamical director reorientation and wave-mixing in liquid crystals and utilize this exclusive reorientation property of liquid crystals to inspire future applications. Some considerations for future research on the continuation of this orientational nonlinearity and wave-mixing study in liquid crystals are listed as the following:

1. Further study in the dynamics of the stimulated orientational scattering in liquid crystals. Experimental observations have shown that the energy transfer between the stimulated beam and the transmitted beam is very dynamic and can not be explained by the steady-state SOS theory. Extensive theoretical analysis of the time-dependent SOS effect is needed to understand this dynamic process and to provide directions for the chaotic study in liquid crystals [Cipparrone 1993, Cipparrone 2001].

2. Explore the utilizations of the SOS effect in other applications beside polarization conversion. The SOS effect is a non-resonant all-optical effect. Combining with unique properties of liquid crystals, such as duality of liquid and crystal, transparency over a wide spectrum range, large optical anisotropy, the SOS effect of liquid crystals is very promising for a wide range of applications, such as the infrared phase-conjugating for wave-front control, adaptive optics in the infrared regime, all-optical beam amplification.

3. Photorefractive soliton study. Spatial solitons in photorefractive materials was first proposed by Calvo [Calvo 2002] and Crosignani [Crosignani 2002]. Compared with conventional spatial solitons, the generation of solitons in photorefractive media requires less power. Observations of spatial solitons in

photorefractive materials have shifted the research of solitons from producing solitons to manipulating solitons for various applications. The supra nonlinearity in carbon nanotube doped liquid crystals will further decrease the power requirement for generating spatial solitons. In addition, the flexibility of liquid crystals can bring additional advantages in device deployment.

Bibliography

[Barbero 2002] G. Barbero, D. Olivero, Phys. Rev. E, Vol. 65, pp. 031701-1—031701-5 (2002).

[Bethune 1993] Bethune D. S., Kiang C. H., Deveries M. S., Gorman G., Savoy R., Vazquez J., Beyers R., Nature, Vol. 363, pp. 605-607 (1993).

[Brown 2002] C. V. Brown, Em. E. Kriezis, S. J. Elston, Journ. Of Appl. Phys., Vol. 91, No. 6, pp. 3495-3500 (2002).

[Calvo 2002] G. F. Calvo, B. Sturman, F. Agullo-Lopez, M. Carrascosa, Phy. Rev. Lett., Vol. 89, No. 3, pp.033902-1—033902-4 (2002).

[Carbone 2001] V. Carbone, G. Cipparrone, G. Russo, Phy. Rev. E, Vol. 63, pp. 051701-1—051701-4

[Chen 2002] Jian Chen, Haiying Liu, Wayne A. Weiner, Mathew D. Halts, David H. Waldeck, Gilbert C. Walker, J. Am. Chem. Soc., Vol 124, pp. 9034-9035 (2002)

[Cipparrone 1993] G. Cipparrone, V. Carboue, C. Versace, C. Umeton, R. Bartolino, Phy. Rev. E, Vol. 47, No. 5, pp. 3741-3744, (1993)

[Cipparrone 2001] G. Cipparrone, A. Mazzulla, P. Pagliusi, A. V. Sukhov, r. F. Usahkov, J. Ot. Soc. Am. B, Vol. 18, No. 2, pp. 182-186 (2001)

[Crosignani 2002] Bruno Crosignani, Greg Salamo, Optics & Photonics News, Vol. 13, No. 2, pp.38-41 (2002).

[Ebbesen 1998] T. W. Ebbesen, H. J. Lezec, H. F. Ghaeml, T. Thio, P. A. Wolff, Nature, Vol. 391, pp. 667-669 (1998)

[Etchegoin 1997] P. Etchegoin and R. T. Philips, Phys. Rev. E 55, 5603 (1997)

[Fan 2003] Yun-Hsing Fan, Hongwen Ren, Shin-Tson Wu, App. Phys. Lett., Vol. 82, No. 18, pp. 2945-2947 (2003)

[Fazio 2003] E. Fazio, W. Ramadan, A. Belardini, A. Bosco, M. Bertolotti, Phys. Rev. E, Vol. 67, pp. 026611-1—026611-8 (2003)

[Furumi 2003] Seiichi Furumi, Shiyoshi Yokoyama, Akira Otomo, Shinro Mashiko, Appl. Phys. Lett., Vol. 82, No. 1, pp. 16-18 (2003)

[Gibbons 1991] Gibbons W. M., Shannon P. J., Sun S. T., Swetlin B. J., Nature, 351 (6321): 49-50, (1991)

[Gooneseker 2000] Arosha Gooneseker, Daniel Wright, W. E. Moerner, App. Phys. Lett. Vol. 76, No. 23, pp. 3358-3360 (2000)

[Gu 1996] Clarie Gu, Jenn-Ken Lien, Foster Dai, J. Opt. Soc. Am. A, Vol. 18, No. 8, pp 1704 -1711 (1996)

[Gunter 1989] P. Gunter and J. P. Huignard, “Photorefractive Materials, and Their Applications”, Vol. 1 and 2, Springer, Berlin (1989)

[Hamada 1992] Hamada N., Sawada S., Oshiyama A., Phys. Rev. Lett., 68 (10): 1579-1581 (1992)

[Hayer 1978] William Hayes, “Scattering of Light by Crystals”, John Wiley & Sons, NY (1978)

[Heanue 1994] J. F. Heanue, M. C. Bashaw, and L. Hesselink, Science 265, 749 (1994)

[Henriot 2003] Michel Henriot, Javier Burguete, Roland Ribotta, Phys. Rev. Lett., Vol. 91, No. 10, pp. 104501-1—104501-4 (2003)

[Hesselink 1993] L. Hesselink, M. C. Bashaw, Optical and Quantum Electronics, 25, pp. S611-S661 (1993)

[Hoppensteadt 1999] F. C. Hoppensteadt and E. M. Izhikevich, Phys. Rev. Letts. 82, pp. 2983-2986 (1999)

[Hooper 2002] I. R. Hooper, J. R. Sambles, Opt. Lett., Vol. 27, No. 24, pp. 2152-2154 (2002)

[Ickimura 2000] Kunihiro Ickimura, Sang-Keun Oh, Masaru Nakagawa, Science, Vol. 288, pp. 1624-1626 (2000)

[Inoue 2002] Inoue, K. Yoshino, Jour. of Appl. Phys., Vol. 91, No.5, pp. 2798-2802 (2002)

[Janossy 1992] Janossy I., Kosa, T., Opt. Lett., 17 (17): 1183-1185, (1992)

[Jenekhe 1998] S. A. Jenekhe and X. L. Chen, Sciences Vol. 279, pp. 1903-1907 (1998)

[Jin 1998] A. J. Jin, M. R. Fisch, M. P. Mahajan, K. A. Crandall, P. Chu, C. Y. Huang, V. Percec, R. G. Petschek, C. Rosenblatt, Eur. Phys. J. B, Vol. 5, pp. 251-255 (1998)

[Jishi 1994] Jishi R. A. , Inomata D., Nakao K., Dresselhaus M. S., Dresshelhaus G., Journ Of The Phys. Soci. Of Jap., Vol. 63, No.6, pp.2252-2260 (1994)

[Johnson 1993] Kristina M. Johnson, Douglas J. McKnight, Ian Underwood, IEEE Journal. of Quantum. Electronics., Vol. 29, No. 2, pp. 699-714 (1993)

[Kaczmark 2002] Malgosia Kaczmark, Min-Yi Shih, Roger S. Cudney, Iam-Choon Khoo, IEEE Jorun. Of. Quan. Elec., Vol. 38, No. 5, pp. 451-457 (2002)

[Kataura 1999] H. Kataura, Y. Kumazawa, Y. Maniwa, I. Umezu, S. Suzuki, Y. Ohtsuka, Y. Achiba, Synthetic Metals, Vol. 103, pp. 2555-2558 (1999)

[Kataura 2000] Hiromichi Kataura, Yoshinori Kumazawa, Noriaki Kojima, Yutaka Maniwa, Ikurou Umezu, Shinichi Masubuchi, Shigeo Kazama, Youshuke Ohtsuka, Shinzo Suzuki, Yohji Achiba, Mol. Cryst. Liq. Cryst., Vol. 340, pp. 757-762 (2000)

[Khoo 1993] I. C. Khoo, S. T. Wu, “Optics and Nonlinear Optics of Liquid Crystals,” World Scientific, Singapore, (1993)

[Khoo 1994a] I. C. Khoo, “liquid crystals”, Wiley Interscience, NY (1994)

[Khoo 1994b] I. C. Khoo, H. Li, Y. Liang, Opt. Lett., Vol. 19, No. 21, pp. 1723-1725 (1994)

[Khoo 1995] I. C. Khoo, Opt. Lett., Vol. 20, No. 20, pp. 2137-2139 (1995)

[Khoo 1996a] I. C. Khoo, Mol. Cryst. Liq. Cryst., Vol. 282, pp. 53-66 (1996)

[Khoo 1996b] I. C. Khoo, IEEE Journ. Of Quan. Elec., Vol. 32, No. 3, pp. 525-534 (1996)

[Khoo 1997] I. C. Khoo, B. D. Guenther, M. Y. Wood,, P. Chen, Min-Yi Shih, Opt. Lett., Vol. 22, No. 16, pp. 1229-1231 (1997)

[Khoo 1998] I. C. Khoo, S. Slussareuko, B. D. Guenther, Min-Yi Shih, P. Chen, W. V. Wood, Opt. lett., Vol. 23, No. 4, pp. 253-255 (1998)

[Khoo 2000] I. C. Khoo, Y. Liang, Phys. Rev. E, Vol. 62, No. 5-B, pp. 6722-6733 (2000)

[Khoo 2002a] I. C. Khoo and J. Ding, Appl. Phys. Lett., Vol. 81, No. 14, pp. 2496-2498 (2002)

[Khoo 2002b] I. C. Khoo, M. Kaczmarek, M. Y. Shih, M. V. Wood, A. Diaz, J. Ding, Y. Zhang, J. Patel, Mol. Cryst. Liq. Cryst., Vol. 374, pp. 315-324 (2002)

[Khoo 2003] I. C. Khoo, J. Ding, Y. Zhang, K. Chen, A. Diaz, Appl. Phys. Lett., Vol. 82, No. 21, pp. 3587-3589 (2003)

[Kumar 1998] Jeyant Kumar, Lian Li, Xin Li Jiang, Dong-Yu Kim, Taek Seung Lee, Sukant Tripathy, Appl. Phys. Lett., Vol 72, No. 17, pp. 2096-2098 (1998)

[Kuroda 2002] Kazuo Kuroda, “Progress in Photorefractive Nonlinear Optics”, Taylor & Francis, NY (2002)

[Lauret 2003] J-S. Lauret, C. Voisin, G. Cassabois, C. delalande, Ph. Roussignol, O. Jost, L. Capes, Phys. Rev. Lett., Vol. 90, No. 5, pp. 057404-1—057404-4, (2003)

[Lee 2001] S. B. Lee, t. Katayama, H. Kajii, H. Araki, K. Yoshimo, Synthetic Metals, Vol. 121, pp. 1591-1592 (2001)

[Lee 2000] Wei Lee, Chi-Shen Chiu, Opt. Lett. Vol. 26, No. 8, pp. 521-523 (2000)

[Lee 2001] Wei Lee, Sheng-Long Yeh, Appl. Phys. Lett., Vol. 79, No. 27, pp. 4488-4490 (2001)

[Lee 2002] Wei Lee, Hui-Yu Chen, Sheng-Long Yeh, Opt. Exp., Vol. 10, No. 11, pp. 482-487 (2002)

[Liu 2002] X. Liu, T. Pichler, M. Knupfer, M. S. Golden, J. Fink, H. Kataura, Y. achiba, K. Hirahara, S. Iijima, Phys. Rev. B, Vol. 65, pp. 045419-1—045419-6 (2002)

[Lynch 2002] Michael D. Lynch, David L. Patrick, Vo2. 2, No. 11, pp. 1197-1201 (2002)

[Meerholz 1994] K. Meerholz, B. L. Volodin, Sandalphon, B. Kippelen & N. Peyhgambarian, Nature, Vol. 371, No. 6, pp. 497-499 (1994)

[Minardi 2002] Stefano Minardi, Gianluca Arrighi, Paolo Di Trapani, Opt. Lett., Vol. 27, No. 23, pp. 2097-2099 (2002)

[Mishira 2000] S. R. Mishra, H. S. Rawat, S. C. Mechendale, K. C. Rustagi, A. K. Sood, Ranjini Bandyopdhyay, A. Govindaraj, C. N. R. Rao, Chem. Phys. Lett., Vol. 317, pp. 510-514 (2000)

[Mosquera 2002] Luis Mosquera, Jaime Frejlich, J. Opt. Soc. Am. B, Vol. 19, No. 12, pp. 2904-2910 (2002)

[O'Flaherty 2003] Sean M. O'Flaherty, Stephanie V. Hold, Margaret E. Brennan, Martin Cadek, Anna Drury, Jonathan N. Coleman, Werner J. Blau, J. Opt. Soc. Am. B, Vol. 20, No. 1, pp. 49-58 (2003)

[Odoulov 1996] S. G. Odoulov, B. I. Sturman, S. Shamonina and K. H. Ringhofer, Opt. Letts., 21, pp. 854-856 (1996)

[Ott 1990] Edward Ott, Celso Grebogi, James A. Yorke, Phys. Rev. Lett., Vol. 64, No. 11, pp. 1196-1199 (1990)

[Peccianti 2000a] M. Peccianti, A. De Rossi, G. Assanto, A. De Luca, C. Umeton, I. C. Khoo, Appl. Phys. Lett., Vol. 77, No. 1, pp. 7-9 (2000)

[Peccianti 2000b] M. Peccianti, G. Assanto, A. De Luca, C. Umeton, M. A. Karpierz, I. C. Khoo, Journ. Of Comm. Tech. and Elec., Vol. 47, No. 7, pp. 790-795 (2000)

[Peccianti 2002] M. Peccianti, K.A. Brzdkiewicz, and G. Assanto, Opt. Lett. 27, 1460 (2002)

[Pepper 1990] D. M. Pepper, J. Feinberg, and N. V. Kukhtarev, "The Photorefractive Effect," in Scientific American, October 1990, p. 62 (1990)

[Pompeo 2002] Francisco Pompeo, Daniel E. Resasco, Nano Lett., Vol. 2, No. 4, pp. 369-373 (2002)

[Purcell 2002] S. T. Purcell, P. Vincent, C. journet, Vu Thien Binh, Phys. Rev. Lett., Vol. 89, No. 27, pp. 276103-1—276103-4 (2002)

[Reznikov 2003] Yurii Reznikov, Olexander Buchnev, Olexander Tereshchenko, Appl. Phys. Lett., Vol. 82, No. 12, pp. 1917-1919 (2003)

[Richter 1997] Richter E, Subbaswamy KR, Phys. Rev. Lett., Vol. 79, No. 14, pp. 2738-2741 (1997)

[Rudenko 1994] E. V. Rudenko, A. V. Sukhov, JETP, Vol 78, No. 6, pp. 875-881 (1994)

[Russo 2000] G. Russo, V. Carbone, G. Cipparrone, Phys. Rev. E, Vol 62, No. 4, pp. 5036-5042 (2000)

[Sakamoto 2003] Kenji Sakamoto, Klyoaki Usami, Manabu Kikegawa, Sukekatsu Ushioda, Journ. Of Appl. Phys., Vol. 93, No. 2, pp. 1039-1043 (2003)

[Saito 1992] Saito R., Fujita M., Dresselhaus G., Dresselhaus M. S.,Phys. Rev. B, 46 (3): 1804-1811 (1992)

[Sandfuchs 2001] O. Sandfuchs, F. Kaiser, and M. R. Belic, Phys. Rev. A 64, 063809 (2001)

[Schwartz 2002] Tal Schwartz, Yaniv Ganor, Raam Urdin, Sharon Shwartz, Mordechai Segev, Opt. Lett., Vol. 27, No. 14, pp. 1229-1231 (2002)

[Shen 1984] Y. R. Shen, The Principles of Nonlinear Optics, Wiley, New York. (1984)

[Simoni 1997] F. Simoni, "Nonlinear Optical Properties of Liquid Crystals", World Scientific, Singapore, (1997)

[Solymar 1996] L. Solymar, D. J. Webb, and A. Grunnet-Jepsen, The Physics and Applications of Photorefractive Materials (Clarendon Press, Oxford, 1996)

[Sturman 1992] B. I. Sturman and V. M. Fridkin, The Photovoltaic and Photorefractive Effects in Noncentrosymmetric Materials (Gordon and Breach, Philadelphia, 1992)

[Sukhov 1990] A. V. Sukhov, Mol., Cryst., Liq., Cryst., 185: 227-237 (1990)

[Tabiryan 1986] N. V. Tabiryan, B. Ya. Zel'dolvich, and A. V. Sukhov, Mol. Cryst. Liq. Cryst. Vol. 136, No.1, pp.1-139 (1986)

[Tabiryan 1998] N. V. Tabiryan and C. Umeton, J. Opt. Soc. Am. B, Vol 15, No. 7 (1998)

[Tabiryan 2001] N. V. Tabiryan, A. V. Sukhov, B. Ya. Zel'dovich, J. Opt. Scio. Am. B, Vol. 18, No. 8, pp. 1203-1205 (2001)

[Titus 2001] C. M. Titus, J. R. Kelly, E. C. Gartland, S. V. Shiyanovskii, J. A. Anderson, P. J. Bos, Opt. Lett., Vol. 26, No. 15, pp. 1188-1190 (2001)

[Tondiglia 2002] Vincent P. Tondiglia, Lalgudi V. Natarajan, Richard L. Sutherland, David Tomlin, Timothy J. Bunning, Advanced Materials, Vol. 14, No. 3, pp187-191 (2002)

[Vavro 2002] J. Vavro, M. C. Llaguno, B. C. Satishkumar, D. E. Luzzi, J. E. Fisher, Appl. Phys. Lett., Vol. 80, No. 8, pp. 1450-1452 (2002)

[Vivien 2002] L. Vivien, D. Riehl, F. Hache, E. Anglaret, Physica B, Vol. 323, pp. 233-234 (2002)

[Wang 1992] Y. Wang, Nature, Vol. 356, pp. 585-587 (1992)

[Wiederrecht 1999] Gary P. Wiederrecht, Michael R. Wasielewski, Appl. Phys. Lett., Vol. 74, No. 23, pp. 3459-3461 (1999)

[Xie 1997] Rui-Hua Xie, Jie Jiang, Appl. Phys. Lett., Vol. 71, No. 8, pp. 1029-1031 (1997)

[Yariv 1991] A. Yariv, "Optical Electronics", Saunders HBJ, New York, (1991)

[Yeh 1993] P. Yeh, Intorduction to Photorefractive Nonlinear Optics (Wiley, New York, 1993)

[Yip 2001] W. C. Yip, H. S. Kwok, App. Phys. Lett., Vol. 78, No. 4, pp. 425-427 (2001)

[Zeldovich 1983] B. Ya. Zel'dovich, S. K. Merzlikin, N. F. Pilipetskii, A. V. Sukhov, N. V. Tabiryan, DAN SSSR, Vol. 273, No. 5, pp. 1116-1118, (in Russian) (1983)

[Zeldovich 1985a] B. Ya. Zeldovich, N. F. Pilipetsky, and V. V. Shkunov, Principles of Phase Conjugation, Springer Series in Optical Sciences Vol. 42 (Springer-Verlag, Berlin, 1985)

[Zeldovich 1985b] B. Ya. Zel'dovich, S. K. Merzlikin, N. F. Pilipetsky, A. V. Sukhov, Sov. Phys. JETP Lett., Vol. 41, No. 10 pp. 514-517, (1985)

[Yu 2000] Francis T. S. Yu, Shizhuo Yin, "Photorefractive Optics", Academic Press, CA (2000)

[Zhang 2000] Guoquan Zhang, Germano Montemezzani, Peter Gunter, Journ. Of Appl. Phys., Vol. 88, No. 4, pp. 1709-1717 (2000)

[Zhang 1992] Yue Zhang, Yiping Cui, Paras N. Prasad, Phys. Rev. B Rapid Comm., Vol 46, No. 15, pp. 9900-9902 (1992)

[Zhou 1994] Zhou O., et al, Science, 263 (5154): 1744-1747 (1994)

VITA

Jianwu Ding

Jianwu Ding was born in Hubei, People's Republic of China in 1976. He received his B. S degree in Physics from the Wuhan Unveristy, P. R. China in 1997. He had two-year M. S. study in the Wuhan University from 1997 to 1999 and one-year Ph. D study in the Texas A&M University from 1999 to 2000 before he entered the Ph. D program in the Pennsylvania State University in the year of 2000. In 2002, he completed his M. S. degree in Electrical Engineering at the Pennsylvania State University. He is a member of SPIE, OSA and IEEE.